HEAT TRANSFER ANALYSIS FOR HOMOGENEOUS BUBBLE NUCLEATION DURING JET IMPINGEMENT QUENCHING

Sheikh Farhan Ahmed

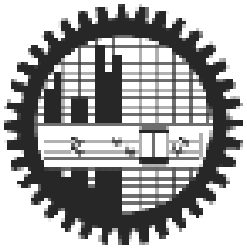

DEPARTMENT OF MECHANICAL ENGINEEIRNG

BANGLADESH UNIVERSITY OF ENGINEERING AND TECHONOLGY

Dhaka, Bangladesh

June 2010

Heat Transfer Analysis for Homogeneous Bubble Nucleation during Jet Impingement Quenching

by

Sheikh Farhan Ahmed

MASTER OF SCIENCE IN MECHANICAL ENGINEERING

Department of Mechanical Engineering

BANGLADESH UNIVERSITY OF ENGINEERING AND TECHONOLGY

June 2010

RECOMMENDATION OF THE BOARD OF EXAMINERS

The thesis titled '**HEAT TRANSFER ANALYSIS FOR HOMOGENEOUS BUBBLE NUCLEATION DURING JET IMPINGEMENT QUENCHING**', submitted by Sheikh Farhan Ahmed, Roll No. 040810005P, Session: April 2008, has been accepted as satisfactory in partial fulfillment of the requirement for the degree of **Masters of Science in Mechanical Engineering** on **June 6, 2010.**

BOARD OF EXAMINERS

Dr. Md. Ashraful Islam Professor Department of Mechanical Engineering BUET, Dhaka	Chairman
Dr. Muhammad Mahbubul Alam Professor and Head Department of Mechanical Engineering BUET, Dhaka	Member (Ex-officio)
Dr. Aloke Kumar Mozumder Associate Professor Department of Mechanical Engineering BUET, Dhaka	Member
Dr. Bodius Salam Professor Department of Mechanical Engineering CUET, Chittagong	Member (External)

CANDIDATE'S DECLARATION

This is hereby declared that this thesis or any part of it has not been submitted elsewhere for the award of any degree or diploma.

_____

Sheikh Farhan Ahmed

Dedicated to my mother

ACKNOWLEDGEMENT

The author is highly grateful to his supervisor, Dr. Md. Ashraful Islam, Professor, Department of Mechanical Engineering, Bangladesh University of Engineering and Technology (BUET), Dhaka, for his continuous and untiring supervision, encouragement and support in accomplishing this research work. His thoughtful observations and comments helped the author a lot to establish a complete and coherent investigation in depth.

The author is also indebted to Dr. Noor Al Quddus, Assistant Professor, Department of Mechanical Engineering, BUET, for his valuable suggestions in modeling the solid block part of this research work.

Finally, the author would like to express his deep gratitude to Dr. Bodius Salam, Professor, Department of Mechanical Engineering, CUET, for his thoughtful comments that have enriched this research work. The author would also like to give special thanks to Dr. Md. Mahbubul Alam, Professor and Head, and Dr. Aloke Kumar Mozumder, Associate Professor, Department of Mechanical Engineering, BUET, for their suggestions and cooperation in the successful completion of this work.

ABSTRACT

Jet impingement quenching is a direct liquid cooling technique with a promise of dealing with high heat flux which may give rise to heterogeneous and / or homogeneous nucleation of bubbles. In the present study, the phenomenon that happens during a brief contact of a liquid jet impinging on a hot solid surface has been analytically investigated.

In liquid analysis, a simple semi-infinite conduction heat transfer model is considered and the heat transfer analysis has been carried out for two different heating conditions, namely with (i) Prescribed Surface Temperature (PST-case) and (ii) Time-dependent Surface Temperature (TST-case). For each of the above cases, explicit equations for temperature distribution within liquid and other parameters have been derived and solved numerically and their outcomes are discussed. Furthermore, the average surface heat flux (q_s) during jet impingement quenching is determined using the concept of critical time (t^*) and compared with the thermodynamic limit of heat flux, which assures the validity of the analytical study. Also the information of the average stored energy and the minimum required energy for bubble formation gives the possibility of homogeneous bubble nucleation during jet impingement quenching. In solid analysis, a two-dimensional cylindrical heat transfer model has been devised and the simulation results are analyzed for a clear understanding of the cooling process of the hot solid surface at the early stages of jet impingement.

It is found that, when sufficient amount of energy is stored in superheated liquid after a particular time of contact of the liquid jet with the hot solid and when this energy becomes greater than the minimum amount of energy required for bubble formation, there is always a possibility for homogeneous bubble nucleation during jet impingement quenching process. As for example, a contact time of 0.025 μs is needed for water in PST case to trigger homogeneous bubble nucleation during such quenching process. From the solid analysis, the present study finds an alternating wet and dry phenomenon at the solid surface at early stages of cooling with a frequency of 16.4 cycles/s. It is also found that a contact period of 0.55 s for steel and 1.1 s for brass is required for a sustainable solid-liquid contact at early stages of jet impingement quenching.

TABLE OF CONTENTS

APPENDICES

LIST OF FIGURES

LIST OF TABLES

NOMENCLATURE

Symbols	Meanings	Units
a	Thermal diffusivity of liquid	$[m^2/s]$
a_s	Thermal diffusivity of the solid	$[m^2/s]$
C_{pl}	Specific heat of liquid	[kJ/kg-K]
C_{pv}	Specific heat of vapor	[kJ/kg-K]
C_v	Molar specific heat at constant volume	[kJ/mole-K]
c	Specific heat	[kJ/kg-K]
$\bar{c}$	Mean molecular velocity	[m/s]
Gb	Gibbs number ($= W_{cr} / k_B T$)	
h	Height of the solid block	[mm]
h_{fg}	Latent heat of vaporization	[kJ/kg]
h_l	Enthalpy of liquid	[J/kg]
h_v	Enthalpy of vapor	[J/kg]
J	Nucleation rate	$[Number/m^3/s]$
J_0	Factor of proportionality of nucleation rate	
K_l	Thermal conductivity of liquid	[W/m-K]
k	Boundary heating rate	[K/s]
k_B	Boltzmann constant	[J/K]
M	Molecular weight	
m	Mass of molecule	[kg]
N_1	Number density of liquid	$[molecules/m^3]$
n	Number density of molecules	
P	Pressure	[Pa]
P_B	Interior pressure of a vapor bubble	[Pa]
P_l	Liquid pressure exterior to a vapor bubble	[Pa]
P_{sat}	Saturation pressure	[Pa]

P_v	Saturated vapor pressure	[Pa]
P_{ve}	Pressure of vapor in equilibrium	[Pa]
q_{max}	Maximum heat flux	[MW/m^2]
$q_{max,max}$	Maximum thermodynamic limit of maximum heat flux	[MW/m^2]
q_s	Average heat flux	[MW/m^2]
$\bar{R}$	Ideal gas constant	[Joule/K-mole]
r	Radius of vapor bubble	[nm]
r_e	Equilibrium radius of vapor bubble	[nm]
r_1	Radius of the solid block	[mm]
s	Entropy	[J/kg-K]
T_o	Saturation temperature at ambient pressure	[°C or K]
T_c	Critical temperature	[°C or K]
T_i	Interface temperature	[°C or K]
T_L / T_{liq}	Temperature inside liquid	[°C or K]
T_l	Jet initial temperature	[°C or K]
T_{lavg}	Average liquid temperature	[°C or K]
T_{max}	Maximum solid surface temperature for a sustainable solid-liquid contact	[°C or K]
T_s / T_{b0}	Surface temperature of solid	[°C or K]
T_{sat}	Saturation temperature	[°C or K]
t	Time elapsed	[μs]
t_{max}	Time to reach T_{max}	[μs]
t^*	Critical time	[μs]
U_{avg}	Total average energy stored in superheated liquid	[J]
u_{avg}	Average amount of energy stored in superheated liquid	[J/molecule]
W_{cr}	Minimum energy required for bubble formation	[J]

x	Depth of liquid from the solid surface	[nm]
x_e	Liquid depth equal to dia of the critical vapor bubble	[nm]

Greek

•	Surface tension of liquid	[N/m]
•	Density	[kg/m^3]
• $_g$	Density of saturated vapor	[kg/m^3]
• $_l$	Density of liquid	[kg/m^3]
• $_v$	Density of vapor	[kg/m^3]
•	Thermal conductivity	[W/m-K]
•	Specific volume	[m^3/kg]
• $_g$	Specific volume of vapor	[m^3/kg]
• P_C	Tensile strength of liquid	[Pa]
μ_l	Chemical potential of liquid	G (Gibbs)
μ_{sat}	Chemical potential in saturated condition	G (Gibbs)
μ_{ve}	Chemical potential of vapor in equilibrium	G (Gibbs)

Abbreviations

ECCS	Emergency Core Cooling System
LOCA	Loss of Coolant Accident
PST	Prescribed Surface Temperature
TST	Time-dependent Surface Temperature

Subscripts

l	Liquid
s	Solid
v	Vapor

1. INTRODUCTION

1.1 Motivation and Background

In this modern challenging world today, demand for each and every industrial product is increasing day by day. Therefore, the major trend in all the industries in recent years has been the development of higher productivity, faster and complex automation in every branches of production with miniaturized system sizes. This drive towards more compact and faster technologies with shrinking system size has resulted in the tremendous increase of heat flux both at the chip and overall package levels in electronics and other industries. Though the number of system components in integrated form has been increased by the evolution of microprocessor and microcontroller-based systems, a consequent higher rate of heat dissipation has also augmented up in an alarming manner. Hence, the rapid development in the industrial productivity with modern technologies today requires a revolutionized thermal management with a high and efficient heat transfer in a small volume and space. Furthermore, many industrial situations require a very quick removal of heat, like in water-cooled nuclear reactors, where it is necessary to control the heat removal rate from the fuel elements during a Loss of Coolant Accident (LOCA). A LOCA is a mode of failure for a nuclear reactor; if not managed effectively, whose result could be the reactor core damage. Each nuclear plant's Emergency Core Cooling System (ECCS) exists specifically to deal with a LOCA. Nuclear reactors generate heat internally and in order to remove this heat and convert it into useful electrical power, a coolant system is used. If this coolant flow is reduced, or lost altogether, the nuclear reactor's emergency shutdown system is designed to stop the fission chain reaction. However, due to radioactive decay, the nuclear fuel will continue to generate a significant amount of heat. If all of the independent cooling trains of the ECCS fail to operate as designed, this heat can increase the fuel temperature to the point of damaging the reactor. In case of such failures, a very quick and highly effective technique is essential in order to avoid any kind of accidents. In addition, high density cooling technology is focused in designing plasma facing surface in fusion reactor.

Thus, the need for new cooling techniques is driven by the continuing increase in heat dissipation of electronic parts and other systems [1]. In many cases, standard techniques

cannot achieve the required cooling performance due to physical limitations in heat transfer capabilities. These limitations are principally related to the limited thermal conductivity of air for convection and other solid materials for conduction. Figure 1.1 shows a comparison of various cooling techniques as a function of the attainable heat transfer in terms of the heat transfer coefficients [2], which concludes that, liquid cooling technique is a must in future for thermal management systems.

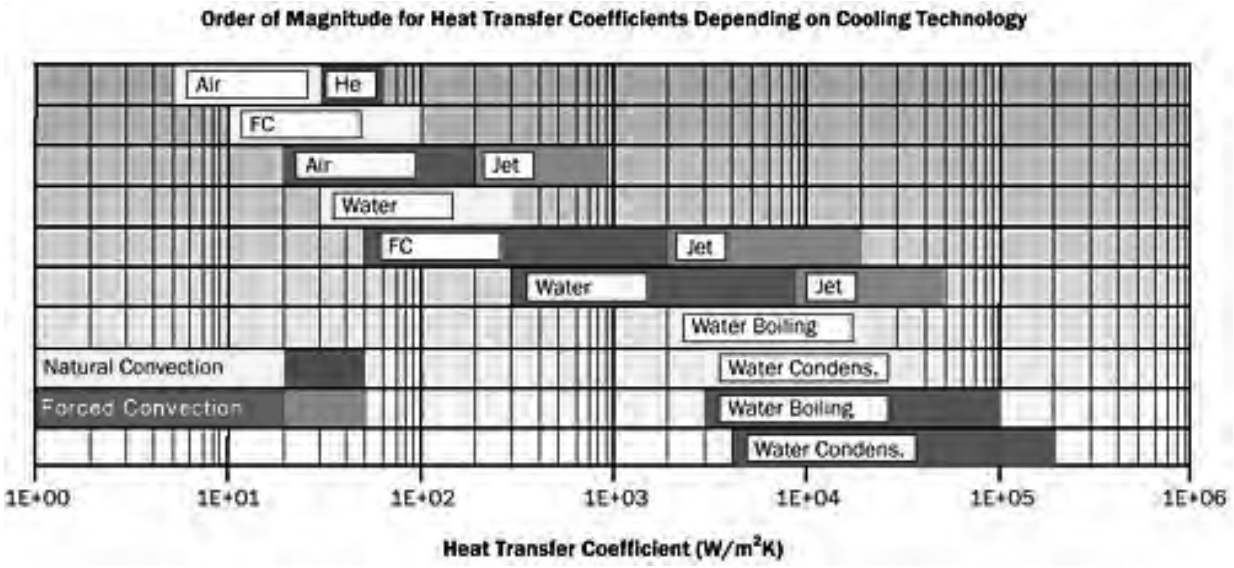

Figure 1.1 Heat transfer coefficient attainable with natural convection, single-phase liquid forced convection and boiling for different coolants [2]

Liquid cooling for industrial applications is generally divided into two main categories- indirect and direct liquid cooling. Indirect liquid cooling is one in which the liquid does not directly contact the components to be cooled. Direct liquid cooling brings the liquid coolant into direct contact with the components to be cooled. Indirect liquid cooling can be achieved in the form of heat pipes, cold plates etc. and direct liquid cooling can appear in the form of immersion cooling and jet impingement. In direct liquid cooling, it is claimed that a cooling of 90 W/cm^2 with a 100°C temperature rise can be achieved using a flow rate of only 8 ml/min [1]. An example of a commercial concept for liquid jet impingement cooling [3] is shown in Fig. 1.2 and jet impingement of a dielectric liquid on the chip surface [3] is shown in Fig. 1.3.

Figure 1.2 Commercially available multiple jet impingement liquid cooling [3]

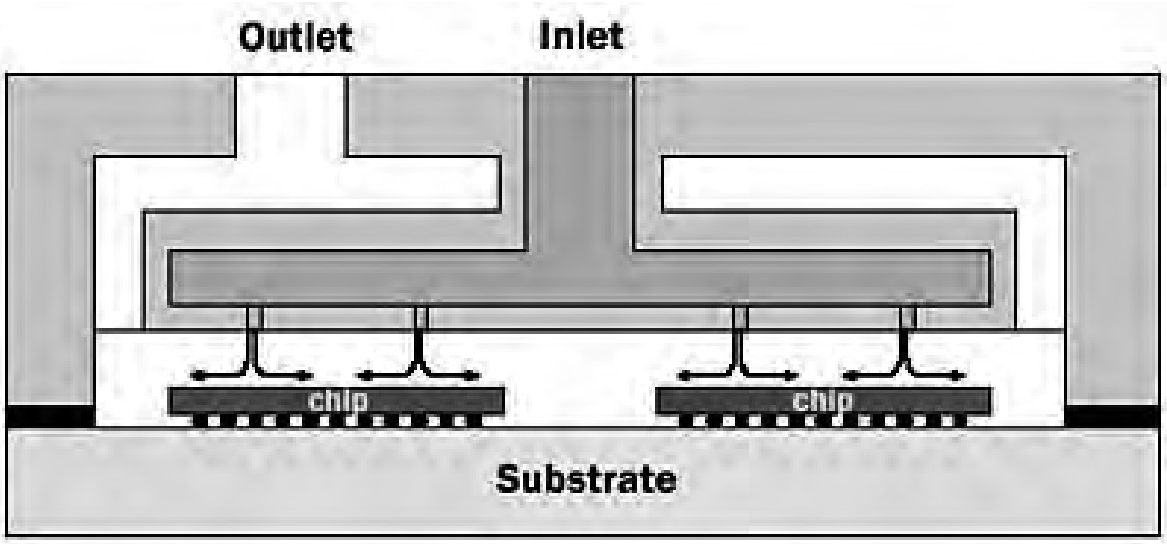

Figure 1.3 Direct liquid jet impingement cooling [3]

For its attractive cooling potential and wide range of industrial applications, jet impingement quenching is an exclusive topic to the researchers and scientists now-a-days. A quench refers to a rapid cooling. Figure 1.4 also proves water jet impingement as the best option among all the indirect cooling available [4].

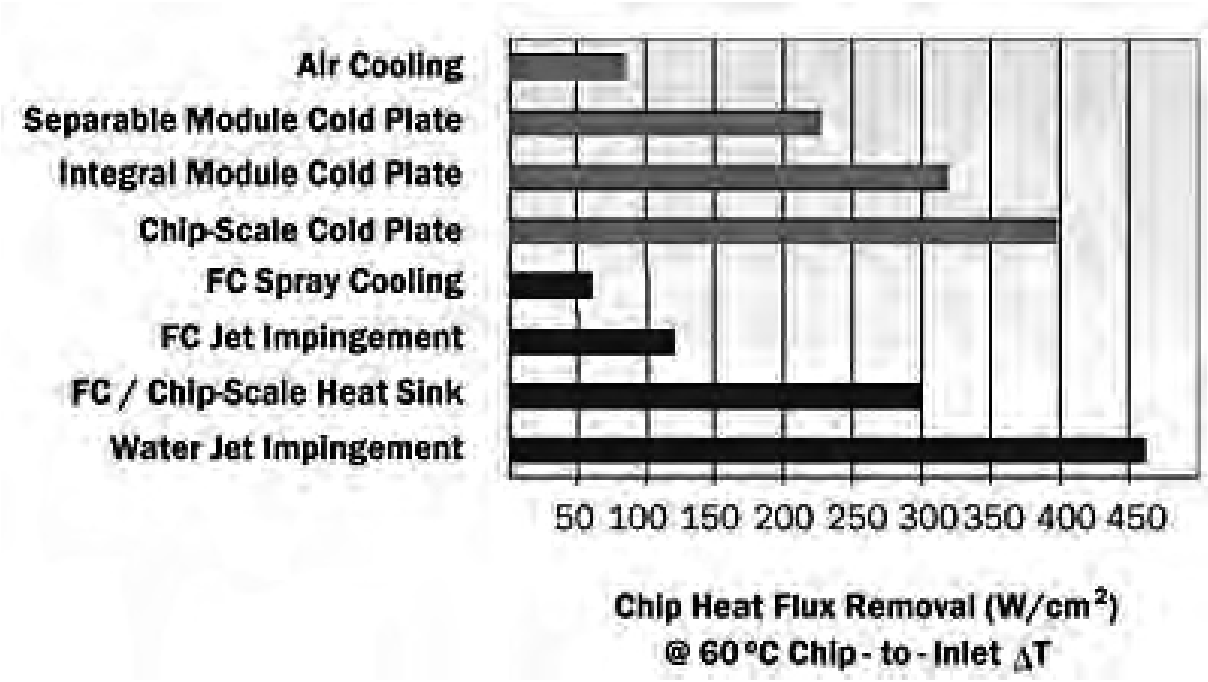

Figure 1.4 Comparison of heat removal capability [4]

Jet impingement cooling method has been used in LOCA analysis, steel manufacturing, metallurgy, microelectronic device making, thermal management processes etc. It might be useful in elucidating poorly understood phenomena such as Leidenfrost phenomena, boiling explosion etc. In spite of many important applications of jet impingement quenching, there are some reasons for which, the understanding of the field of quenching and wetting front propagation is far from a mature science. One of the major reasons is that, during quenching high temperature material, different cooling modes such as film boiling, nucleate boiling and transient from film to nucleate boiling coexists on the surface and these modes changes with time. Especially, during the transient, the surface temperature and surface heat flux dramatically change, which are hardly measured. As

such, current study is devoted to explicate the heat transfer characteristics for homogeneous bubble nucleation during jet impingement quenching.

1.2 Phase Stability in Classical Thermodynamics

According to classical thermodynamics, the stability of a phase of pure substance depends upon two criteria- the thermal stability and the mechanical stability. The thermal stability of a phase is satisfied by the relation, $C_v > 0$ where, C_v is the molar specific heat at constant volume, and the mechanical stability is satisfied by the relation, $(\partial P/\partial V)_T < 0$. Now, as C_v for all substances are theoretically greater than zero, so the criterion of thermal stability is satisfied and only the mechanical stability is a necessary and sufficient condition for the stability of a phase of pure substance.

Now, in real phase transition process, liquid can be superheated above its equilibrium saturation temperature. Liquid, which is superheated to this temperature, exists in a non-equilibrium condition, which is known as metastable state. Liquid in metastable state is mechanically stable although it is not in thermodynamic equilibrium.

1.3 Homogeneous Nucleation

Nucleation is the onset of a phase transition in a small region. The phase transition can be the formation of a bubble or of a crystal from a liquid. Creation of liquid droplets in saturated vapor or the creation of gaseous bubble in a saturated liquid is also characterized by nucleation. Nucleation of crystalline, amorphous, and even vacancy clusters in solid materials is also important, for example to the semiconductor industry.

1.3.1. Thermodynamic aspect

When a liquid comes in contact with a solid surface whose temperature is above the temperature of the liquid, heat is transferred from the hot solid surface to the ambient liquid by free convection. As the surface temperature increases, reaching the saturation temperature of the liquid, small gaseous bubbles begin to form at some of the cavities of the surface and tend to grow with further increase of surface temperature. This type of bubble nucleation occurring at the solid-liquid interface is known as heterogeneous bubble nucleation. On the otherhand, bubble nucleation may also occur completely within a liquid at any liquid-liquid interface. This type of bubble nucleation is known as homogeneous bubble nucleation. One particular case of homogeneous bubble nucleation is that, occurring within a superheated liquid in the metastable region.

In a thermodynamically stable liquid system, fluctuations of local molecular density take place spontaneously. Extreme density fluctuations, that may give rise to small bubble embryo is known as ‘Heterophase Fluctuation’. In equilibrium condition, the radius of such a bubble embryo is known as equilibrium radius of vapor embryo, r_e, whose expression is derived in Appendix A.1.

Now, a bubble embryo of radius $r = r_e$ is in an unstable equilibrium because of the decrease of embryo radius into the range $0 < r < r_e$ by the loss of just one molecule from it. So, if a bubble embryo of radius $r < r_e$ is formed due to the density fluctuation in the metastable liquid, it will collapse. On the other hand, an embryo of radius $r = r_e$ grows spontaneously by gaining just one molecule due to density fluctuation. This spontaneous growth of bubbles results in Homogeneous nucleation of the vapor phase in the system.

1.3.2. Kinetic theory

In a pure liquid, surface tension is the macroscopic manifestation of the intermolecular forces that tend to hold molecules together and prevent the formation of large holes. The

liquid pressure, P_l exterior to a bubble of radius, r, will be related to the interior pressure, P_B, by-

$$P_B - P_l = \frac{2}{}$$

equilibrium with its surroundings after its creation, then the increment of energy that must be deposited consists of two parts. First, energy must be deposited to account for that stored in the surface of the bubble. By definition of the surface tension, • , that amount is • per unit surface area for a total of $4\bullet r_e^{2}\bullet$. But, in addition, the liquid has to be displaced outward in order to create the bubble, and this implies work done on or by the system. The pressure difference involved in this energy increment is the difference between the pressure inside and outside of the bubble (which, in this evaluation, is • P_C) given by Eq. (1.2). The work done is the volume of the bubble multiplied by this pressure difference, or $4\bullet r_e^{3}\bullet P_C/3$, and this is the work done by the liquid to achieve the displacement implied by the creation of the bubble. Thus the net energy, W_{cr}, which must be deposited to form the bubble, is-

$$W_{cr} = 4\pi r_e^2\sigma - \frac{4}{3}\pi r_e^3\Delta P_C = \frac{4}{3}\pi r_e^2\sigma \tag{1.3}$$

It can also be useful to eliminate r_e from Eq. (1.2) and Eq. (1.3) to write the expression for the critical deposition energy as-

$$W_{cr} = \frac{16\pi\sigma^3}{3(\Delta P_C)^2} \tag{1.4}$$

It was, in fact, Gibbs [6] who first formulated this expression. For more detailed considerations the reader is referred to the works of Skripov [5] and many others.

The final step in homogeneous nucleation theory is an evaluation of the mechanisms by which energy deposition could occur and the probability of that energy reaching the magnitude, W_{cr}, in the available time. Then Eq. (1.4) yields the probability of the liquid being able to sustain a tension of • P_C during that time. In the body of a pure liquid completely isolated from any external radiation, the issue is reduced to an evaluation of the probability that the stochastic nature of the thermal motions of the molecules would lead to a local energy perturbation of magnitude, W_{cr}. Most of the homogeneous nucleation

theories therefore relate W_{cr} to the typical kinetic energy of the molecules, namely $k_B T$ (k_B is Boltzmann's constant) and the relationship is couched in terms of a Gibbs number,

$$Gb = \frac{W_{cr}}{k_B T} \tag{1.5}$$

It follows that a given Gibbs number will correspond to a certain probability of a nucleation event in a given volume during a given available time. It is worth mentioning that other basic relations for W_{cr} have been proposed. For example, Lienhard and Karimi [7] find that a value of W_{cr} related to $k_B T_C$ (where T_C is the critical temperature) rather than $k_B T$ leads to a better correlation with experimental observations.

A number of expressions have been proposed for the precise form of the relationship between the nucleation rate, J, defined as the number of nucleation events occurring in a unit volume per unit time and the Gibbs number, Gb, but all take the general form-

$$J = J_0 e^{-Gb} \tag{1.6}$$

Where, J_0 is some factor of proportionality. Various functional forms have been suggested for J_0. A typical form is that given by Blander and Katz [8], namely-

$$J_0 = N_1 \left(\frac{2\sigma}{\pi m}\right)^{\frac{1}{2}} \tag{1.7}$$

Where, N_1 is the number density of the liquid (molecules/m^3) and 'm' is the mass of a molecule. Though J_0 may be a function of temperature, the effect of an error in J_0 is small compared with the effect on the exponent, Gb, in Eq. (1.6).

1.4 Literature Review

1.4.1 Fundamentals of homogeneous nucleation

Studies of the fundamental physics of the formation of vapor voids in the body of a pure liquid date back to the pioneering work of Gibbs [6]. The modern theory of homogeneous nucleation is due to Volmer and Weber [9], Farkas [10], Becker and Doring [11], Zeldovich [12] and others. For reviews of the subject, the reader is referred to the books of Frenkel [13] and Skripov [5], to the recent text by Carey [14] and to the reviews by Blake [15], Bernath [16], Cole [17], Lienhard and Karimi [7] and Blander and Katz [8].

Jet impingement cooling of a hot surface may give rise to heterogeneous and/or homogeneous nucleation of bubbles which is yet to be explored. A number of interesting phenomena have been reported for jet impingement quenching. Piggot et al. [18] reported a delay to the movement to the wetting front. In addition, they observed a number of completely different flow patterns during quenching of 6.3-25.3 mm diameter heated rods from an initial temperature of 700°C with a subcooled water jet. The most dramatic phenomena occurred for the case where the outermost layer of the heated rod was a 1 mm thick gold tube. The quench began with quiet film boiling and then a white patch of around 5 mm in diameter appeared beneath the jet. The liquid film then broke into tiny droplets in a spray pattern, which was followed by an oscillating liquid sheet that lifted from the surface of the rod. Finally, the wetting front moved forward over the heated surface.

A number of unusual phenomena have been reported for quench cooling by Ishigai et al. [19] during performing experiments with a planar, subcooled, free-surface water jet impingement on a surface with an initial temperature of approximately 1000°C. They found that a region of almost constant heat flux appeared in the transition regime for liquid subcooling greater than 15°C.

Hatta et al. [20] considered quench cooling of a 10 mm thick stainless steel plate from an initial temperature of around 900°C using a subcooled laminar water jet of 80K. Visual observations indicated an almost instantaneous drop in surface temperature to below 500°C

since the metal color in a small circle beneath the jet changed from glowing red to black immediately when the jet contacted the surface. From this, they concluded that direct liquid-solid contact occurred without any noticeable period of film boiling in spite of the high temperature.

A comprehensive review of jet impingement boiling was also made by Wolf et al. [21]. They observed that in contrast to research on nucleate boiling and critical heat flux, there is a scarcity of concrete studies relating to jet impingement for the film boiling and transition regimes. Liu and Wang [22] carried out an experimental investigation to measure heat transfer to an impinging jet during film boiling on a high temperature plate. They reported a significant increase in the heat flux with liquid subcooling and heat fluxes in the range from 0.2 to 2 MW/m^2 for film boiling. These figures are over an order of magnitude greater than film boiling at the minimum heat flux condition for pool boiling which reflects the heat transfer enhancement of impinging jets.

Some recent works include Hammad et al. [23], Woodfield et al. [24], Mozumder et al. [25] and Islam et al. [26,27]. Most of these recent studies have been performed by quenching a cylindrical block of initial temperatures ranging from 250-400°C. These studies included flow visualization, surface temperature, surface heat flux, cooling curves, boiling curves, resident time or wetting delay and boiling sound. All of them were determined using the experimental setup, shown as Fig. 1.5, which contains five major components, a heated block, a fluid flow system, a data acquisition system, a high-speed video camera and a sound measuring unit. The heated block was of cylindrical shape with 94 mm diameter and 59 mm height. Sixteen thermocouples were located at two different depths, 2.1 mm and 5 mm from the surface. At each depth, eight thermocouples were inserted along the r-axis. When all the desired experimental conditions were fulfilled, then the shutter was opened for the water jet to strike the center of the flat surface of the heated block. The high speed video camera starts simultaneously at the signal of opening shutter to record the flow pattern over the heated block surface and at the same time, the 16 thermocouples measure the temperatures inside the heated block. Sound has also been recorded simultaneously at the same time with the microphone. Islam et al. [28] reported

some excellent video images at early stages of jet impingement quenching (Fig. 1.6 is an example of such an image) and demonstrated a clue towards development of a model of heat transfer. Therefore, the nature of the phase change phenomena and characteristics of heat transfer for impinging jets at early stages in the high temperature context is yet to be understood clearly. Islam et al. [29] tried to find out the average amount of energy stored in the superheated liquid (U_{avg}) and compared it with the minimum energy (W_{cr}) which must be supplied to form a bubble cluster, in order to find the possibility of homogeneous bubble nucleation during jet impingement quenching. Most recently, Islam et al. [30] analyzed the possibility of homogeneous bubble nucleation during the impingement of water and ethanol jet and found a very strong possibility of such a nucleation process.

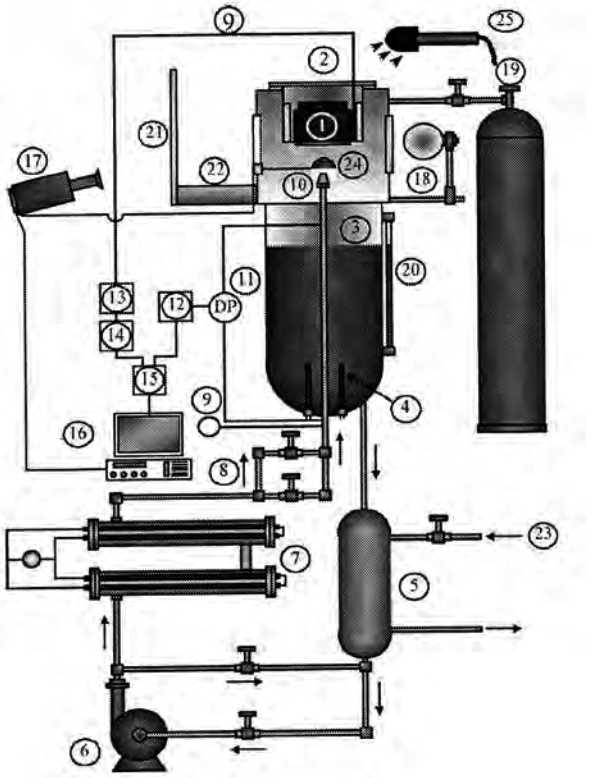

Figure 1.5 Schematic diagram of the experimental setup [25]. (1) Tested block, (2) block holder, (3) liquid tank, (4) heater, (5) heat exchanger, (6) pump, (7) auxiliary heater, (8) regulating valve, (9) thermocouple, (10) nozzle, (11) differential pressure, (12) dynamic strain meter, (13) ice box, (14) voltage amplifier, (15) A/D converter, (16) computer, (17) high-speed video camera, (18) spot light, (19) nitrogen cylinder, (20) level gauge, (21) glass frame, (22) vessel, (23) cooling water, (24) rotary shutter, (25) microphone.

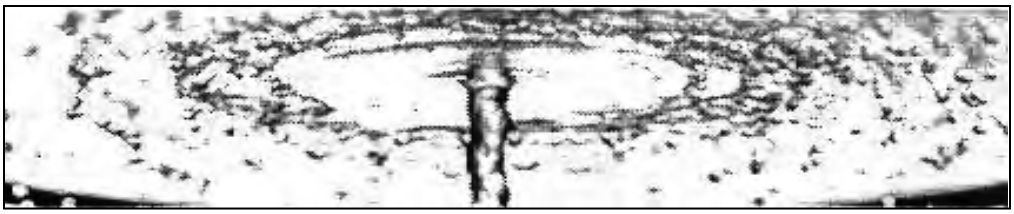

Figure 1.6 A video image 30 ms after jet impingement during jet impingement quenching [28]

1.4.2 Upper limit of heat flux

It is a well-known information in process heat transfer, that boiling and condensation yield the highest known heat transfer coefficient and in order to transfer a great deal of energy rapidly, under fairly low driving temperature differences, these processes must be incorporated. For their vast use in process heat transfer, several investigators have worked hard to find the upper limit on these heat fluxes. The highest heat flux that can be achieved in a phase-transition process was given by Schrage [31] who made reference to antecedents of the idea extending back into 19^{th} century. It was Gambill and Green [32], who first used inlet tangential-slot swirl-flow generators with water at pressure up to 7 MPa and at axial velocities up to 30 m/s to measure the burnout heat flux. He obtained burnout heat fluxes as high as 172.8 MW/m^2. When this study was later extended to swirl flows induced by internal twisted tapes, Gambill et al. [33] obtained maximum heat flux upto 117.8 MW/m^2 in water and Gambill and Bundy [34] obtained q_{max} up to 28.4 MW/m^2 in ethylene Glycol.

Ornatskii and Vinyarskii [35] have observed q_{max} in water flowing axially in small (0.5 mm I. D.) tubes at speed up to 90 or 100 m/s, and attained a value of maximum heat flux of 224.5 MW/m^2. Japanese investigators, like Monde and Katto [36] and Katto and Shimizu [37] have measured maximum heat flux in a different kind of system- a liquid jet impinging perpendicularly upon a heated disc. The set of experiments using water jets at atmospheric pressure yielded several values of q_{max} in excess of 10 MW/m^2. Monde and Katto's highest value was 18.26 MW/m^2.

Later researchers like Tien and Lienhard [38,39] independently made the calculations, done previously by Scharge [31] in a simple approximate way, in reference to boiling burnout. The simple forms of the expression, derived by Lienhard, are used in the present study to find the thermodynamically attainable maximum heat flux, $q_{max.max}$.

1.4.3 Effect of boundary heating rate

A number of experiments have been done where the boundary heating rate effects on homogeneous nucleation and the dynamics of bubble formation are observed. A number of methods are also used in this respect and between several methods which are available to study the limit of liquid superheat, only pulsed heating method, in which, a heater immersed in liquid, is heated so rapidly that the nucleation from pre-existing nuclei does not occur, has enabled to study the dynamics of a large number bubbles formed by fluctuation nucleation. In the conventional studies of Skripov et al. [40] and Derewnicki et al. [41] for pulse heating method, the rate of temperature rise was limited to about 11×10^6 K/s. Such a lower rate of temperature rise cannot confirm the occurrence of fluctuation nucleation. To overcome this situation, in further studies of Iida et al. [42,43], a thin film heater immersed in a liquid at atmospheric pressure was heated at an extremely high rate of temperature rise up to 93×10^6 K/s, which is about ten times that of conventional studies.

Glod et al. [44] investigated the explosive vaporization of water close to its superheat limit at the microscale level using a short and ultrathin (only 10μm in diameter) Platinum wire, where it was possible to obtain a novel visualization and simultaneously pressure and temperature measurements in the vapor microregion, thus accomplishing a step forward in understanding the complex behavior of explosive vapor nucleation, growth, and subsequent collapse, despite experimental difficulties posed by the very short time and length scales of the phenomena. In their investigation, Glod et al. transferred a very large amount of energy to the liquid during a very short time period. The wire or heater temperature increased rapidly (at a rate higher than 10^7K/s) and after a few microseconds, the liquid in contact with the source boiled explosively. They successfully used a maximum heating rate of 86×10^6 K/s and obtained a maximum nucleation temperature of 303°C for water. They

came to a number of very interesting conclusions about temperature rising rates from this investigation, such as, the heating rate has to be higher than 60×10^6 K/s in order to reach the maximum nucleation temperature of 303°C for water and for lower heating rates, heterogeneous nucleation seemed to be the governing boiling mechanism. For a lower heating rate of 10^5 K/s, the nucleation temperature was found as around 275°C. For a lower heating rate of 10^5 K/s, it was observed that the nucleation was initiated by a single vapor bubble, growing from a cavity on the wire surface which then triggered the boiling on the entire wire surface, which showed clearly that heterogeneous nucleation would be the mechanism to govern the boiling process for lower rate of heating.

Okuyama et al. [45] investigated the dynamics of boiling succeeding spontaneous nucleation of a small film heater immersed in ethyl alcohol at high heating rates, ranging from 10^7 K/s to approximately 10^9 K/s, under which spontaneous nucleation was dominant for the inception of boiling. The heating rate was widely varied up to approximately two orders of magnitude larger than the minimum rate, (which is approximately 1.0×10^7 K/s for ethyl alcohol) required for realizing spontaneous nucleation, and its effects on the formation, growth and collapse processes of the coalesced bubble were investigated. They came to a conclusion that vapor production became negligibly small at an infinitely large rate of surface temperature increase and the superheat energy at boiling incipience decreased with the increase in the heating rate, because boiling is always initiated at around the homogeneous nucleation temperature, regardless of the magnitude of the heating rate for a sufficiently large rate.

Most recently, Hasan et al. [46] developed a numerical model using a control volume approach to simulate the process of rapid heating with time-dependent boundary temperature condition. They aimed at a comparative study of their simulation results with earlier experimental observations and came to a number of interesting conclusions, such as, the simulations results are close to the experimental counterparts for lower values of boundary heating rate (approximately 3.73×10^7 K/s), but for higher values (approximately 1.8×10^9 K/s), simulations results predicted earlier attainment of maximum liquid temperature, in other words, earlier occurrence of boiling explosion. It is also found from

their investigations that the magnitude of maxima of average liquid temperature increased for higher values of boundary heating rate.

1.5 Scope and Objectives of the Study

All the previous studies, mentioned in the earlier section apprehended the possibility of homogeneous bubble nucleation on the basis of the minimum energy stored in liquid. The heat fluxes were not taken into consideration in those studies. Therefore, as a follow up of the previous investigations, the present has the following specific objectives to achieve-

a. To establish a theoretical model of heat transfer for the liquid during jet impingement quenching and to carry out heat transfer analysis for different heating conditions and also for different working fluids, like water and ethanol.
b. To derive explicit equations for the temperature distribution, average liquid temperature and average internal energy within the liquid and to solve them numerically in order to achieve a complete temperature history within the liquid during the quenching process.
c. To investigate the effect of different parameters like jet initial temperature, block initial temperature, block material, working fluid, contact time and boundary heating rate, on the heat transfer characteristics of liquid during jet impingement quenching process.
d. To determine the average surface heat flux during the quenching process using a new concept of critical time, t^*, and to compare it with the thermodynamic limit of maximum heat flux.
e. To examine the possibility of homogeneous bubble nucleation during jet impingement quenching process by the information of the stored energy in liquid as well as the thermodynamic limit of maximum heat flux.
f. To develop an analytical model of heat transfer for the solid surface in order to achieve a clear view of its cooling process and the surface heat flux variation during jet impingement quenching.

g. To extensively analyze the change of solid surface temperature and the alternating wet and dry phenomenon at early stages of jet impingement quenching process.

2. ANALYTICAL MODELING AND SIMULATION

2.1 Liquid Analysis

2.1.1 Mathematical model

A promising method for simulating the heat transfer process from the hot solid object to the impinging liquid is based on the consideration of the liquid in brief contact with the hot solid during jet impingement quenching as one dimensional semi-infinite solid through which heat from the hot solid is conducted. A semi-infinite solid is one, which is bounded by the plane x = 0 and extends to infinity in the direction of x positive. The mathematical model for the present study is depicted in Fig. 2.1. Due to the consideration of the hot solid as a one dimensional semi-infinite solid, a simple conduction analysis can find the temperature distribution within the liquid. Hence, this temperature distribution is dependent on the initial temperature of the liquid jet by which the impingement on the hot solid is done, the temperature of the solid-liquid interface during the jet impingement, the thermal diffusivity of both liquid and solid, the depth of liquid from the hot solid impinging surface and the brief time of contact of the liquid jet with the hot solid surface.

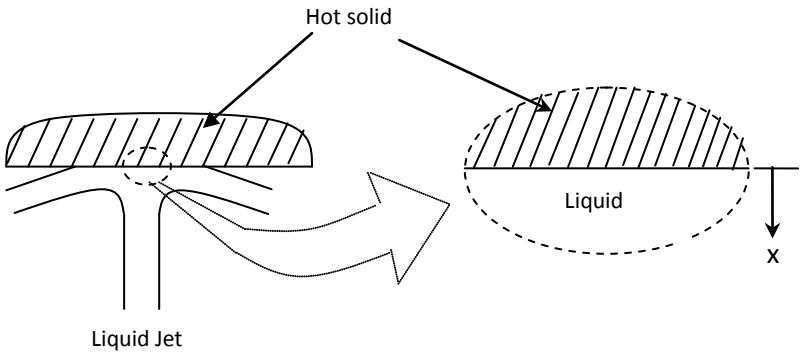

Figure 2.1 One-dimensional semi-infinite solid model

As mentioned above, the present model is based on transient one dimensional heat conduction in a semi-infinite solid and hence, the governing equation of the model is given by-

$$\frac{\delta^2 T}{\delta x^2} = \frac{1}{a}\frac{\delta T}{\delta t} \;\; ; \;\; 0 < x < \infty \qquad (2.1)$$

Where, ‘a’ is the thermal diffusivity of liquid.

2.1.2 Boundary conditions

The present mathematical model is solved for two boundary conditions at the plane, x = 0

i) Prescribed Surface Temperature (PST)
ii) Time-dependent Surface Temperature (TST)

The initial condition is given by-

$$T = T_l \;\; ; \;\; 0 < x < ø \qquad (2.2)$$

Where, T_l is the jet initial temperature.

PST case. This boundary condition predicts a fixed temperature at the surface x = 0 for a particular type of solid block material, liquid jet and their corresponding initial temperatures. Though maintaining a fixed temperature at a surface is practically very difficult, but it is assumed in this investigation that a prescribed temperature of a surface can be maintained for a very short period of time. The temperature, T at the plane x = 0 is given by-

$$T = T_i \qquad (2.3)$$

Where, T_i is the interface temperature. It is calculated according to Carslaw and Jaeger [47] using the following equation-

$$\frac{(T_s - T_i)}{(T_i - T_l)} = \sqrt{\frac{(\rho c \lambda)_l}{(\rho c \lambda)_s}} \tag{2.4}$$

Where, T_s is the surface temperature of solid, '•', 'c' and '•' are, respectively, the density, specific heat and thermal conductivity and the subscripts 'l' and 's' stand for liquid and solid respectively. The detailed derivation of the interface temperature is given in Appendix A.2.

The temperature distribution within the liquid for PST case can be derived using the assumption of a continuous heat flux over the surface of separation of solid and liquid. The temperature distribution is given by the equation-

$$T(x,t) = T_l + (T_i - T_l)\ \text{erfc}\left(\frac{x}{\sqrt{4at}}\right) \tag{2.5}$$

Where, 'x' is the depth of liquid from the solid surface and't' is the time elapsed after jet comes in contact with the surface. The detailed derivation of the temperature distribution within the liquid for PST case is mentioned in Appendix A.3.1.

The boundary condition for PST case is verified by substituting x = 0 in equation (2.5) –

$$T\ (0,t) = T_l + (T_i - T_l)\ \text{erfc}\ (0)$$

$$= T_l + (T_i - T_l) \times 1$$

$$= T_i\ \text{, which is the required boundary condition.}$$

The initial condition is verified by substituting t = 0 in equation (2.5) -

$$T\ (x,0) = T_l + (T_i - T_l)\ \text{erfc}\ (ø)$$

$$= T_l + (T_i - T_l) \times 0$$

$= T_l$, which is the required initial condition.

From the definition of heat capacity, the amount of energy stored in the superheated liquid with reference to saturated liquid is the amount of heat needed to change the temperature of the liquid from its saturation temperature to the superheat temperature of the liquid T(x,t), i.e.,

$$u(x,t) = mc\Delta T = mc[T(x,t) - T_0]$$

Now in a unit mass basis, this stored energy will be-

$$u(x,t) = c(T(x,t) - T_0) \tag{2.6}$$

Where, 'c' is the specific heat of the liquid and 'T_0' is the reference temperature, which can reasonably be the saturation temperature at the ambient pressure.

The average of the stored energy over the depth of liquid is-

$$u_{avg}(x_e,t) = \frac{1}{x_e}\int_0^{x_e} u(x,t)dx \tag{2.7}$$

Where, x_e is the liquid depth equal to the diameter of the critical vapor embryo in the superheated liquid. The value of x_e (=$2r_e$) is not known. It depends on the liquid temperature which in turn depends on the contact time t. The equilibrium embryo size is given by equation (2.8) according to Carey [14]-

$$r_e = \frac{2\sigma}{P_{sat}(T_l)\exp\left[\frac{v_l\{P_l - P_{sat}(T_l)\}}{RT_l}\right] - P_l} \tag{2.8}$$

Equation (2.7) can be simplified as follows-

$$u_{avg}(x_e, t) = c\left(T_l + \frac{T_i - T_l}{\frac{x_e}{\sqrt{4at}}}\left[\frac{1}{\sqrt{\pi}} - \text{ierfc}\left(\frac{x_e}{\sqrt{4at}}\right)\right] - T_0\right) \tag{2.9}$$

Here,

$$\text{ierfc}\left(\frac{x_e}{\sqrt{4at}}\right) = \frac{1}{\sqrt{\pi}} e^{-\left(\frac{x_e}{\sqrt{4at}}\right)^2} - \frac{x_e}{\sqrt{4at}}\text{erfc}\left(\frac{x_e}{\sqrt{4at}}\right)$$

The detailed derivations of the equilibrium embryo size, r_e is shown in Appendix A.1.

In order to get an estimate of x_e, the average temperature of the liquid over a certain volume of the liquid in contact is considered as given in the following equation-

$$T_{lavg}(x_e, t) = \frac{1}{x_e}\int_0^{x_e} T\,(x, t)\,dx \tag{2.10}$$

Equation (2.10) can be manipulated analytically to have a simplified shape as follows-

$$T_{lavg}(x_e, t) = T_l + \frac{T_i - T_l}{\frac{x_e}{\sqrt{4at}}}\left[\frac{1}{\sqrt{\pi}} - \text{ierfc}\left(\frac{x_e}{\sqrt{4at}}\right)\right] \tag{2.11}$$

Equation (2.9) can be simplified using average liquid temperature as follows-

$$u_{avg}(x_e, t) = c\left(T_{lavg}(x_e, t) - T_0\right) \tag{2.12}$$

Therefore, the total average internal energy over the volume x_e^3 of the liquid is given by-

$$U_{avg}(x_e, t) = \rho_l x_e^3 u_{avg}(x_e, t) \tag{2.13}$$

Where, ρ_l is the density of liquid at T_{lavg}.

For the detailed calculations for finding the simplified expressions of average liquid temperature, T_{lavg} and the average internal energy, u_{avg}, the readers are recommended to see Appendix A.3.2 and A.3.3 respectively.

TST case. This boundary condition predicts the surface temperature at x = 0 as a time-varying one, where the temperature T on the plane x = 0 is assumed to vary linearly with time, given by-

$$T = kt \tag{2.14}$$

Where, 'k' is a constant, representing the rate of change in boundary surface temperature and't' is the time elapsed after jet comes in contact with the surface. A linear variation of temperature is assumed neglecting non-linear ones in order to avoid any calculation complexity. The boundary heating rate, k values are taken from Iida et al. [42].

The temperature distribution within the liquid for TST case, derived from Carslaw and Jaeger [47], is given by the expression-

$$T(x,t) = T_l + 4kti^2\,\mathrm{erfc}\left(\frac{x}{\sqrt{4at}}\right) \tag{2.15}$$

Where,

$$i^2\mathrm{erfc}\left(\frac{x}{\sqrt{4at}}\right) = \frac{1}{4}\left[\mathrm{erfc}\left(\frac{x}{\sqrt{4at}}\right) - 2\frac{x}{\sqrt{4at}}\,\mathrm{ierfc}\left(\frac{x}{\sqrt{4at}}\right)\right]$$

The boundary condition for TST case is verified by substituting x = 0 in equation (2.14) –

$$T(0,t) = T_l + 4kt \times \frac{1}{4}[\mathrm{erfc}(0) - 2(0)\mathrm{ierfc}(0)]$$

$$= T_l + kt, \text{ which is the required boundary condition.}$$

The initial condition is verified by substituting t = 0 in equation (2.14) –

$$T(x, 0) = T_l + 0$$

$$= T_l \text{ , which is the required initial condition.}$$

The average liquid temperature in TST case can be presented in a simplified form as-

$$T_{lavg}(x_e, t) = T_l + \frac{kt}{\frac{x_e}{\sqrt{4at}}} \frac{2}{3}\left[\frac{1}{\sqrt{\pi}} - 6i^3\text{erfc}\left(\frac{x_e}{\sqrt{4at}}\right)\right] \quad (2.16)$$

Where,

$$i^3\text{erfc}\left(\frac{x_e}{\sqrt{4at}}\right) = \frac{1}{6}[\text{ierfc}\left(\frac{x_e}{\sqrt{4at}}\right) - \frac{1}{2}\frac{x_e}{\sqrt{4at}}\text{erfc}\left(\frac{x_e}{\sqrt{4at}}\right) + (\frac{x_e}{\sqrt{4at}})^2\text{ierfc}(\frac{x_e}{\sqrt{4at}})]$$

The average of the stored energy over the depth of the liquid is given by-

$$u_{avg}(x_e, t) = \frac{1}{x_e}\int_0^{x_e} u(x, t)dx$$

This equation can be simplified for TST case as-

$$u_{avg}(x_e, t) = c\left(T_l + \frac{kt}{\frac{x_e}{\sqrt{4at}}} \frac{2}{3}\left[\frac{1}{\sqrt{\pi}} - 6i^3\text{erfc}\left(\frac{x_e}{\sqrt{4at}}\right)\right] - T_0\right) \quad (2.17)$$

Therefore, the total average internal energy over the volume x_e^3 of the liquid is given by-

$$U_{avg}(x_e, t) = \rho_l x_e^3 u_{avg}(x_e, t)$$

Where, $\bullet_l$ is the density of liquid at T_{lavg}.

For more details of the calculation procedures of the temperature distribution, average liquid temperature and average stored energy in liquid for TST case, the reader is referred to Appendix A.4.1, A.4.2 and A.4.3 respectively.

2.1.3 Critical time

The critical time, t^* is a new concept, used in the present investigation. This new concept of analytical investigation has differentiated the present approach of heat transfer analysis with the previous ones. The critical time is the one, at which, the temperature on the opposite side $x = x_e$ of the cluster reaches saturation temperature, T_{sat} at environmental pressure, i.e. the condition for critical time is expressed as-

$$T\,(x_e, t^*) = T_{sat} \tag{2.18}$$

The present simulation method explains that, with the value of the critical time in hand, it is been checked whether the assumed average temperature required to calculate equation (2.8) is equal to the average temperature at the time t^* in the cluster. Such a procedure results in a combination of values of average liquid temperature, T_{lavg}, liquid depth, x_e and critical time, t^* from equations (2.10), (2.8) and (2.18) respectively using iterative procedure.

The average heat flux at critical time is also calculated and is compared with the maximum heat flux, which decides the validity of this analytical investigation, using the new concept of critical time.

PST case. According to the definition of critical time, t^* in equation (2.18), the following expression for PST case is achieved-

$$T_l + (T_i - T_l)\,\mathrm{erfc}\left(\frac{x_e}{\sqrt{4at^*}}\right) = T_{sat}$$

This equation can be rearranged in a more simplified form as-

$$\operatorname{erf}\left(\frac{x_e}{\sqrt{4at^*}}\right) = \frac{T_i - T_{sat}}{T_i - T_l} \tag{2.19}$$

Therefore, the value of t^* for PST case can be calculated using equation (2.19) and iterative procedure.

For detailed calculations, it is recommended to go through Appendix A.5.1.

TST case. From the definition of critical time in equation (2.18), the expression for TST case is achieved as-

$$T_l + 4kt^* i^2 \operatorname{erfc}\left(\frac{x_e}{\sqrt{4at^*}}\right) = T_{sat}$$

Further simplification of the above equation gives the expression of critical time for TST case as-

$$t^* = \frac{\frac{T_{sat} - T_l}{k}}{\left[1 - \operatorname{erf}\left(\frac{x_e}{\sqrt{4at^*}}\right) - \frac{2x_e}{\sqrt{\pi}} \exp\left(\frac{-x_e{}^2}{4at^*}\right) + \frac{2x_e{}^2}{\sqrt{4at^*}} - \frac{2x_e{}^2}{\sqrt{4at^*}} \operatorname{erf}\left(\frac{x_e}{\sqrt{4at^*}}\right)\right]} \tag{2.20}$$

For more details of the calculations, readers can consult Appendix A.5.2.

2.1.4 Average and maximum heat flux

The average heat flux can be derived in this new approach of investigation by integrating the heat flux over a time duration of the critical time, t^* and the expression is found as-

$$q_s = -(T_s - T_l)\frac{\sqrt{(\rho c\lambda)_l}}{1+\sqrt{(\rho c\lambda)_l/(\rho c\lambda)_s}}\frac{1}{\sqrt{t^*}} \tag{2.21}$$

Where, q_s is the average heat flux, T_s is the initial temperature of the heated solid block and T_l is the initial temperature of the impinging liquid jet.

For the expression of the maximum thermodynamic limit of maximum heat flux, $q_{max,max}$, the author has extracted some useful information from the works of Gambill and Lienhard [48] and the theory of molecular dynamics. The final simplified form of expression for $q_{max,max}$ is found as-

$$q_{max,max} = \rho_g h_{fg}\sqrt{\frac{\bar{R}T}{2\pi M}} \tag{2.22}$$

Where, '$\bullet_g$' is the density of saturated vapor, 'h_{fg}' is the latent heat of vaporization, '$\bar{R}$' is the ideal gas constant, 'T' is the temperature and 'M' is the molecular weight.

The detailed derivation is given in Appendix A.6.

2.1.5 Minimum required energy

The minimum amount of energy required to form a vapor bubble, W_{cr} is derived from the kinetic theory of homogeneous bubble nucleation, which is expressed as-

$$W_{cr} = \frac{4}{3}\pi {r_e}^2 \sigma \tag{2.23}$$

Where, r_e is the equilibrium radius of the vapor bubble and $\bullet$ is the liquid surface tension.

For detailed calculations, the author recommends to consult Appendix A.7.

2.1.6 Solution procedure

As mentioned in chapter 1, the present study starts with the development of a theoretical model of heat transfer for the liquid during jet impingement quenching. The simulation is based on a one dimensional semi-infinite solid model, through which, heat from the hot solid is conducted. The analysis is done for two different working fluids and three different solid block materials. After selecting suitable boundary conditions, the mathematical model is solved numerically using MATLAB programming language. For TST boundary condition, the analysis is also accomplished for different boundary heating rates. An iterative procedure is followed in this study, assuming an initial guess value of the liquid depth, x_e under consideration and a set of values are recorded for the average liquid temperature, T_{lavg}, average internal energy in liquid, U_{avg}, liquid depth, x_e, equilibrium radius of vapor bubble, r_e, minimum required energy to form bubbles, W_{cr}, average heat flux, q_s, maximum heat flux, q_{max}, contact time, t, and critical time, t^*. The amount of heat, transferred from the hot solid is quantified and the possibility of homogeneous bubble nucleation is examined from the information of the stored energy in liquid and the minimum required energy for bubble formation.

The following steps are followed to calculate T_{lavg}, U_{avg}, q_s and q_{max}-

i) For any time t, an initial guess is made for x_e

ii) Properties are taken at 100^oC

iii) Value of x_e is stored as x_{eold}

iv) Using Eq. (2.10), T_{lavg} is calculated and properties are again taken at T_{lavg}

v) Using Eq. (2.8), the value of r_e is computed and then x_e is taken to be $2r_e$

vi) The critical time t^* is calculated using Eq. (2.18) and the heat flux q_s at time t^* is calculated from Eq. (2.21)

vii) The maximum heat flux q_{max} and minimum required energy W_{cr} are calculated using Eq. (2.22) and (2.23) respectively

viii) Step (*iii*) is repeated until absolute value of $((x_e-x_{eold})/x_{eold})$ is less than 0.0001

ix) U_{avg} is calculated using Eq. (2.13)

x) The values of t, t^*, r_e, x_e, T_{lavg}, U_{avg} and W_{cr} are recorded

xi) The values of q_s and q_{max} are compared, whether q_s is greater than q_{max}

xii) The value of time is incremented and then steps (ii) to (xi) are repeated

The error function and relevant functions are shown in Appendix B and the flow chart of the algorithm has been given in the Appendix C.

2.2 Solid Analysis

2.2.1 Introduction

Islam et al. [28] has exhibited changes in solid surface temperatures with time at the center and at different depths of a 500°C steel block during quenching by a 20°C and 5 m/s water jet and reported the limiting surface temperature, T_{max}, that allows stable solid-liquid contact during quenching, as 355.5°C for steel. They also reported the time for reaching T_{max} for a sustainable solid-liquid contact (t_{max}) as 800 ms. The same experiment was done by them for a 550°C brass block with a 50°C and 5 m/s water jet and values of T_{max} and t_{max} were found as approximately 343°C and 1.2 s respectively.

Now, the phenomena, that happens at early stages of jet impingement quenching before the solid surface reaches the temperature, T_{max}, was not understood properly from these investigations. Neither video images nor temperature history during jet impingement quenching of a high temperature surface could give useful information about these early phenomena. Therefore, Islam et al. [28] demonstrated a conceptual change in surface temperature within the first few seconds of jet impingement quenching, which is shown as Fig. 2.2. The concept shows that, the surface temperature instantaneously reaches the interface temperature (shown as T^* in the figure), as the liquid comes in contact with it and a solid-liquid contact is maintained for a very short duration of time. Heat transfer occurs from solid to liquid by conduction and the surface temperature at this brief contact is assumed as constant.

The liquid molecules that come in contact with the hot solid surface are momentarily transformed into vapor molecules after the brief contact due to homogeneous nucleation and the solid surface becomes dry as the vapor molecules prevent the jet from making any contact with the solid surface. Therefore, the solid surface temperature increases again because of the heat conduction from the region far from the surface.

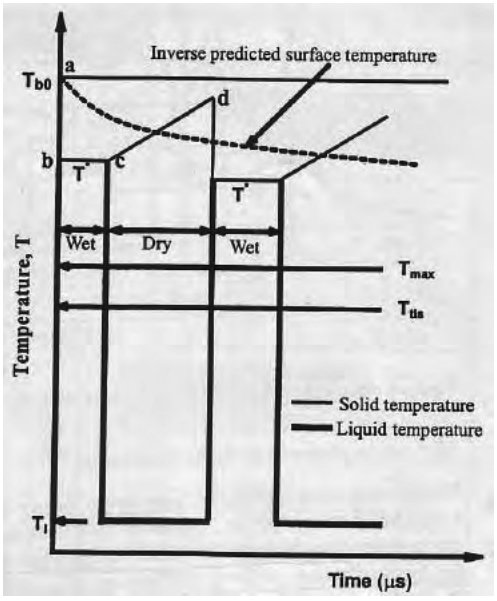

Figure 2.2 Conceptual cooling phenomena at early stages of jet impingement quenching [28]

According to this conceptual solid surface temperature changing phenomenon at the early stages of jet impingement quenching, there will be alternating events of wet and dry phenomena at the surface with an unascertained frequency. In order to have a clear understanding of this unascertained event, the present investigation assumes a model of two dimensional solid heated block on which, liquid impingement occurs.

2.2.2 Mathematical model

Woodfield [49] formulated a one dimensional transition boiling model in Cartesian coordinate, which accounted for the direct coupling between the solid and liquid during contact.

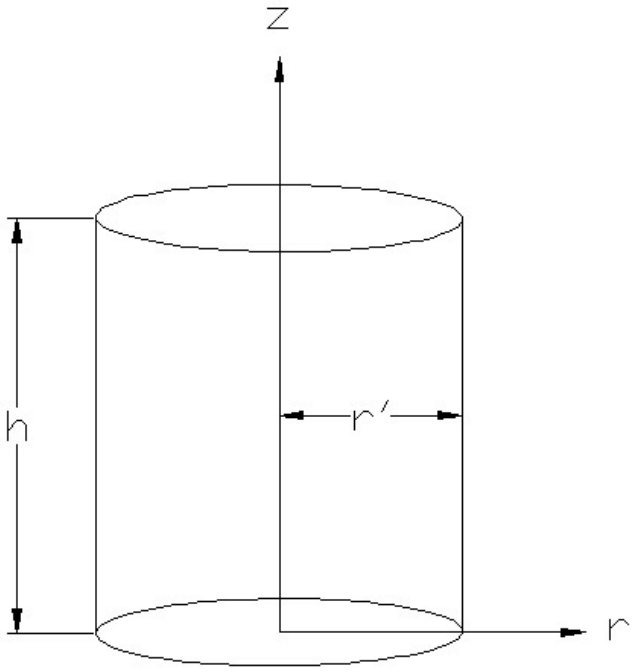

Further development on his investigation is made in the present study by devising a two dimensional cylindrical heat transfer model, shown as Fig. 2.3. The model serves more realistic features like those of the investigations done previously by a number of researchers [26-30], where a cylindrical heated block was quenched by jets of water. The present model is based on transient two-dimensional heat conduction in a cylindrical solid block and hence, the governing equation of the model is given by-

$$\frac{\delta^2 T}{\delta r^2} + \frac{1}{r}\frac{\delta T}{\delta r} + \frac{\delta^2 T}{\delta z^2} = \frac{1}{a_s}\frac{\delta T}{\delta t} \quad ; \qquad 0 < r < r$$

Where, 'a_s' is the thermal diffusivity of the solid material, r' is the radius and 'h' is the height of the solid cylindrical block.

2.2.3 Boundary conditions

The present mathematical model is analyzed for the following boundary conditions-

i) The top surface of the cylindrical block is taken as the block initial temperature, T_{b0}, i.e.,

$$T(r, h, t) = T_{b0}$$

ii) The bottom surface of the block (on which the liquid jet impinges) is taken as the interface temperature, T_i during a short period of contact and as a time-varying temperature, bt (where 'b' is a time-varying constant) during another short period of non-contact of the liquid jet with the surface, i.e.,

$$T(r, 0, t) = \{ T_i , \quad 0 < t \leq \tau_1 \qquad \text{(Wet region)}$$

$$bt , \quad \tau_1 < t \leq \tau_2 \qquad \text{(Dry region)}$$

iii) The cylinder circumference is considered as insulated, i.e.,

$$\frac{\delta T}{\delta r}_{(r}$$

2.2.4 Solution procedure

The two dimensional solid model, formulated in the previous sections is solved and analyzed numerically based on Finite Element Method (FEM), using a dedicated FEM modeling and simulation software, namely COMSOL. The transient conduction heat transfer module is used here for steel and brass materials. Both surface plots as well as a number of cross-section point plots are drawn from the temperature history, taken from the post processing data of the simulated model mentioned above. Such plots serve a clear insight of the wet and dry phenomena at the early stages of jet impingement quenching as well as the transient changes of the solid surface temperature and surface heat flux at different depths of the solid.

3. RESULTS AND DISCUSSIONS

The present study aims at providing a complete and coherent investigation of homogeneous bubble nucleation and the heat transfer analysis during this process. Successful outcomes regarding this homogeneous nucleation research could be useful in elucidating many other poorly understood phenomena, such as, Vapor Explosions, Leidenfrost Effect etc. Therefore, in order to gain a better insight of heat transfer characteristics during this type of nucleation process, a solid heated block is taken into consideration and is quenched by jets of water and ethanol as explained in Chapter 2. In detailed analysis, a number of parameters like liquid temperature, T_{liq}, average liquid temperature, T_{lavg}, equilibrium radius of vapor bubbles, r_e, average internal energy, U_{avg}, minimum energy required to form a bubble, W_{cr}, average heat flux, q, maximum thermodynamic limit of heat flux, q_{max} etc. are changed and the corresponding variations are presented in this chapter. A comparative study is also presented here by changing some parameters like, liquid jet initial temperature, T_l, solid block initial temperature, T_{b0}, block material, contact time, t, working fluids, boundary heating rates, k, etc. and the corresponding effects are evaluated for two boundary conditions: the Prescribed Surface Temperature (PST) case and the Time-dependent Surface Temperature (TST) case.

The present study uses the homogenous nucleation temperature of water as 300°C and of ethanol as 190°C, taken from Blander and Katz [8]. For general study, the boundary heating rate is taken as 37.7×10^6 K/s for water and 10.7×10^6 K/s for ethanol, from Iida et al. [42]. The study also uses a reasonable limit to increase the boundary heating rate for water and ethanol from the analysis of Glod et al. [44] and Okuyama et al. [45].

3.1 Liquid Temperature

The present analysis finds a significant variation of liquid temperature, T_{liq}, with liquid depth, x, for a particular jet initial temperature, block initial temperature, contact time and boundary heating rate. Besides, the analysis also finds a number of parameters like, jet initial temperature, contact time and boundary heating rate, which can influence a great deal on the variation of liquid temperature with liquid depth. All these effects and their corresponding variations are discussed in this section.

3.1.1 Depthwise liquid temperature change

Figure 3.1.1 shows the variation of liquid temperature, T_{liq} with liquid depth, x, for different contact times in TST case, when a 50°C water jet impinges on a 350°C steel block surface. It shows that, at a particular time of contact, water temperature decreases linearly with water depth. For example, water temperature decreases from 313°C to 280°C over the liquid depth shown (0 to 250 nm) for a contact time of 7 μs. The figure also illustrates the effect of contact time on the variation of water temperature with depth of water. It is evident from the figure that, with an increase in contact time, liquid temperature increases for a particular liquid depth due to more time available for energy transfer in case of higher contact times. As for example, water temperature increases from 210°C to 280°C when the contact time reaches from 5 μs to 7 μs at a liquid depth of 250 nm. A similar type of variation is found for water in PST case.

Figure 3.1.2 shows the same variation with ethanol as working fluid for different contact times in TST case, where a 10°C ethanol jet impinges on a 220°C steel block surface. Here also the temperature of ethanol decrease linearly with its depth for any contact time, e.g., the ethanol temperature decreases from 202°C to 176°C over the liquid depth shown (0 to 250 nm) for a contact time of 18 μs. The figure also shows the effect of contact time on the variation of ethanol temperature with its depth. It is evident from the figure that, liquid temperature increases significantly for higher contact times for a particular liquid depth due

to the same reasons mentioned earlier. For example, the temperature of ethanol increases from 38°C to 176°C when the time of contact increases from 4 μs to 18 μs at a liquid depth of 250 nm. A similar kind of variation is achieved for ethanol in PST case.

3.1.2 Effect of jet initial temperature

The initial temperature of the liquid jet before the impingement is one of the major variables that have significant effects on the liquid temperature, average liquid temperature, equilibrium radius of vapor bubble, etc. for both PST and TST cases.

Figure 3.1.3 shows the effect of jet initial temperature on the variation of liquid temperature with liquid depth for TST case at 16 μs of contact, when ethanol jet of different initial temperatures impinges on steel block of temperature 220°C. Liquid temperature decreases linearly with liquid depth just like the earlier variations, e.g., the liquid temperature decreases from 208°C to 202°C over the depth of ethanol shown for a 40°C jet initial temperature. Again, for a particular liquid depth, ethanol temperature increases with jet initial temperature. For example, at a liquid depth of 100 nm, ethanol temperature increases from 172°C to 202°C when the jet initial temperature increase from 10°C to 40°C. For higher values of jet initial temperature, the stored energy in impinging liquid itself is very high and energy transfer does not occur significantly from the heated solid block to the impinging jet. Therefore, the liquid temperature remains high before impingement. Again, for lower values of jet initial temperatures, though energy transfer occurs significantly from solid block to impinging jet, liquid temperature cannot become higher than that with a higher jet initial temperature. It is also observed from the figure that, ethanol temperature remains well above its homogeneous nucleation temperature of 190°C, when the impinging ethanol jet temperature is initially 30°C or more for a contact time of 16 μs. Thus, it can be seen that, for the initiation of homogeneous bubble nucleation for ethanol with a contact time of 16 μs, the jet initial temperature must exceed at least 30°C. Similar kind of effect is found for water as working fluid.

3.1.3 Effect of boundary heating rate

Hasan et al. [46] has numerically simulated the boiling explosion phenomenon for rapid liquid heating with time-dependent boundary temperature (TST) condition and presented a comparative study of their simulation results with some earlier experimental observations of Glod et al. [44] and Okuyama et al. [45]. They have surprisingly found some very significant effects of the boundary heating rate on the initiation and growth of homogeneous bubbles. With this knowledge, the present study has tried to gain a better insight of the effects of the boundary heating rates on the temperature distributions in TST cases and has reached to a number of important results.

Figure 3.1.4 shows the effect of boundary heating rate, k, on the variation of the liquid temperature with liquid depth when a 50°C water jet impinges on the 350°C steel block at a contact time of 7.0 μs. Though the liquid temperature decreases significantly with liquid depth for any boundary heating rate, the figure is a clear indication of a higher liquid temperature for a higher boundary heating rate at a particular depth of liquid. For example, at 100 nm liquid depth and 7.0 μs of contact, the liquid temperature is approximately 298°C for $k = 37.7\times10^6$ K/s and is 327°C for a higher boundary heating rate of $k = 42\times10^6$ K/s. It happens due to faster rate of heat transfer from the hot solid surface to the impinging liquid for higher boundary heating rates and consequently a faster rise in liquid temperature.

Figure 3.1.5 shows the effect of boundary heating rate on the variation of liquid temperature with liquid depth for ethanol as working fluid. The figure shows a decrease of liquid temperature with liquid depth for any boundary heating rate, but a significant increase in liquid temperature for a higher boundary heating rate due to the reasons mentioned earlier. For example, at 50 nm depth of ethanol and 13 μs of contact, the liquid temperature increases from approximately 140°C to 197°C, when the heating rate increases from 10.7×10^6 K/s to 15.0×10^6 K/s.

3.2 Average Liquid Temperature

It is found from the present investigation that, the average liquid temperature significantly varies with contact time for a particular jet initial temperature, block initial temperature, block material and boundary heating rate. A significant variation of average liquid temperature is also found when a number of parameters, like the jet initial temperature, block initial temperature, block material, working fluid and boundary heating rate are changed. The present section aims at discussing all these effects and their corresponding variations.

3.2.1 Change of average liquid temperature with contact time

Figure 3.2.1 shows the variation of average liquid temperature, T_{lavg}, with contact time for both the boundary conditions, when a 50°C water jet impinges on a 350°C steel block. It shows that, T_{lavg} increases with contact time for both the boundary conditions, though at different rates. The reason behind such a variation is that, for higher contact times, there will be more time available to transfer heat from the solid surface to the impinging liquid and therefore, a higher rate of heat transfer occurs for higher time of contact. The figure also indicates a much higher rate of change of average liquid temperature for TST case than for the PST case. For example, after 7 μs of contact, T_{lavg} is about 317°C for PST case and about 325°C for TST case. This may happen due to a much higher solid surface temperature for a high heating rate in TST case and a consequent high heat transfer rate from solid surface to liquid. But there is just a constant prescribed temperature of the solid surface for PST case and consequently, the heat transfer rate will be lower. Therefore, the rate of increase in T_{lavg} will also be lower in PST case. It is also observed that, T_{lavg} exceeds the homogeneous nucleation temperature of water earlier for PST case than for TST case. Hence, under similar conditions, an earlier attainment of homogeneous nucleation temperature can be achieved for PST than for TST case. For example, contact times of 7 μs in TST case and 0.03 μs in PST case are needed to reach the homogeneous nucleation temperature for water. Fig. 3.2.2 shows the same variations of T_{lavg} for ethanol

as working fluid and an earlier attainment of homogeneous nucleation temperature in PST case than for TST case is also observed.

3.2.2 Effect of jet initial temperature

Figure 3.2.3 shows the effect of jet initial temperature, T_l on the variation of average liquid temperature, T_{lavg} with time for TST case when water jets of different initial temperatures impinge on steel block of temperature 350°C. It shows that, for a particular jet initial temperature, the average liquid temperature increases with contact time, e.g., after 5 μs of contact, T_{lavg} becomes approximately 200°C for a jet initial temperature of 25°C. The figure also demonstrates a significant increase in T_{lavg} with the enhancement of jet initial temperature for a particular contact time. As for example, after 5 μs of contact, T_{lavg} is approximately 200°C for a 25°C temperature water jet, which becomes approximately 282°C for a 95°C water jet. This is because, for higher liquid initial temperature, the stored energy in impinging liquid jet itself is very high and heat transfer does not occur significantly from the heated solid block to the liquid jet. Therefore, the average liquid temperature is high before jet impingement. On the otherhand, for lower values of jet initial temperature, though energy transfer occurs significantly from heated solid block to the impinging liquid jet, T_{lavg} cannot become higher than that, with a higher jet initial temperature. The figure also demonstrates an earlier attainment of homogeneous nucleation temperature (300°C) for higher values of T_l, due to the increase in average liquid temperature with the increase of T_l. For example, it takes about 7.3 μs of contact for a 25°C water jet to reach homogeneous nucleation temperature of 300°C, but only 5.5 μs is needed for a 95°C water jet to reach this temperature limit. Similar kind of variation is found for water in PST case.

Figure 3.2.4 shows the effect of jet initial temperature on the variation of average liquid temperature with time for TST case with a heating rate of 10.7×10^6 K/s, but in this case, an ethanol jet impinges on steel block of temperature 220°C. The same kind of variation like water is found in this case. For example, after 15 μs of contact, T_{lavg} increases from

approximately 158°C to 190°C when the ethanol jet temperature increases from 10°C to 40°C in TST boundary condition. The same phenomenon of an earlier attainment of homogeneous nucleation temperature for ethanol (190°C) is achieved due to the increase of T_{lavg} with jet initial temperature of ethanol. For example, a contact time of 15 μs is required for a 40°C ethanol jet to reach the homogeneous nucleation temperature of ethanol, whereas a contact time of 18 μs is needed when the jet temperature becomes 10°C. Similar kind of variation is found for ethanol in PST boundary condition.

3.2.3 Effect of block initial temperature

The initial temperature of the heated solid block before the impingement of the liquid jet is another important variable, having significant effects on parameters like- average liquid temperature, equilibrium radius of vapor bubble etc for both PST and TST cases.

Figure 3.2.5 shows the effect of the block initial temperature, T_{b0} on the variation of average liquid temperature, T_{lavg} with time, when a 20°C water jet impinges on steel block of two different initial temperatures in PST case. As mentioned earlier, T_{lavg} increases with contact time, but it is also observed that, T_{lavg} increases significantly with the block initial temperature. For example, after 10 μs of contact, T_{lavg} increases from 268°C to 315°C when the block initial temperature increases from 300°C to 350°C. A higher block initial temperature enhances the heat transfer rate from the solid surface to the impinging liquid and therefore, the average liquid temperature also becomes higher for relatively higher block initial temperatures. The illustration also shows that a block initial temperature of 300°C is not enough to reach the homogeneous nucleation temperature of water and for 350°C solid block, it takes approximately 0.028 μs of contact to reach this temperature. Therefore, a block initial temperature of 350°C with a contact time of at least 0.028 μs is required for homogenous bubble nucleation for water in PST case. It should be mentioned here that under similar conditions, Islam et al. [28] has found the time to reach the homogeneous nucleation temperature limit as 0.02 μs which is very close to the present

finding of 0.028 μs. Same type of variation is achieved for water in TST boundary condition.

In figure 3.2.6, the same effect of block initial temperature on the variation of average liquid temperature with time is shown with a 10°C ethanol jet impingement on steel block surface of two different initial temperatures in PST case. Due to the same reason of higher heat transfer rate for higher block initial temperatures, the average liquid temperature of ethanol increases with increasing block initial temperature. For example, at 10 μs of contact, T_{lavg} of ethanol increases from 140°C to 210°C when the block initial temperature increases from 150°C to 220°C. Identical effect is found for ethanol in TST case.

3.2.4 Effect of block material

In order to get a better insight of the heat transfer analysis during jet impingement quenching, the block materials are also changed and the corresponding effects on parameters like average liquid temperature, equilibrium radius of vapor embryo etc. are analyzed thoroughly.

Figure 3.2.7 shows the effect of block material on the variation of average liquid temperature, T_{lavg} with contact time, when a 50°C water jet impinges on 350°C block of different materials in PST case. Though the same increase in T_{lavg} with time is observed for all the materials, the figure shows that, T_{lavg} is the highest for Copper and the lowest for Steel for a particular time of contact. For example, at 10 μs of contact, T_{lavg} becomes 317°C for steel, 331°C for brass and 337°C for copper as block material. The thermal properties like conductivity play important roles in this regard. Due to higher thermal conductivity (366 W/m-°C at 350°C) of copper than steel (43.5 W/m-°C at 350°C), a greater volume of the copper block is cooled by the impinging water jet and therefore, T_{lavg} increases significantly due to higher rate of heat transfer from the copper block to the impinging water jet. On the other hand, the steel block is cooled locally near the surface, i.e., the steel block is only skin-cooled and therefore, a much lower energy transfer occurs

between steel block surface and the impinging water jet and consequently, T_{lavg} becomes much lower for steel than the copper block. The thermal conductivity of Brass (147 W/m-°C at 350°C) lies in between copper and steel, and therefore, the value of T_{lavg} for brass is also in between those for steel and copper. It is also found from the figure that, under such conditions, T_{lavg} exceeds the homogeneous nucleation temperature for water (300°C) after a contact time of 0.026 μs for steel and relatively lower contact times are needed for brass and copper to exceed such temperature limit. Therefore, homogeneous bubble nucleation is possible for steel as block material after 0.026 μs of contact.

In case of ethanol jet impingement, the same phenomenon is observed, which is shown in Fig. 3.2.8, where a 10°C ethanol jet impinges on 220°C block of different materials in PST case. The average liquid temperature is the highest for copper and the lowest for steel. For example, T_{lavg} of ethanol increases upto 210°C for steel, 213°C for brass and 216°C for copper as block material after 10 μs of contact. The higher thermal conductivity (373 W/m-°C at 220°C) of copper than steel (47.4 W/m-°C at 220°C) is responsible for this variation which has already been discussed. The thermal conductivity of brass (144.6 W/m-°C at 220°C) is in between steel and copper and hence, T_{lavg} for brass lies in between those for steel and copper. It is also found that, T_{lavg} exceeds the homogeneous nucleation temperature of ethanol (190°C) after a contact time of 0.2 μs for steel, 0.022 μs for brass and 0.01 μs for copper as block material. Therefore, homogeneous nucleation temperature can be reached earlier for copper than for steel due to higher thermal conductivity of copper. The time to reach this temperature in case of brass lies in between those for steel and copper for the same reasons mentioned above. The same kind of effect is achieved for both water and ethanol in case of TST boundary condition.

3.2.5 Effect of working fluids

The working fluids play an important role on the characteristics of heat transfer between the solid surface and the impinging liquid jet. Therefore, the present study emphasizes on investigating the effects of working fluids on various parameters like average liquid

temperature, equilibrium radius of vapor bubble, average internal energy, maximum thermodynamic limit of maximum heat flux etc.

Figure 3.2.9 depicts such a variation, where average liquid temperature, T_{lavg} is varied with time, when a 40°C jet of water and ethanol impinge on steel block surface in TST case. The average liquid temperature as usually increases with contact time, but for an identical liquid jet temperature of 40°C, T_{lavg} for water is found much higher than ethanol, although their rate of changes are almost similar for both the working fluids. For example, T_{lavg} increases from 210°C to 315°C when the working fluid changes from ethanol to water after 10 μs of contact. The thermal conductivity of water is much higher than that for ethanol and therefore, T_{lavg} of water is also higher than that of ethanol for a particular time of contact. Moreover, for both the cases, T_{lavg} exceeds the corresponding homogeneous nucleation temperature. Similar effects are found in PST case also.

3.2.6 Effect of boundary heating rate

Figure 3.2.10 shows the effect of boundary heating rate, k, on the variation of average liquid temperature, T_{lavg}, with time, when a 50°C water jet impinges on steel block of 350°C. It is observed from the depiction that, the average liquid temperature increases significantly with contact time for any boundary heating rate. Again, a higher boundary heating rate yields an earlier attainment of homogeneous nucleation temperature of water (300°C), e.g. it takes 6.8 μs to reach the homogeneous nucleation temperature limit with a heating rate, $k = 37.7\times10^6$ K/s, but only 5.9 μs is needed for a higher heating rate, $k = 42\times10^6$ K/s. It happens due to faster rate of heat transfer from the hot solid surface to the impinging liquid for higher boundary heating rates and consequently, faster rise in the average liquid temperature.

3.3 Equilibrium Radius of Vapor Bubble

It has been found in the present investigation, that the equilibrium radius of vapor bubbles changes significantly with contact time for a constant block initial temperature, jet initial temperature, boundary heating rate and block material. Besides, a number of parameters like the jet initial temperature, block initial temperature, block material and working fluids are also found, that have a significant influence on the variation of equilibrium vapor radius with time. This section will demonstrate and explain such variations, their cause and effects on the heat transfer characteristics during jet impingement quenching.

3.3.1 Change of equilibrium radius with contact time

Figure 3.3.1 shows the variation of equilibrium radius of vapor bubble, r_e, with contact time for both the boundary conditions, when a 50°C water jet impinges on a 350°C steel block. It is observed that, the values of r_e decreases with time for both the cases. This is because, T_{lavg} increases with contact time and the liquid pressure increases with the increase of T_{lavg}. Consequently, the size of the vapor bubble decreases with an increase in contact time. The figure also shows that, for PST case, a steady and converged solution of r_e is achieved after 0.01 μs of contact and for TST case, values of r_e are found after 2 μs of contact and beyond that, r_e changes significantly.

Figure 3.3.2 shows the same variation with ethanol as working fluid, when a 10°C ethanol jet impinges on a 220°C steel block. Like water, decrease in r_e is observed with contact time and stable solutions of r_e are found after 1.0 μs of contact in PST case. But for TST case, values of r_e are found after approximately 10 μs of contact beyond which, a significant variation of r_e is observed.

3.3.2 Variation of equilibrium radius with average liquid temperature and contact time

Figure 3.3.3 shows the variation of equilibrium radius of vapor bubble, r_e, in combination with the average liquid temperature, T_{lavg} with time, when 50°C water jet impinges on a 350°C steel block surface in TST case with a heating rate of 37.7×10^6 K/s. The values of r_e decreases with contact time and at the same time, the average liquid temperature increases with the period of contact. This is because, the liquid pressure increases with the increase of T_{lavg} and consequently, the size of the vapor bubble decreases. For a contact time beyond approximately 6.5 μs, the average liquid temperature remains well above the homogeneous nucleation temperature of 300°C for water. Such a variation shows us the possibility of homogeneous bubble nucleation for this particular case after 6.5 μs of contact.

Figure 3.3.4 illustrates the variation of r_e, in combination with average liquid temperature with time, when a 10°C ethanol jet impinges on steel block surface of temperature 220°C in TST case with a heating rate of 10.7×10^6 K/s. For ethanol as working fluid, the same decrease of r_e is observed and for the contact time beyond 18 μs, T_{lavg} remains well above the homogeneous nucleation temperature of 190°C for ethanol, which concludes about the possibility of homogeneous bubble nucleation of ethanol after 18 μs of contact for this particular case.

3.3.3 Effect of jet initial temperature

Figure 3.3.5 shows the effect of jet initial temperature on the variation of equilibrium radius of vapor embryo, r_e with time for PST case when water jets of different initial temperatures impinge on steel block of temperature 350°C. It illustrates that, r_e decreases with contact time for any jet initial temperature within the range shown (0.01 to 10 μs) due to the same reason mentioned earlier. For example, r_e decreases from 2.6 nm to 2.25 nm for a jet initial temperature of 25°C. It is also clear from the illustration that, there is a

significant decrease in r_e with the enhancement of jet initial temperature for a particular contact time. For example, after 10 μs of contact, r_e decreases from 2.25 nm to approximately 1.65 nm when the jet initial temperature increases from 25°C to 95°C. It has been discussed earlier that T_{lavg} increases with the increase in jet initial temperature and the equilibrium radius decreases with increase in T_{lavg}. Therefore, r_e decreases significantly with jet initial temperature.

A similar kind of effect is observed from Fig. 3.3.6 with the same surroundings but for a different boundary condition- TST case with a heating rate of 37.7×10^6 K/s. For this particular case, the rate of change of r_e for different jet initial temperatures is higher than that for PST case. Again, a significant decrease in r_e is achieved with an increase in jet initial temperature for a particular time of contact. For example, after 4 μs of contact r_e decreases from 78 nm to 13 nm, when jet initial temperature increases from 25°C to 95°C.

Figure 3.3.7 and 3.3.8 show the effect of jet initial temperature on the variation of r_e with time for PST and TST cases respectively with ethanol as working fluid for a boundary heating rate of 10.7×10^6 K/s and similar type of changes are observed for those cases.

3.3.4 Effect of block initial temperature

Figure 3.3.9 shows the effect of the block initial temperature on the variation of equilibrium radius of vapor embryo, r_e with time, when a 50°C water jet impinges on steel block of different initial temperatures in PST case. The equilibrium vapor radius decreases with contact time for any block initial temperature. As T_{b0} increases, r_e decreases for a particular contact time. This is because of the fact that, the average liquid temperature increases with block initial temperature due to higher rate of heat transfer from the block surface to the impinging liquid, which creates a higher liquid pressure inside and a consequent decrease of r_e. For example, after 10 μs of contact, equilibrium vapor radius, r_e decreases from approximately 7.5 nm to 1.8 nm, when the block initial temperature increases from 300°C to 350°C.

Figure 3.3.10 shows the same effect of T_{b0}, on the variation of r_e with time, when a 10°C ethanol jet impinges on steel block surfaces of two different initial temperatures in PST case. For the same reasons mentioned earlier, r_e decreases also for ethanol with an increase in block initial temperature. For example, r_e decreases from 35 nm to 2 nm after 10 μs of contact, when the initial temperature of the steel block increases from 150°C to 220°C. Similar phenomena are achieved for both water and ethanol in TST cases.

3.3.5 Effect of block material

Figure 3.3.11 shows the effect of block material on the variation of equilibrium radius of vapor bubble, r_e with time, when a 50°C water jet impinges on 350°C blocks of different materials. Though a usual decrease of r_e is observed with contact time for any kind of block material, it is also found from the figure that, the values of r_e are the highest for steel and the lowest for copper as block material for a particular time of contact. For example, at 10 μs of contact, r_e becomes 2 nm for steel, 1.3 nm for brass and 0.9 nm for copper as block material. This is because of the reason mentioned earlier, that the average liquid temperature, T_{lavg} is the highest for copper for a particular time of contact and consequently, r_e becomes the lowest. Again, r_e achieves higher values for steel due to its lower values of average liquid temperature. For the same reason, the value of r_e for brass lies in between those for steel and copper. Identical effects are found for ethanol and in TST boundary condition.

3.3.6 Effect of working fluids

Figure 3.3.12 shows the effect of working fluids on the variation of equilibrium radius of vapor bubbles, r_e with time when 40°C water and ethanol jets impinge on steel block surface in PST case. The figure is a clear indication of relatively higher values of r_e for ethanol than for water for a particular jet initial temperature and contact time. For example, after 0.1 μs of contact, r_e becomes 2.55 nm for ethanol and 2.25 nm for water. It has

already been discussed that the average liquid temperature of water is much higher than that of ethanol due to higher thermal conductivity of water. Consequently, the equilibrium vapor radius remains lower for water than ethanol at a particular contact time.

Figure 3.3.13 shows the effect of working fluids on the variation of equilibrium radius of vapor bubble with time for TST case with a boundary heating rate of 10.7×10^6 K/s, when 40°C water and ethanol jets impinge on steel surface. The same effect, like the PST case is observed here, with a higher value of r_e for ethanol than for water. The rate of change of r_e is almost the same for both the working fluids.

3.4 Liquid Internal Energy

The average internal energy of liquid, U_{avg}, also varies with contact time for both the boundary conditions and it has been found in the present analysis, that the working fluid has a strong influence on the variation of average internal energy with contact time. The analysis of U_{avg} is also important for the comparison with the minimum amount of energy required for bubble formation, which will demonstrate the possibility of homogeneous bubble nucleation during jet impingement quenching. This section will explain the variation of U_{avg}, the influence of working fluids on this variation, as well as the comparison of U_{avg} and the minimum energy required for bubble formation.

3.4.1 Change of liquid internal energy with contact time

Figure 3.4.1 shows the variation of average internal energy stored in the superheated liquid, U_{avg}, with contact time for both the boundary conditions, when a 50°C water jet impinges on the 350°C steel block. The figure shows that, the average stored energy, though at different rates, decreases with contact time and for both the boundary conditions, U_{avg} exceeds the minimum amount of energy required for bubble formation (W_{cr}). This is

because of the fact that, with an increase in contact time, U_{avg} of liquid tries to reach W_{cr}, which will be discussed later in this chapter.

Figure 3.4.2 depicts the same variation of U_{avg} with time for both the boundary conditions, when a 10°C ethanol jet impinges of a 220°C steel block surface. It shows that, for both the cases, U_{avg} exceeds W_{cr} for ethanol as working fluid under the above mentioned conditions.

3.4.2 Effect of working fluids

Figure 3.4.3 illustrates the effect of working fluids on the variation of average internal energy, U_{avg} with contact time for PST case, when 40°C water and ethanol jets impinge on steel block surface. Though U_{avg} decreases with contact time for any working fluid, it is observed that, the values of U_{avg} are much higher for water for a particular contact time than for ethanol. For higher thermal conductivity of water than ethanol for a particular jet initial temperature, the average liquid temperature of water becomes much higher than that of ethanol and therefore, the stored internal energy also becomes much higher for water. For example, after 0.1 μs of contact, U_{avg} of water becomes 80×10^{-18} J, which is higher than that of ethanol (44×10^{-18} J).

Figure 3.4.4 shows the similar effect with the 40°C jets, but for a different boundary condition- TST case with a heating rate of 10.7×10^{6} K/s. Similar kind of effect is found here like the PST case, with a higher average internal energy for water than for ethanol for identical jet initial temperature and contact time.

3.4.3 Comparison with minimum required energy

A comparative study of the average amount of energy stored in the superheated liquid, U_{avg}, and the minimum amount of energy required to form a vapor bubble, W_{cr}, would be an indication of the possibility of the occurrence of homogeneous bubble nucleation.

Figure 3.4.5 depicts such a comparison where the variation of U_{avg}, W_{cr}, as well as the average liquid temperature, T_{lavg} with contact time is shown, when a water jet of initial temperature 50°C impinges on 350°C steel block surface in TST case with a heating rate of 37.7×10^6 K/s. It is clear from the figure that, U_{avg} is much higher than W_{cr} for a particular time of contact and the average liquid temperature reaches the homogeneous nucleation temperature for water (300°C) within approximately 5.8 μs. So, it can be concluded from the figure, that there is a strong possibility of homogeneous bubble nucleation for water after 5.8 μs of contact in this particular boundary condition.

Figure 3.4.6 shows the same variation for water in PST case and it is observed that U_{avg} is much higher than W_{cr} for any time of contact and the average liquid temperature exceeds the homogeneous nucleation temperature for water after approximately 0.025 μs of contact. Consequently, there is a high probability of homogeneous bubble nucleation for water after 0.025 μs in PST case.

Figure 3.4.7 shows the variation of U_{avg}, W_{cr} and T_{lavg} with time when a 10°C ethanol jet impinges on 220°C steel block surface in TST case with a heating rate of 10.7×10^6 K/s. The figure shows that, for ethanol as working fluid, U_{avg} is much higher than W_{cr} for a particular contact time and the average liquid temperature, T_{lavg} reaches the homogeneous nucleation temperature of ethanol (190°C) within 18 μs. So, it can be concluded that, there is a strong possibility of homogeneous bubble nucleation of ethanol for TST case after 18 μs of contact.

Figure 3.4.8 shows a similar variation for ethanol in PST case and shows that, it takes approximately 0.2 μs of contact for ethanol jet with the steel block surface, for the initiation of homogeneous bubble nucleation in PST boundary condition.

For a particular jet initial temperature, thermal properties like conductivity (•), specific heat (c) and density (•) of water are much higher than those of ethanol and therefore, it takes more time in case of ethanol to take heat from the hot solid surface than water.

3.5 Heat Flux

A validation of the present analytical investigation is achieved by comparing the average heat flux, q attained in the study with the maximum heat flux, q_{max}.

Figure 3.5.1 shows the variation of average and maximum heat flux with time for water in TST case, when a 50°C water jet impinges on steel block of temperature 350°C. It is depicted that, q never exceeds q_{max} throughout the investigation; rather q_{max} is well above q for any contact time. For example, after 8 μs, q_{max} becomes 1.7×10^5 MW/m^2, which is approximately 169.6×10^3 MW/m^2 higher than q at that contact time. Since average heat flux never exceeds the maximum heat flux for any period of contact, therefore, it can be decided that the present analytical method of investigation, used here by the new concept of critical time, t^* is correct and valid for water in TST case. Though q_{max} attains a very large value and seems practically unreachable, it only shows the maximum thermodynamically attainable heat flux which cannot be exceeded in practical analysis.

Figure 3.5.2 illustrates similar variation with a different boundary condition- PST case for water. The average heat flux never exceeds the maximum heat flux in this condition also; rather, q_{max} reaches 1.22×10^5 MW/m^2 after 10 μs of contact, which is approximately 59×10^3 MW/m^2 higher than q at that contact time. So, it is evident that, the new approach of investigation is also valid for water in PST case as q never exceeds q_{max} in this particular case also.

Figure 3.5.3 shows the variation of q and q_{max} with time in PST case, when a 10°C ethanol jet impinges on steel block surface of temperature 220°C. Like the variation for water mentioned above, it is also observed for ethanol that q never exceeds q_{max} in any contact time and after 10 μs of contact, q_{max} becomes 1.65×10^4 MW/m^2, which is approximately

8.5×10^3 MW/m^2 higher than q. Fig. 3.5.4 illustrates the same variation for ethanol in TST case and again finds that, q_{max} is higher than q for any contact time. So, it is also evident that, the present analytical method of investigation is valid for ethanol both in PST and in TST boundary conditions.

3.5.1 Effect of working fluids

Figure 3.5.5 depicts the theoretically attainable maximum heat fluxes, $q_{max,max,}$ for the two working fluids, used in this investigation. It is found from the depiction that, a maximum heat flux of 4.8×10^6 MW/m^2 can be reached theoretically for water and 1.7×10^5 MW/m^2 for ethanol. It has already been mentioned in Fig. 3.5.1, 3.5.3 and 3.5.4 respectively that, the present investigation finds a maximum heat flux of 1.8×10^5 MW/m^2 for water in TST case and 1.6×10^4 MW/m^2 for ethanol in both PST and TST cases. Therefore, it is observed that it might not be possible to reach the maximum thermodynamically attainable heat flux, $q_{max,max,}$ due to some practical facts. One notable fact is that, it is impossible to collect every vapor molecule, leaving a liquid-vapor interface without permitting any vapor molecule to return to the liquid, which is assumed in the derivation for the expression of $q_{max,max.}$ Many vapor molecules will inevitably be returned to the interface by molecular collisions.

As mentioned earlier, these heat fluxes for both the working fluids are very large and indicate only maximum thermodynamic limiting values of heat fluxes.

3.6 Variation of Solid Surface Temperature at Initial Stages

In the solid analysis part of the present investigation, a significant variation of the solid surface temperature with contact time is found for a particular jet initial temperature, block initial temperature and block material and such variation matches with the earlier results, found by a number of researchers like Islam et al. [28].

Figure 3.6.1 shows such a variation of solid surface temperature with time for steel at the early stages of jet impingement quenching in a radial position of 18.8 mm, when a 20°C water jet impinges on a 500°C steel surface. The upper horizontal solid line in the figure indicates the block initial temperature, T_{b0}, for steel, which is taken as 500°C in this investigation. The lower dash double-dotted horizontal line shows the limiting surface temperature of steel, which allows a sustainable solid-liquid contact during quenching. The interface temperature is indicated as T_i in the figure.

The figure illustrates a clear alternating wet and dry event occurring at the solid block surface. Whenever the liquid comes in contact with the solid surface, the surface temperature instantaneously assumes the interface temperature, T_i. Such solid-liquid contact is very much unstable and heat is transferred to the liquid by conduction during this short period of contact. As this wet solid-liquid contact of the surface exists for a very short period of time, there would not be enough time to conduct heat towards the solid surface from the region far from it. Therefore, heat conduction does not occur within the solid in this short-existing and unstable wet state and solid surface temperature remains fixed at the interface temperature.

After this brief contact, the figure shows an increase in surface temperature. This is because, the liquid molecules, in contact with the hot surface, store the heat conducted to them during the brief contact and this heat excites enough liquid molecules to form vapor molecules instantaneously. Now, such vapor molecules prevent the liquid jet to come in direct contact with the solid surface, making the surface dry again. At this dry state, there would be enough time to conduct heat towards the solid surface from the region far from it and therefore, heat conduction occurs within the solid towards the solid impinging surface. Thus, the surface temperature increases again. Such a dry and wet event completes one cycle and the surface is now prepared for the next cycle of dry and wet event.

At the beginning of the next cycle, the surface temperature instantaneously reaches the next interface temperature, which is lower than that of the previous cycle. The wet event persists for a relatively longer time than the wet event of the previous cycle and thus, the cycle, in

this case, takes a little longer time to complete than the previous one. After the wet condition of the surface, formation of vapor occurs that prevent any direct contact of the liquid jet with the solid surface. But the maximum temperature of each dry state cannot cross that of the previous cycle.

In a similar way, it takes more and more time of contact to complete each cycle of wet and dry event and each cycle temperature becomes lower than the previous one. Eventually, after a particular time of contact, the surface temperature lowers down to the limiting temperature, T_{max}, of 355.5°C for steel [28], where a stable solid-liquid contact is achieved, diminishing the alternating wet and dry events during first few seconds of jet impingement quenching. Such a wet and dry cycle achieves a frequency of 16.4 cycles/s. The dashed line in the figure illustrates the average surface temperature during the alternating wet and dry event.

Now, Islam et al. [28] in their investigation found the time to reach the limiting temperature, T_{max} as 0.8 s. The present investigation finds the time to reach the sustainable solid-liquid contact, t_{max}, as 0.55 s, which is close to the findings of Islam et al.

Below this limiting temperature of 355.5°C and after a time t_{max} = 0.55 s of solid-liquid contact, the surface is cooled below T_{max} and a stable solid-liquid contact is maintained during the quench.

Figure 3.6.2 depicts the same variation of solid surface temperature with time in a radial position of 18.8 mm at early stages of jet impingement quenching, but in this case, a 50°C water jet impinges on a brass block of initial temperature 550°C. The lower dash double-dotted horizontal line shows the limiting surface temperature of brass for a sustainable solid-liquid contact during quenching, which is found as 343°C by Islam et al. [26] and the dashed line indicates the average solid surface temperature during the wet and dry cycle.

The same alternating wet and dry phenomenon is achieved for brass, but the time required for a stable solid-liquid contact for brass in this case is found as 1.1 s, which is close to the

findings by Islam et al. [26], who have achieved a sustainable solid-liquid contact of water jet with brass surface after 1.2 s.

3.7 Transient Variation of Surface Heat Flux

Figure 3.7.1 shows the variation of surface heat flux distribution with time for a particular radial position of 18.8 mm, when a 50°C water jet impinges on a 350°C steel block. The surface heat flux distribution in the figure shows that, after the jet first strikes the hot surface, the heat flux increases drastically and reaches its maximum value within a very short period of time. For example, within approximately 0.2 s, the heat flux reaches its maximum value upto 4.75×10^6 W/m^2. At this early stage, phase change heat transfer occurs during a very short period of contact and homogeneous bubble nucleation also occurs within this short contact period.

Beyond the peak heat flux, single phase convection heat transfer takes place resulting in a decrease of heat flux until the surface is fully cooled down. Such a surface heat flux variation pattern completely agrees with the surface heat flux distribution with time, obtained from inverse solutions by Monde [50].

4. CONCLUSIONS AND RECOMMENDATIONS

4.1 Conclusions

Jet impingement quenching is a direct liquid cooling technology with all the promise to be the future solution of efficient and faster heat removal. The present study has analytically investigated the effect of various parameters on the heat transfer performance of this process. The study has assumed the hot solid as a one-dimensional semi-infinite solid and hence, a simple conduction analysis is enough to find the temperature distribution within the liquid as well as the effect of various parameters on it. Two different working fluids, namely, water and ethanol as well as two different boundary conditions have been considered during the liquid analysis which gives some information on the possibility of homogeneous bubble nucleation during such quenching processes. The solid analysis is done by devising a two-dimensional cylindrical heat transfer model that serves a realistic feature like some previous investigations. Following conclusions can be drawn from the data presented and the subsequent analysis-

1. The heat transfer performance of the jet impingement quenching process is significantly influenced by a number of parameters like, the time of contact between the hot solid surface and the impinging liquid jet, the initial temperature of the liquid jet, the initial temperature of the solid block, the type of block material, the type of working fluids and the boundary heating rate.

2. For both the boundary conditions considered in the present analysis, there is a possibility of homogeneous bubble nucleation during the jet impingement quenching process, depending upon the time of contact.

3. A contact time of 0.02-0.03 μs (for water) and 0.2-0.25 μs (for ethanol) is needed to trigger homogeneous bubble nucleation for the conditions, where impinging surface has a fixed temperature throughout the cooling process.

4. A contact time of 6.0-7.0 μs (for water) and 15-18 μs (for ethanol) is required to initiate homogeneous bubble nucleation for the conditions, where the impinging surface temperature drops at a rate depending on time.

5. For both the boundary conditions, the average internal energy of the liquid exceeds the minimum amount of energy required for bubble formation. Therefore, when water or ethanol is heated above their respective thermodynamic limit of superheat, there is always a chance of homogeneous bubble nucleation during jet impingement quenching process.

6. Throughout the investigation, the average heat flux never exceeds the thermodynamic limit of maximum heat flux, which concludes that, the present new method of investigation, using the concept of critical time, is valid. Therefore, there is indeed a possibility of homogeneous bubble nucleation during jet impingement quenching process.

7. At the early stages of jet impingement quenching process, an alternating wet and dry event is observed during the cooling process of the solid block surface and a stable solid-liquid contact is achieved after a fixed time of contact, beyond which, such alternating wet and dry phenomenon diminishes. The present analysis finds the time to reach a sustainable solid-liquid contact as 0.55 s for steel and 1.1 s for brass as block material. These values closely match with the findings of some previous researchers [26].

8. The surface heat flux variation of the solid block, obtained in the present investigation, completely agrees with the surface heat flux distribution, obtained from inverse solutions of Monde [50]. Therefore, such a variation well-explains the heat transfer characteristics of the hot solid surface.

4.2 Recommendations

The present investigation is conducted for a set of parameters that influence the heat transfer characteristics of homogeneous bubble nucleation. However, in order to supplement the present analytical results as well as for further enhancement of understanding the effects of various parameters both for solid and for liquid analysis, a little more advanced studies are needed. The recommendations for future work are listed below-

a. A comprehensive heat transfer analysis with different working fluids, other than water and ethanol is required for the determination of the most suitable working fluid for the most effective heat removal process.

b. A conjugate heat transfer analysis, incorporating convection mode of heat transfer with the conduction analysis can provide some useful information about the heat transfer characteristics during homogeneous bubble nucleation.

c. The effect of the velocity of the impinging liquid jet can be incorporated in the liquid analysis, resulting in a more pragmatic investigation.

d. The effect of stagnation pressure at the point of impingement on the solid surface can be taken into consideration.

e. Further investigation is required for an exact knowledge of the size of the vapor bubbles, number of molecules in a vapor bubble and nucleation rate etc. for a better understanding of the physics involved in homogeneous bubble nucleation.

f. A numerical solution approach from direct mathematical model of heat transfer for the solid block can be more effective in understanding the heat transfer performance of the solid block surface.

g. A quantum mechanical model of the energy stored in the liquid can provide a more accurate stored energy scenario inside liquid, during jet impingement quenching.

APPENDICES

Appendix A Detailed Derivations

A.1 Equilibrium radius of vapor embryo, r_e

Let us consider a bubble with inside pressure as the saturated vapor pressure, P_v and of radius, r, inside a liquid with temperature, T_L and liquid pressure, P_l.

Now, at equilibrium, the temperature of the vapor and the liquid must be the same and the chemical potential in the two phases must be equal.

So,

$$°_l = °_{ve} \tag{A.1}$$

Where, μ_l is the chemical potential of the liquid and μ_{ve} is that of vapor in equilibrium.

Now, from Young-Laplace equation,

$$P_{ve} = P_l + \frac{2\sigma}{r_e} \tag{A.2}$$

Where, σ is the surface tension of the liquid and r_e is the equilibrium radius of the vapor bubble.

Again, from Gibbs-Duhem equation,

$$d\mu = -sdT + vdP \tag{A.3}$$

Where, ‘s’ is the entropy and ‘v’ is the specific volume.

Integrating the above equation at constant temperature from saturation pressure $P = P_{sat}$ to an arbitrary pressure, P, we obtain,

$$\mu - \mu_{sat} = \int_{P_{sat}}^{P} v dP \tag{A.4}$$

From the ideal gas law for the vapor phase, we know,

$$v = \frac{RT_l}{P} \tag{A.5}$$

Where, R is the ideal gas constant.

Using this value in equation (A.4),

$$\mu - \mu_{sat} = \int_{P_{sat}}^{P} \frac{RT_l}{P} dP$$

$$= RT_l \int_{P_{sat}}^{P} \frac{dP}{P}$$

$$\gg \mu - \mu_{sat} = RT_l \ln\left[\frac{P}{P_{sat}}\right]$$

For the chemical potential of the vapor and its equilibrium, this equation becomes,

$$\mu_{ve} = \mu_{sat,v} + RT_l \ln\left[\frac{P_{ve}}{P_{sat}}\right] \tag{A.6}$$

Again, for liquid phase, due to the incompressibility of liquid, v has a constant value for the saturated liquid at T_l , i.e. $v = v_l$. So from equation (A.4), we have,

$$\mu_l - \mu_{sat,l} = v_l \int_{P_{sat}}^{P} dP$$

$$= v_l [P_l - P_{sat}(T_l)]$$

$$\gg \mu_l = \mu_{sat,l} + v_l\,[P_l - P_{sat}(T_l)] \tag{A.7}$$

Now, substituting equation (A.6) and (A.7) into the equilibrium condition (A.1), we get,

$$\mu_{sat,l} + v_l\,[P_l - P_{sat}(T_l)] = \mu_{sat,v} + RT_l \ln\left[\frac{P_{ve}}{P_{sat}}\right]$$

$$\gg RT_l \ln\left[\frac{P_{ve}}{P_{sat}}\right] = v_l\,[P_l - P_{sat}(T_l)]$$

$$\gg P_{ve} = P_{sat}(T_l)\exp\left[\frac{v_l\{P_l - P_{sat}(T_l)\}}{RT_l}\right]$$

Putting this value in equation (A.2),

$$P_{sat}(T_l)\exp\left[\frac{v_l\{P_l - P_{sat}(T_l)\}}{RT_l}\right] = P_l + \frac{2\sigma}{r_e}$$

$$\gg r_e = \frac{2\sigma}{P_{sat}(T_l)\exp\left[\frac{v_l\{P_l - P_{sat}(T_l)\}}{RT_l}\right] - P_l}$$

Therefore, the expression for the equilibrium radius of vapor embryo is-

$$r_e = \frac{2\sigma}{P_{sat}(T_l)\exp\left[\frac{v_l\{P_l - P_{sat}(T_l)\}}{RT_l}\right] - P_l}$$

A.2 Interface temperature, T_i

For the semi-infinite solid model assumed in the investigation, the region $x > 0$ is of one substance with thermodynamic properties- K_l, $\bullet_l$, c_l, a_l and $x < 0$ of another with properties K_s, $\bullet_s$, c_s and a_s, where, 'K', '•', 'c' and 'a' are, respectively, the thermal conductivity, the density, specific heat and thermal diffusivity and the subscripts 'l' and's' stand for liquid and solid respectively.

Now, the flux is continuous over the surface of separation. So,

$$K_l \frac{\delta T_1}{\delta x} = K_s \frac{\delta T_2}{\delta x} \tag{A.8}$$

Where, T_1 and T_2 denote the temperatures in the regions $x > 0$ and $x < 0$ respectively.

Again, it can be assumed that, at the surface of separation, the temperatures in the two media are the same, so

$$T_1 = T_2 = T_i = \text{Interface temperature} \tag{A.9}$$

At $x > 0$, the initial temperature (at, $t = 0$) is T_l

At $x < 0$, the initial temperature (at, $t = 0$) is T_s

Now, we seek solutions of type,

$$T_1 = A_1 + B_1 \text{erf}\left(\frac{x}{\sqrt{4ta_l}}\right) \tag{A.10}$$

$$T_2 = A_2 + B_2 \text{erf}\left(\frac{x}{\sqrt{4ta_s}}\right) \tag{A.11}$$

Applying initial conditions in (A.10) and (A.11),

$$T_l = A_1 + B_1 \tag{A.12}$$

$$T_s = A_2 + B_2 \tag{A.13}$$

Applying condition (A.9) in (A.10) and (A.11),

$$A_1 = A_2 \tag{A.14}$$

Applying condition (A.8) in (A.10) and (A.11),

$$B_1 K_l \frac{1}{\sqrt{a_l}} = -B_2 K_s \frac{1}{\sqrt{a_s}}$$

$$\gg B_1 \sqrt{(\rho_l c_l K_l)} = -B_2 \sqrt{(\rho_s c_s K_s)}$$

$$\gg B_2 = -B_1 \frac{\sqrt{(\rho_l c_l K_l)}}{\sqrt{(\rho_s c_s K_s)}} \tag{A.15}$$

Subtracting (A.13) from (A.12),

$$B_1 - B_2 = T_l - T_s$$

$$\gg B_1 + B_1 \frac{\sqrt{(\rho_l c_l K_l)}}{\sqrt{(\rho_s c_s K_s)}} = T_l - T_s$$

$$\gg B_1 \left[1 + \frac{\sqrt{(\rho_l c_l K_l)}}{\sqrt{(\rho_s c_s K_s)}}\right] T_l - T_s$$

$$\gg B_1 = \frac{T_l - T_s}{\frac{\sqrt{(\rho_l c_l K_l)} + \sqrt{(\rho_s c_s K_s)}}{\sqrt{(\rho_s c_s K_s)}}}$$

$$= \frac{(T_l - T_s)\sqrt{(\rho_s\, c_s\, K_s)}}{\sqrt{(\rho_s\, c_s\, K_s)} + \sqrt{(\rho_l\, c_l\, K_l)}} \qquad (A.16)$$

Substituting this value in (A.15),

$$B_2 = \frac{(T_s - T_l)\sqrt{(\rho_l\, c_l\, K_l)}}{\sqrt{(\rho_s\, c_s\, K_s)} + \sqrt{(\rho_l\, c_l\, K_l)}} \qquad (A.17)$$

So, from (A.12),

$$A_1 = T_l - \frac{(T_l - T_s)\sqrt{(\rho_s\, c_s\, K_s)}}{\sqrt{(\rho_s\, c_s\, K_s)} + \sqrt{(\rho_l\, c_l\, K_l)}}$$

$$= \frac{T_l\sqrt{(\rho_s\, c_s\, K_s)} + T_l\sqrt{(\rho_s\, c_s\, K_s)} - T_l\sqrt{(\rho_s\, c_s\, K_s)} + T_s\sqrt{(\rho_s\, c_s\, K_s)}}{\sqrt{(\rho_s\, c_s\, K_s)} + \sqrt{(\rho_l\, c_l\, K_l)}}$$

$$= \frac{T_l\sqrt{(\rho_l\, c_l\, K_l)} + T_s\sqrt{(\rho_s\, c_s\, K_s)}}{\sqrt{(\rho_s\, c_s\, K_s)} + \sqrt{(\rho_l\, c_l\, K_l)}}$$

Now, from (A.10), at the interface, $x = 0$ and $T_l = T_i$. Therefore,

$$T_i = A_1 + 0$$

$$\gg T_i = A_1 = \frac{T_l\sqrt{(\rho_l\, c_l\, K_l)} + T_s\sqrt{(\rho_s\, c_s\, K_s)}}{\sqrt{(\rho_s\, c_s\, K_s)} + \sqrt{(\rho_l\, c_l\, K_l)}}$$

This is the expression for the interface temperature.

A.3 Derivations for PST case

A.3.1 Temperature distribution within the liquid

We have, temperature distribution within the liquid,

$$T\ (x,t) = A_1 + B_1\ \mathrm{erf}(\frac{x}{\sqrt{4at}})$$

Substituting the values of A_1 and B_1 from Appendix A.2,

$$T\ (x,t)\ = \frac{T_l \sqrt{(\rho_l\, c_l\, K_l)}\ +\ T_s \sqrt{(\rho_s\, c_s\, K_s)}}{\sqrt{(\rho_s\ c_s\ K_s)} + \sqrt{(\rho_l\ c_l\ K_l)}} + \frac{(T_l\ -\ T_s\ )\sqrt{(\rho_s\ c_s\ K_s)}}{\sqrt{(\rho_s\ c_s\ K_s)} + \sqrt{(\rho_l\ c_l\ K_l)}}\,\mathrm{erf}\,(\frac{x}{\sqrt{4at}})$$

$$=\ T_i\ +\ \mathrm{erf}\,(\frac{x}{\sqrt{4at}})\ \left[\frac{T_l\ \sqrt{(\rho_l\, c_l\, K_l)} + T_l \sqrt{(\rho_s\ c_s\ K_s)} -\ T_l \sqrt{(\rho_l\ c_l\ K_l)} -\ T_s \sqrt{(\rho_s\, c_s\, K_s)}}{\sqrt{(\rho_s\ c_s\ K_s)} + \sqrt{(\rho_l\ c_l\ K_l)}}\right]$$

$$=\ T_i\ +\ \mathrm{erf}\,(\frac{x}{\sqrt{4at}})\ \left[T_l\ -\ \ ^{T_l}\sqrt{(}\right.$$

$$= T_i \operatorname{erfc}\left(\frac{x}{\sqrt{4at}}\right) + T_l - T_l \operatorname{erfc}\left(\frac{x}{\sqrt{4at}}\right)$$

$$= T_l + (T_i - T_l) \operatorname{erfc}\left(\frac{x}{\sqrt{4at}}\right)$$

$$\therefore T(x,t) = T_l + (T_i - T_l) \operatorname{erfc}\left(\frac{x}{\sqrt{4at}}\right)$$

This is the expression for the temperature distribution within the liquid for PST case.

A.3.2 Average liquid temperature, T_{lavg}

We have the temperature distribution within the liquid for PST case,

$$T(x,t) = T_l + (T_i - T_l) \operatorname{erfc}\left(\frac{x}{\sqrt{4at}}\right)$$

Now, the average liquid temperature,

$$T_{lavg}(x_e,t) = \frac{1}{x_e}\int_0^{x_e} T(x,t)\,dx$$

$$= \frac{1}{x_e}\int_0^{x_e}\left[T_l + (T_i - T_l) \operatorname{erfc}\left(\frac{x}{\sqrt{4at}}\right)\right]dx$$

$$= \frac{1}{x_e}\left[T_l x_e + (T_i - T_l)\int_0^{x_e} \operatorname{erfc}\left(\frac{x}{\sqrt{4at}}\right)dx\right]$$

$$= T_l + \frac{T_i - T_l}{x_e}\int_0^{x_e} \operatorname{erfc}\left(\frac{x}{\sqrt{4at}}\right)dx$$

Let,

$$\frac{x}{\sqrt{4at}} = \eta$$

and thus,

$$dx = \sqrt{4at}\, d\eta$$

For x = 0, • = 0.

For $x = x_e$,

$$\eta = \frac{x_e}{\sqrt{4at}} = \eta_e$$

Therefore,

$$T_{lavg}(x_e, t) = T_l + \frac{T_i - T_l}{\sqrt{4at}\,\eta_e}\int_0^{\eta_e} \text{erfc}(\eta)\sqrt{4at}\; d\eta$$

$$= T_l + \frac{T_i - T_l}{\eta_e}\int_0^{\eta_e} \text{erfc}(\eta)\; d\eta$$

$$= T_l + \frac{T_i - T_l}{\eta_e} I$$

Where the integral,

$$I = \int_0^{\eta_e} \text{erfc}(\eta)\; d\eta$$

But,

$$\int_x^{\infty} i^{n-1}\text{erfc}(\xi)\; d\xi = i^n\, \text{erfc}(x)$$

Therefore,

$$I = \int_0^{\infty} \text{erfc}\,(\eta)\ d\eta - \int_{\eta_e}^{\infty} \text{erfc}\,(\eta)\ d\eta$$

$$= I_1 - \text{ierfc}\,(\eta_e)$$

Where,

$$I_1 = \int_0^{\infty} \text{erfc}\,(\eta)\ d\eta$$

$$= \int_0^{\infty} [1 - \text{erf}\,(\eta)]\ d\eta$$

$$= -\int_0^{\infty} \left\{\frac{d}{d\eta}[1 - \text{erf}\,(\eta)]\eta\right\} d\eta$$

But,

$$\frac{d}{dx}[\text{erf}\,(x)] = \frac{2}{\sqrt{\pi}}\, e^{-x^2}$$

$$\therefore I_1 = \int_0^{\infty} -\left[-\frac{2}{\sqrt{\pi}}\, e^{-\eta^2}\right] \eta\, d\eta$$

$$= \frac{2}{\sqrt{\pi}} \int_0^{\infty} \eta\, e^{-\eta^2}\ d\eta$$

Let, $\eta^2 = z$ and thus, $2\bullet\, d\bullet = dz$

For, $\bullet = 0$, $z = 0$

For, $\bullet = \bullet$, $z = \bullet$

Therefore,

$$I_1 = \frac{1}{\sqrt{\pi}} \int_0^{\infty} e^{-z}\, dz$$

$$= \frac{1}{\sqrt{\pi}}$$

Therefore, the integral,

$$I = \frac{1}{\sqrt{\pi}} - \text{ierfc}\,(\eta_e)$$

Thus, average liquid temperature,

$$T_{lavg}\,(x_e, t) = T_l + \frac{T_i - T_l}{\eta_e} \left[\frac{1}{\sqrt{\pi}} - \text{ierfc}\,(\eta_e)\right]$$

A.3.3 Average internal energy, U_{avg}

The amount of energy stored in the liquid,

$$u(x,t) = c(T(x,t) - T_0)$$

$$= c\left(T_l + \frac{T_i - T_l}{\eta_e}\left[\frac{1}{\sqrt{\pi}} - \text{ierfc}(\eta_e)\right] - T_0\right)$$

Where, c is the specific heat of the liquid and T_0 is the saturation temperature taken as the reference temperature.

Now, the average of the stored energy over the depth of the liquid is-

$$u_{avg}(x_e,t) = \frac{1}{x_e}\int_0^{x_e} u(x,t)dx$$

$$= \frac{c}{x_e}\int_0^{x_e}\left(T_l + \frac{T_i - T_l}{\eta_e}\left[\frac{1}{\sqrt{\pi}} - \text{ierfc}(\eta_e)\right] - T_0\right)dx$$

$$= c\left(T_l + \frac{T_i - T_l}{\eta_e}\left[\frac{1}{\sqrt{\pi}} - \text{ierfc}(\eta_e)\right] - T_0\right)$$

Thus, the total average internal energy over the volume, x_e^3 of the liquid is,

$$U_{avg}(x_e,t) = \rho_l x_e^3 u_{avg}(x_e,t)$$

• $_l$ is the liquid density

Therefore,

$$U_{avg}(x_e,t) = \rho_l x_e^3 c\left(T_l + \frac{T_i - T_l}{\eta_e}\left[\frac{1}{\sqrt{\pi}} - \text{ierfc}(\eta_e)\right] - T_0\right)$$

A.4 Derivations for TST case

A.4.1 Temperature distribution within the liquid

If time-dependent surface temperature,

$$\Phi\,(t) = V_0 t^{n/2}$$

Where 'n' is any positive integer, then

$$\overline{\Phi}\,(S) = \frac{\Gamma(1 + n/2}{P^{1+n/2}} \qquad [47]$$

If • (t) = k't, where k' is a constant, representing the rate of change in surface temperature, then,

$$\overline{\Phi}\,(S) = \frac{k'\Gamma(1+1}{P^{1+1}} = \frac{2k'}{P^2} = \frac{k}{P^2}$$

Where, 'k' is the rate of boundary temperature rise (K/s).

So from Laplace transform,

$$\bar{v} = \frac{k}{P^2}\, e^{-qx}$$

Therefore, from the table of Laplace transform,

$$v = k\left[\left(t + \frac{x^2}{2a}\right)\,\mathrm{erfc}\,\left(\frac{x}{\sqrt{4at}}\right) - x\left(\frac{t}{\pi a}\right)^{1/2} e^{-\frac{x^2}{4at}}\right]$$

$$= kt\left[\left(1 + \frac{x^2}{2at}\right)\,\mathrm{erfc}\,\left(\frac{x}{\sqrt{4at}}\right) - \frac{x}{\sqrt{\pi at}}\, e^{-\frac{x^2}{4at}}\right]$$

$$= kt\left[\mathrm{erfc}\,\left(\frac{x}{\sqrt{4at}}\right) + \frac{x^2}{2at}\,\mathrm{erfc}\,\left(\frac{x}{\sqrt{4at}}\right) - \frac{x}{\sqrt{\pi at}}\, e^{-\frac{x^2}{4at}}\right]$$

$$= 4kt\left[\frac{1}{4}\text{erfc}\left(\frac{x}{\sqrt{4at}}\right)+\frac{1}{4}\frac{x^2}{2at}\text{ erfc}\left(\frac{x}{\sqrt{4at}}\right)-\frac{1}{2\sqrt{\pi}}\frac{x}{\sqrt{4at}}e^{-\frac{x^2}{4at}}\right]$$

$$= 4kt\left[\frac{1}{4}\text{erfc}\left(\frac{x}{\sqrt{4at}}\right)-\frac{1}{2}\frac{x}{\sqrt{4at}}\left\{\frac{1}{\sqrt{\pi}}\,e^{-\frac{x^2}{4at}}-\frac{x}{\sqrt{4at}}\text{ erfc}\left(\frac{x}{\sqrt{4at}}\right)\right\}\right]$$

$$= 4kt\left[\frac{1}{4}\text{erfc}\left(\frac{x}{\sqrt{4at}}\right)-\frac{1}{2}\frac{x}{\sqrt{4at}}\text{ ierfc}\left(\frac{x}{\sqrt{4at}}\right)\right]$$

$$= 4kti^2\text{ erfc}\left(\frac{x}{\sqrt{4at}}\right)$$

So, the temperature distribution for zero initial temperature is

$$T = 4kti^2\text{ erfc}\left(\frac{x}{\sqrt{4at}}\right)$$

Now, if the initial temperature is non-zero and $T = T_l$ for $t = 0$ in $0 < x < \bullet$, then,

$$T = T_l + 4kti^2\text{ erfc}\left(\frac{x}{\sqrt{4at}}\right)$$

This is the expression for the temperature distribution within the liquid for TST case.

A.4.2 Average liquid temperature, T_{lavg}

We have the temperature distribution within the liquid for TST case,

$$T(x,t) = T_l + 4kti^2\text{ erfc}\left(\frac{x}{\sqrt{4at}}\right)$$

Now, the average liquid temperature,

$$T_{lavg}\,(x_e, t) \;=\; \frac{1}{x_e}\int_0^{x_e} T\,(x, t)\,dx$$

$$= \frac{1}{x_e}\int_0^{x_e}\left[T_l + 4kti^2\ \text{erfc}\ \left(\frac{x}{\sqrt{4at}}\right)\right]\,dx$$

$$= \frac{1}{x_e}\left[T_l\,x_e + \;4kt\int_0^{x_e} i^2\text{erfc}\ \left(\frac{x}{\sqrt{4at}}\right)\,dx\right]$$

$$= T_l \;+\; \frac{4kt}{x_e}\int_0^{x_e} i^2\text{erfc}\ \left(\frac{x}{\sqrt{4at}}\right)\,dx$$

Let,

$$\frac{x}{\sqrt{4at}} = \;\eta$$

and thus,

$$dx = \;\sqrt{4at}\,d\,\eta$$

For, $x = 0,\ \bullet = 0$

For $x = x_e$,

$$\eta = \;\frac{x_e}{\sqrt{4at}} = \;\eta_e$$

Therefore,

$$T_{lavg}\,(x_e, t) = \;T_l \;+\; \frac{4kt\,\sqrt{4at}}{\sqrt{4at}\,\eta_e}\int_0^{\eta_e} i^2\text{erfc}\,(\eta)\;\;d\eta$$

$$= T_l \;+\; \frac{kt}{\eta_e}\int_0^{\eta_e} 4i^2\text{erfc}\,(\eta)\;\;d\eta$$

$$= T_l + \frac{kt}{\eta_e} I$$

Where the integral,

$$I = \int_0^{\eta_e} 4i^2 erfc\,(\eta)\ d\eta$$

But,

$$i^2 erfc\,(x) = \frac{1}{4}\,[erfc\,(x) - 2x\,ierfc\,(x)]$$

$$\therefore I = 4 \times \frac{1}{4} \int_0^{\eta_e} [erfc\,(\eta) - 2\eta\,ierfc\,(\eta)]\,d\eta$$

Again,

$$ierfc\,(\eta) = \frac{1}{\sqrt{\pi}}\,e^{-\eta^2} - \eta\,erfc\,(\eta)$$

Thus,

$$I = \int_0^{\eta_e} \left[erfc\,(\eta) - \frac{2}{\sqrt{\pi}}\eta\,e^{-\eta^2} + 2\eta^2 erfc\,(\eta)\right] d\eta$$

$$= \int_0^{\eta_e} erfc\,(\eta)\ d\eta - \frac{2}{\sqrt{\pi}} \int_0^{\eta_e} \eta\,e^{-\eta^2}\ d\eta + 2\int_0^{\eta_e} \eta^2 erfc\,(\eta) d\eta$$

$$= I_1 - \frac{2}{\sqrt{\pi}}\,I_2 + 2\,I_3$$

Now,

$$I_1 = \int_0^{\eta_e} erfc\,(\eta)\ d\eta$$

$$= \frac{1}{\sqrt{\pi}} - \ ierfc\,(\eta_e)$$

$$I_2 = \int_0^{\eta_e} \eta\,e^{-\eta^2}\ d\eta$$

Let, $\eta^2 = z$ and thus $2\bullet d\bullet = dz$

$$\therefore I_2 = \frac{1}{2}\int_0^{\eta_e} e^{-z}\, dz$$

$$= -\frac{1}{2}\left[e^{-\eta_e^2} - 1\right]$$

$$= \frac{1}{2}\left[1 - e^{-\eta_e^2}\right]$$

And,

$$I_3 = \int_0^{\eta_e} \eta^2 \text{erfc}\,(\eta) d\eta$$

Now,

$$\int \eta^2 \text{erfc}\,(\eta) d\eta = \text{erfc}\,(\eta) \int \eta^2 d\eta - \int \left[\frac{d}{d\eta}\,\text{erfc}\,(\eta) \int \eta^2 d\eta\right] d\eta$$

$$= \text{erfc}\,(\eta)\,\frac{\eta^3}{3} - \int \left(-\frac{2}{\sqrt{\pi}}\, e^{-\eta^2}\right)\frac{\eta^3}{3}\, d\eta$$

$$= \frac{\eta^3}{3}\,\text{erfc}\,(\eta) + \frac{2}{3\sqrt{\pi}} \int \eta^3\, e^{-\eta^2}\, d\eta$$

$$= \frac{\eta^3}{3}\,\text{erfc}\,(\eta) + \frac{2}{3\sqrt{\pi}}\, I_4$$

Where the integral,

$$I_4 = \int \eta^3\, e^{-\eta^2}\, d\eta$$

$$= \int \eta . \eta^2 \, e^{-\eta^2} \, d\eta$$

Let, $\bullet^2 = u$ and thus, $2\bullet \, d\bullet = du$

So

$$I_4 = \frac{1}{2} \int u \, e^{-u} \, du$$

$$= \frac{1}{2} \left[u \int e^{-u} \, du - \int \left(\frac{d}{du} \, u \int e^{-u} \, du \right) du \right]$$

$$= \frac{1}{2} \left[-ue^{-u} + \int e^{-u} \, du \right]$$

$$= \frac{1}{2} \left[- ue^{-u} - e^{-u} \right]$$

$$= -\frac{1}{2} \, e^{-u} [1 + u]$$

$$= -\frac{1}{2} \, e^{-\eta^2} [1 + \eta^2]$$

Thus,

$$\int \eta^2 \text{erfc}\,(\eta) d\eta = \frac{\eta^3}{3} \, \text{erfc}\,(\eta) - \frac{2}{3\sqrt{\pi}} \, \frac{1}{2} \, [1 + \eta^2] e^{-\eta^2}$$

$$= \frac{\eta^3}{3} \, \text{erfc}\,(\eta) - \frac{1}{3\sqrt{\pi}} e^{-\eta^2} [1 + \eta^2]$$

So,

$$I_3 = \frac{\eta_e^3}{3} \, \text{erfc}\,(\eta_e) - \frac{1}{3\sqrt{\pi}} e^{-\eta_e{}^2} - \frac{1}{3\sqrt{\pi}} \left[e^{-\eta_e{}^2} (1 + \eta_e{}^2) - 1 \right]$$

$$= \frac{\eta_e^3}{3}\ \text{erfc}\ (\eta_e) - \frac{1}{3\sqrt{\pi}} e^{-\eta_e{}^2} - \frac{1}{3\sqrt{\pi}} \eta_e{}^2 e^{-\eta_e{}^2} + \frac{1}{3\sqrt{\pi}}$$

Therefore,

$$I = \frac{1}{\sqrt{\pi}} - \text{ierfc}\ (\eta_e) - \frac{2}{\sqrt{\pi}} \frac{1}{2} \left[1 - e^{-\eta_e^2}\right] + \frac{2}{3} \eta_e^3\ \text{erfc}\ (\eta_e) - \frac{2}{3\sqrt{\pi}}\ e^{-\eta_e{}^2} - \frac{2}{3\sqrt{\pi}}\ \eta_e{}^2 e^{-\eta_e{}^2} + \frac{2}{3\sqrt{\pi}}$$

$$= \frac{1}{\sqrt{\pi}} - \text{ierfc}\ (\eta_e) - \frac{1}{\sqrt{\pi}} + \frac{1}{\sqrt{\pi}}\ e^{-\eta_e^2} + \frac{2}{3}\ \eta_e^3\ \text{erfc}\ (\eta_e) - \frac{2}{3\sqrt{\pi}}\ e^{-\eta_e{}^2} - \frac{2}{3\sqrt{\pi}}\ \eta_e{}^2 e^{-\eta_e{}^2} + \frac{2}{3\sqrt{\pi}}$$

$$= \frac{2}{3}\ \eta_e^3\ \text{erfc}\ (\eta_e) + \frac{1}{3\sqrt{\pi}}\ e^{-\eta_e{}^2} - \text{ierfc}\ (\eta_e) - \frac{2}{3\sqrt{\pi}}\ \eta_e{}^2 e^{-\eta_e{}^2} + \frac{2}{3\sqrt{\pi}}$$

$$= \frac{2\eta_e{}^2}{3} \left[\eta_e\ \text{erfc}\ (\eta_e) - \frac{1}{\sqrt{\pi}}\ e^{-\eta_e^2}\right] - \text{ierfc}\ (\eta_e) + \frac{1}{3\sqrt{\pi}}\ e^{-\eta_e{}^2} + \frac{2}{3\sqrt{\pi}}$$

Now,

$$\text{ierfc}\ (\eta_e) = \frac{1}{\sqrt{\pi}}\ e^{-\eta_e^2} - \eta_e\ \text{erfc}\ (\eta_e)$$

$$\gg \frac{1}{\sqrt{\pi}}\ e^{-\eta_e^2} = \text{ierfc}\ (\eta_e) + \eta_e\ \text{erfc}\ (\eta_e)$$

$$\gg \frac{1}{3\sqrt{\pi}}\ e^{-\eta_e^2} = \frac{1}{3}\ [\text{ierfc}\ (\eta_e) + \eta_e\ \text{erfc}\ (\eta_e)]$$

So,

$$I = \frac{2\eta_e{}^2}{3}\left[-\text{ierfc}\left(\eta_e\right)\right] - \text{ierfc}\left(\eta_e\right) + \frac{1}{3}\left[\text{ierfc}\left(\eta_e\right) + \eta_e\,\text{erfc}\left(\eta_e\right)\right] + \frac{2}{3\sqrt{\pi}}$$

$$= -\frac{2\eta_e{}^2}{3}\,\text{ierfc}\left(\eta_e\right) - \text{ierfc}\left(\eta_e\right) + \frac{1}{3}\text{ierfc}\left(\eta_e\right) + \frac{1}{3}\,\eta_e\,\text{erfc}\left(\eta_e\right) + \frac{2}{3\sqrt{\pi}}$$

$$= \frac{2}{3}\left[\frac{1}{\sqrt{\pi}} - \left\{\text{ierfc}\left(\eta_e\right) - \frac{1}{2}\eta_e\,\text{erfc}\left(\eta_e\right) + \eta_e{}^2\text{ierfc}\left(\eta_e\right)\right\}\right]$$

$$= \frac{2}{3}\left[\frac{1}{\sqrt{\pi}} - 6\text{i}^3\text{erfc}\left(\eta_e\right)\right]$$

Thus, average liquid temperature

$$T_{lavg}\left(x_e, t\right) = T_l + \frac{kt}{\eta_e}\,\frac{2}{3}\left[\frac{1}{\sqrt{\pi}} - 6\text{i}^3\text{erfc}\left(\eta_e\right)\right]$$

A.4.3 Average internal energy, U_{avg}

The amount of energy stored in the liquid,

$$u(x,t) = c(T(x,t) - T_0)$$

$$= c\left(T_l + \frac{kt}{\eta_e}\,\frac{2}{3}\left[\frac{1}{\sqrt{\pi}} - 6\text{i}^3\text{erfc}\left(\eta_e\right)\right] - T_0\right)$$

Where, c is the specific heat of the liquid and T_0 is the saturation temperature taken as the reference temperature.

Now, the average of the stored energy over the depth of the liquid is-

$$u_{avg}(x_e, t) = \frac{1}{x_e} \int_0^{x_e} u(x, t)dx$$

$$= \frac{c}{x_e} \int_0^{x_e} \left(T_l + \frac{kt}{\eta_e} \frac{2}{3} \left[\frac{1}{\sqrt{\pi}} - 6i^3 \text{erfc}\,(\eta_e) \right] - T_0 \right) dx$$

$$= c \left(T_l + \frac{kt}{\eta_e} \frac{2}{3} \left[\frac{1}{\sqrt{\pi}} - 6i^3 \text{erfc}\,(\eta_e) \right] - T_0 \right)$$

Thus, the total average internal energy over the volume x_e^3 of the liquid is,

$$U_{avg}(x_e, t) = \rho_l x_e^3 u_{avg}(x_e, t)$$

• $_l$ is the liquid density.

Therefore,

$$U_{avg}(x_e, t) = \rho_l x_e^3 c \left(T_l + \frac{kt}{\eta_e} \frac{2}{3} \left[\frac{1}{\sqrt{\pi}} - 6i^3 \text{erfc}\,(\eta_e) \right] - T_0 \right)$$

A.5 Critical Time, t^*

A.5.1 PST case

We have, the temperature distribution within the liquid for PST case,

$$T\,(x,t) = T_l + (T_i - T_l)\,\mathrm{erfc}\,(\frac{x}{\sqrt{4at}})$$

Now, by the definition of the critical time,

$$T\,(x_e, t^*) = T_{sat}$$

So, from the temperature distribution,

$$T_l + (T_i - T_l)\,\mathrm{erfc}\left(\frac{x_e}{\sqrt{4at^*}}\right) = T_{sat}$$

$$\gg 1 - \mathrm{erf}\left(\frac{x_e}{\sqrt{4at^*}}\right) = \frac{T_{sat} - T_l}{T_i - T_l}$$

$$\gg \mathrm{erf}\left(\frac{x_e}{\sqrt{4at^*}}\right) = 1 - \frac{T_{sat} - T_l}{T_i - T_l}$$

$$\therefore \mathrm{erf}\left(\frac{x_e}{\sqrt{4at^*}}\right) = \frac{T_i - T_{sat}}{T_i - T_l}$$

The critical time, t^* can be calculated using this relation.

A.5.2 TST case

We have, the temperature distribution within the liquid for TST case,

$$T(x,t) = T_l + 4kti^2\ \mathrm{erfc}\left(\frac{x}{\sqrt{4at}}\right)$$

$$= T_l + 4kt\ \frac{1}{4}\left[\mathrm{erfc}\left(\frac{x}{\sqrt{4at}}\right) - 2x\ \mathrm{ierfc}\left(\frac{x}{\sqrt{4at}}\right)\right]$$

$$= T_l + kt[1 - \mathrm{erf}\left(\frac{x}{\sqrt{4at}}\right) - 2x\left\{\frac{1}{\sqrt{\pi}}\exp\left(\frac{-x^2}{4at}\right) - \frac{x}{\sqrt{4at}}\mathrm{erfc}\left(\frac{x}{\sqrt{4at}}\right)\right\}]$$

$$= T_l + kt[1 - \mathrm{erf}\left(\frac{x}{\sqrt{4at}}\right) - \frac{2x}{\sqrt{\pi}}\exp\left(\frac{-x^2}{4at}\right) + \frac{2x^2}{\sqrt{4at}}\left\{1 - \mathrm{erf}\left(\frac{x}{\sqrt{4at}}\right)\right\}]$$

$$= T_l + kt[1 - \mathrm{erf}\left(\frac{x}{\sqrt{4at}}\right) - \frac{2x}{\sqrt{\pi}}\exp\left(\frac{-x^2}{4at}\right) + \frac{2x^2}{\sqrt{4at}} - \frac{2x^2}{\sqrt{4at}}\mathrm{erf}\left(\frac{x}{\sqrt{4at}}\right)]$$

From the definition of critical time,

$$T\ (x_e, t^*) = T_{sat}$$

Therefore, for TST case,

$$T_l + kt^*\left[1 - \mathrm{erf}\left(\frac{x_e}{\sqrt{4at^*}}\right) - \frac{2x_e}{\sqrt{\pi}}\exp\left(\frac{-{x_e}^2}{4at^*}\right) + \frac{2{x_e}^2}{\sqrt{4at^*}} - \frac{2{x_e}^2}{\sqrt{4at^*}}\mathrm{erf}\left(\frac{x_e}{\sqrt{4at^*}}\right)\right] = T_{sat}$$

$$\gg t^* = \frac{\frac{T_{sat} - T_l}{k}}{\left[1 - \mathrm{erf}\left(\frac{x_e}{\sqrt{4at^*}}\right) - \frac{2x_e}{\sqrt{\pi}}\exp\left(\frac{-{x_e}^2}{4at^*}\right) + \frac{2{x_e}^2}{\sqrt{4at^*}} - \frac{2{x_e}^2}{\sqrt{4at^*}}\mathrm{erf}\left(\frac{x_e}{\sqrt{4at^*}}\right)\right]}$$

This is the expression for critical time in TST case.

A.6 Maximum thermodynamic limit of maximum heat flux, $q_{max,max}$

According to Tien and Lienhard [38-39], if each and every vapor molecules that leave a liquid-vapor interface is collected without permitting any vapor molecules to return to the liquid, then, the maximum thermodynamic limit of maximum heat flux will be-

$$q_{max,max} = (mJ)h_{fg} \quad (W/m^2)$$

Where, m = mass of molecules (Kg)

J = flux of molecules

h_{fg} = latent heat of vaporization (J/Kg)

But from Kinetic theory,

$$J = \frac{n\bar{c}}{4}$$

n = number density of molecules

$\bar{c}$ = mean molecular velocity

So,

$$q_{max,max} = \frac{mn\bar{c}}{4} h_{fg}$$

Again, average speed of Maxwellian gas,

$$\bar{c} = \sqrt{\frac{8RT}{\pi}}$$

'R' is the ideal gas constant on a unit mass basis

$$\therefore \; q_{max,max} = \frac{mn}{4} h_{fg} \sqrt{\frac{8RT}{\pi}}$$

$$= mn\, h_{fg} \sqrt{\frac{8RT}{16\pi}}$$

$$= mn\, h_{fg} \sqrt{\frac{RT}{2\pi}}$$

But, mn = • $_g$ = density of saturated vapor

Therefore,

$$q_{max,max} = \rho_g h_{fg} \sqrt{\frac{RT}{2\pi}}$$

$$= \rho_g h_{fg} \sqrt{\frac{\bar{R}T}{2\pi M}}$$

'$\bar{R}$' is the ideal gas constant and 'M' is the molecular weight.

So, the expression for the maximum thermodynamic limit of maximum heat flux,

$$q_{max,max} = \rho_g h_{fg} \sqrt{\frac{\bar{R}T}{2\pi M}}$$

A.7 Minimum required energy for bubble formation, W_{cr}

We know, for a bubble inside a liquid, the liquid pressure P_l, exterior to a bubble of radius, r, will be related to the interior pressure P_B by Young-Laplace equation-

$$P_B - P_l = \frac{2\sigma}{r}$$

Where, • is the surface tension of the liquid.

If the temperature, T is uniform and the bubble contains only vapor, then the interior pressure P_B will be the saturated vapor pressure P_v (T), and the exterior liquid pressure P_l, which is equal to P_v - 2• /r, will have to be less than P_v in order to produce equilibrium conditions.

So, if the maximum size of vacancy present is r_e, then the tensile strength of the liquid, • P_C, will be-

$$\Delta P_C = \frac{2\sigma}{r_e}$$

Assuming that the critical nucleus is in thermodynamic equilibrium with its surrounding, after its formation, the increment of energy that must be deposited consists of the energy that is to be deposited to account for that stored in the surface of the bubble and the energy to displace the liquid outward in order to create the bubble.

The pressure difference involved in this energy increment is the difference between the pressure inside and outside of the bubble, which, in this investigation, is • P_C. The work done is the volume of the bubble multiplied by this pressure difference, which is equal to 4/3• r_e^3• P_C, and this is the work done by the liquid to achieve the displacement implied by the formation of the bubble.

Thus, the net energy, which must be deposited to form the bubble, is-

$$W_{cr} = 4\pi r_e{}^2\sigma - \frac{4}{3}\pi r_e{}^3\Delta P_C$$

$$= 4\pi r_e{}^2\sigma - \frac{4}{3}\pi r_e{}^3\frac{2\sigma}{r_e}$$

$$= \frac{4}{3}\pi r_e{}^2\sigma$$

$$\therefore\ W_{cr} = \frac{4}{3}\pi r_e{}^2\sigma$$

This is the expression for the net energy required to form a vapor bubble.

Appendix B Error Function and Related Functions

The error function,

$$\mathrm{erf}(x) = \frac{2}{\sqrt{\pi}} \int_0^x e^{-\xi^2}\, d\xi$$

So,

$$\mathrm{erf}(\infty) = 1$$

And,

$$\mathrm{erf}(-x) = -\mathrm{erf}(x)$$

Also we have,

$$\mathrm{erfc}(x) = 1 - \mathrm{erf}(x) = \frac{2}{\sqrt{\pi}} \int_x^\infty e^{-\xi^2}\, d\xi$$

Successive derivatives of the error function,

$$\Phi_n(x) = \frac{d^n}{dx^n} \mathrm{erf}(x)$$

So,

$$\Phi_1(x) = \frac{2}{\sqrt{\pi}} e^{-x^2}$$

And,

$$\Phi_2(x) = -\frac{4}{\sqrt{\pi}} x e^{-x^2}$$

For error functions, we can write,

$$i^n\text{erfc}(x) = \int_x^\infty i^{n-1}\,\text{erfc}(\xi)d\xi$$

for n = 1,2,3……

With,

$$i^0\text{erfc}(x) = \text{erfc}(x)$$

Integrating by parts, we can write,

$$\text{ierfc}(x) = \frac{1}{\sqrt{\pi}}e^{-x^2} - x\text{erfc}(x)$$

And,

$$i^2\text{erfc}(x) = \frac{1}{4}[(1+2x^2)\text{erfc}(x) - \frac{2}{\sqrt{\pi}}xe^{-x^2}]$$

$$= \frac{1}{4}[\text{erfc}(x) - 2x\text{ierfc}(x)]$$

So, the general recurrence formula becomes,

$$2ni^n\text{erfc}(x) = i^{n-2}\text{erfc}(x) - 2xi^{n-1}\text{erfx}(x)$$

In order to verify this formula, let us substitute n = 1, 2 etc. and compare them with the previously achieved ones.

For n = 1,

$$2\text{ierfc}(x) = \text{i}^{-1}\text{erfc}(x) - 2x\text{i}^{0}\text{erfc}(x)$$

$$= \frac{2}{\sqrt{\pi}}e^{-x^2} - 2x\text{ierfc}(x)$$

Therefore,

$$\text{ierfc}(x) = \frac{1}{\sqrt{\pi}}e^{-x^2} - x\text{ierfc}(x)$$

This is the same as previously derived.

For n = 2,

$$4\text{i}^{2}\text{erfc}(x) = \text{i}^{0}\text{erfc}(x) - 2x\text{i}^{1}\text{erfc}(x)$$

Therefore,

$$\text{i}^{2}\text{erfc}(x) = \frac{1}{4}[\text{erfc}(x) - 2x\text{ierfc}(x)]$$

This is again the same as previously derived.

Thus, it can be assumed that the recurrence formula for integration is correct.

Again, substituting, n = 3, into the recurrence formula,

$$6\text{i}^{3}\text{erfc}(x) = \text{i}^{1}\text{erfc}(x) - 2x\text{i}^{2}\text{erfc}(x)$$

$$= \text{ierfc}(x) - 2x\frac{1}{4}[\text{erfc}(x) - 2x\text{ierfc}(x)]$$

$$\gg 6\mathrm{i}^3\mathrm{erfc}(\mathrm{x}) = \mathrm{ierfc}(\mathrm{x}) - \frac{1}{2}\mathrm{xerfc}(\mathrm{x}) + \mathrm{x}^2\mathrm{ierfc}(\mathrm{x})$$

Therefore,

$$\mathrm{i}^3\mathrm{erfc}(\mathrm{x}) = \frac{1}{6}[\mathrm{ierfc}(\mathrm{x}) - \frac{1}{2}\mathrm{xerfc}(\mathrm{x}) + \mathrm{x}^2\mathrm{ierfc}(\mathrm{x})]$$

Appendix C Flow Chart

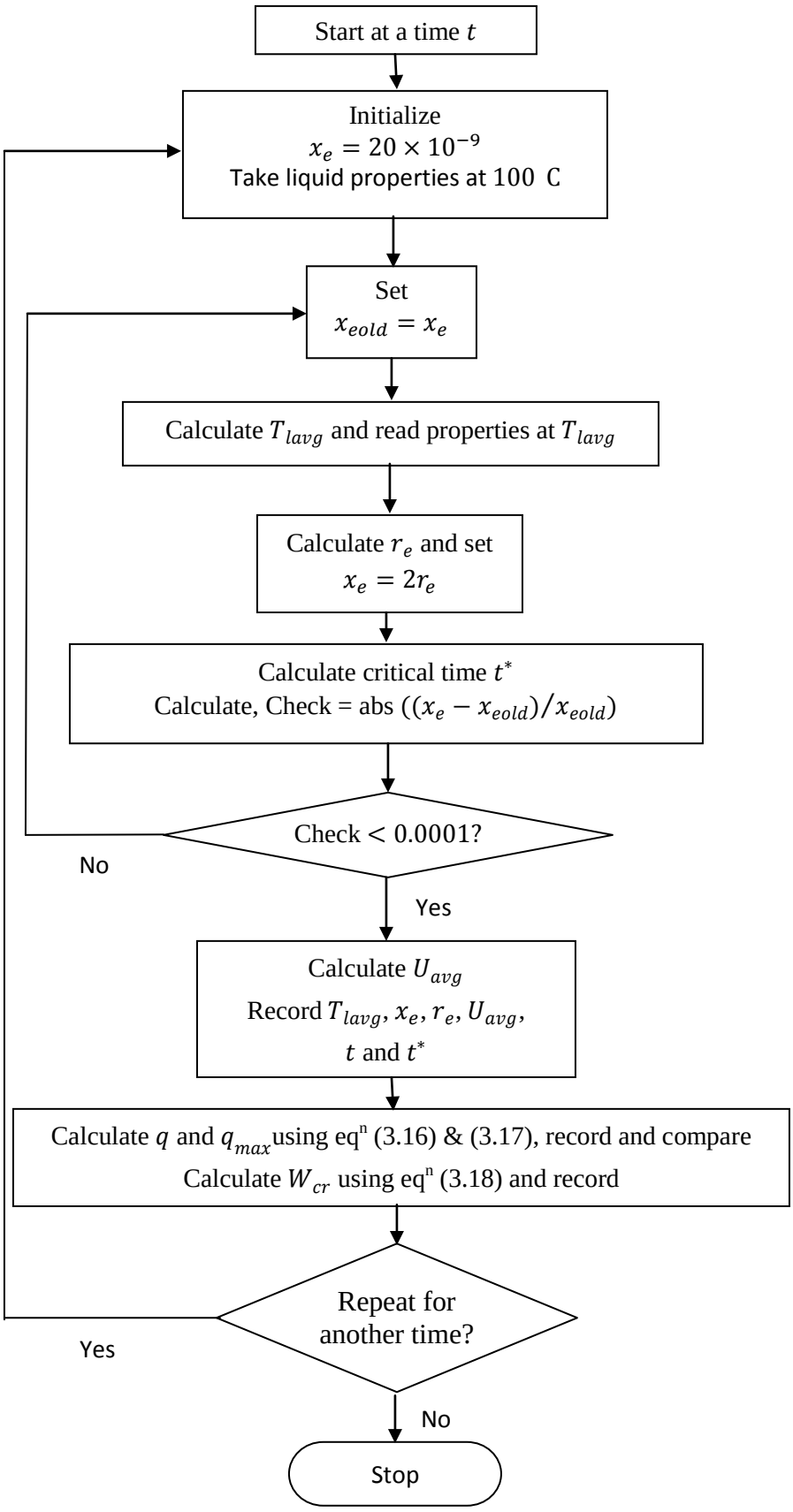

Appendix D Thermodynamic Properties

Table D.1 Thermodynamic Properties of Water

Temp. (°C)	Pressure (MPa)	Liquid Density (kg/m^3)	Vapor Sp. volume (m^3/kg)	Enthalpy kJ/kg		Specific heat kJ/kg-K		Liquid Thermal Conductivity mW/mK	Liquid surface tension (mN/m)
				Liquid	Vapor	Liquid	Vapor		
0	0.61	999.8	205.99	0.00	25.00	4.220	1.884	561.0	75.65
10	1.23	999.7	106.30	42.02	25.19	4.196	1.895	580.0	74.22
20	2.34	998.2	57.757	83.91	25.37	4.184	1.906	598.4	72.74
30	4.25	995.6	32.878	125.7	25.55	4.180	1.918	615.5	71.19
40	7.38	992.2	19.515	167.5	25.73	4.180	1.931	630.6	69.60
50	12.35	988.0	12.027	209.3	25.91	4.182	1.947	643.6	67.94
60	19.95	983.2	7.6672	251.1	26.08	4.185	1.965	654.3	66.24
70	31.20	977.7	5.0395	293.0	26.26	4.190	1.986	663.1	64.48
80	47.41	971.8	3.4052	335.0	26.43	4.197	2.012	670.0	62.67
90	70.18	965.3	2.3591	377.0	26.59	4.205	2.043	675.3	60.82
100	101.42	958.3	1.6718	419.1	26.75	4.216	2.080	679.1	58.91
110	143.38	950.9	1.2093	461.4	26.91	4.228	2.124	681.7	56.96
120	198.67	943.1	0.8912	503.8	27.05	4.244	2.177	683.2	54.97
130	270.28	934.8	0.6680	546.3	27.20	4.261	2.239	683.7	52.93
140	361.54	926.1	0.5084	589.1	27.33	4.283	2.311	683.3	50.86
150	476.16	917.0	0.3924	632.1	27.45	4.307	2.394	682.0	48.74
160	618.23	907.4	0.3067	675.4	27.57	4.335	2.488	680.0	46.59
170	792.19	897.5	0.2425	719.0	27.67	4.368	2.594	677.0	44.41
180	1002.8	887.0	0.1938	763.0	27.77	4.405	2.713	673.3	42.19
190	1255.2	876.1	0.1563	807.4	27.85	4.447	2.844	668.8	39.95
200	1554.9	864.7	0.1272	852.2	27.92	4.469	2.990	663.3	37.67
210	1907.7	852.7	0.1042	897.6	27.97	4.551	3.150	657.0	35.38
220	2319.6	840.2	0.0860	943.5	28.00	4.615	3.329	649.7	33.07
230	2797.1	827.1	0.0715	990.1	28.02	4.688	3.528	641.3	30.74
240	3346.9	813.4	0.0597	1037	28.02	4.772	3.754	631.8	28.39
250	3976.2	798.9	0.0500	1085	28.00	4.870	4.011	621.2	26.04
260	4692.3	783.6	0.0421	1134	27.96	4.986	4.308	609.2	23.69
270	5503.0	767.5	0.0356	1185	27.89	5.123	4.656	595.9	21.34
280	6416.6	750.3	0.0301	1236	27.79	5.289	5.073	581.1	18.99
290	7441.8	731.9	0.0255	1290	27.66	5.493	5.582	565.0	16.66
300	8587.9	712.1	0.0216	1345	27.49	5.750	6.220	547.4	14.36
310	6865.1	690.7	0.0183	1402	27.27	6.085	7.045	528.7	12.09
320	11284.3	667.1	0.0154	1462	27.00	6.537	8.159	509.2	9.86
330	12858.1	640.8	0.0129	1525	26.66	7.186	9.753	489.1	7.70
340	14600.7	610.7	0.0107	1594	26.21	8.210	12.240	468.5	5.63

Table D.2 Thermodynamic Properties of Ethanol

Temperature (K)	Pressure (kPa)	Liquid Density (kg/m^3)	Vapor Density (kg/m^3)	Enthalpy kJ/kg	Specific heat kJ/kg-K		Liquid Thermal Conductivity mW/mK	Liquid surface tension (mN/m)
					Liquid	Vapor		
351.45	101.3	757.0	1.435	963.0	3.00	1.83	153.6	17.7
373	226	733.7	3.175	927.0	3.30	1.92	150.7	15.7
393	429	709.0	5.841	885.5	3.61	2.02	146.5	13.6
413	753	680.3	10.25	834.0	3.96	2.11	141.9	11.5
433	1256	648.5	17.15	772.9	4.65	2.31	137.2	9.3
453	1960	610.5	27.65	698.9	5.51	2.80	134.8	6.9
473	2940	564.0	44.40	598.3	6.16	3.18	129.1	4.5
483	3560	537.6	56.85	536.7	6.61	3.78	125.6	3.3
503	5100	466.2	101.1	387.3	-	6.55	108.0	0.9
513	6020	420.3	160.2	280.5	-	-	79.11	0.34

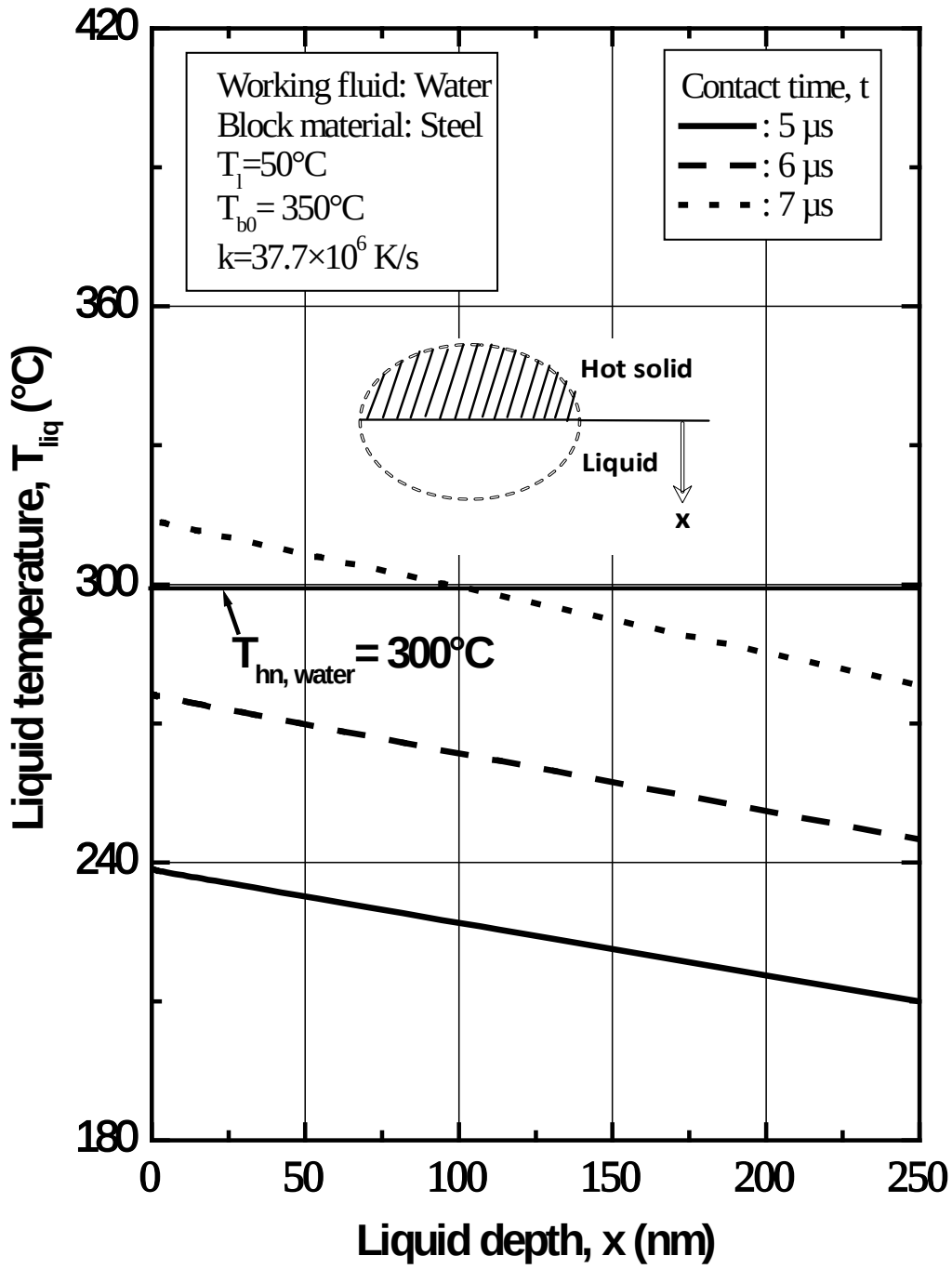

Figure 3.1.1 Variation of liquid temperature with liquid depth for water in TST case

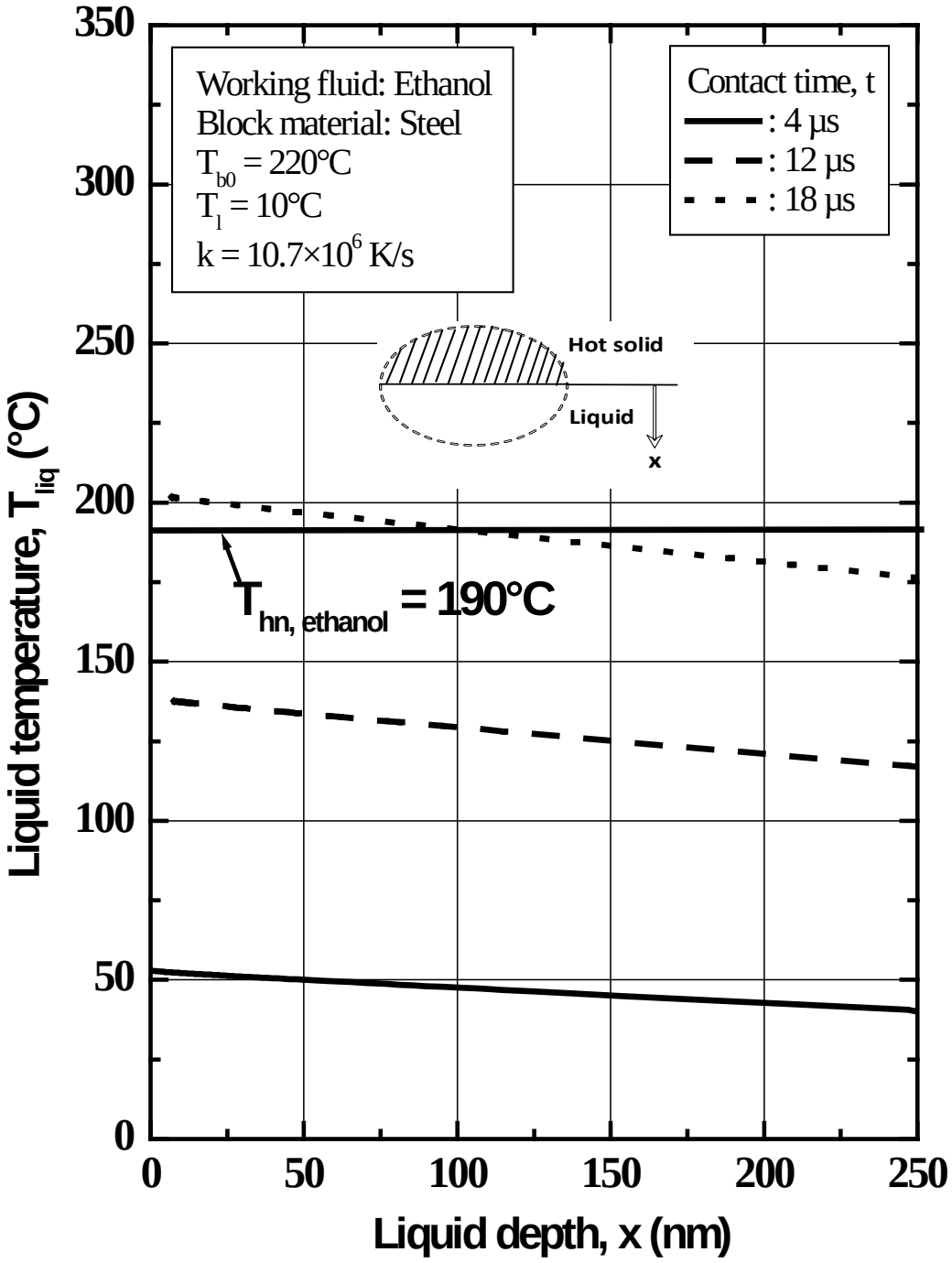

Figure 3.1.2 Variation of liquid temperature with liquid depth for ethanol in TST case

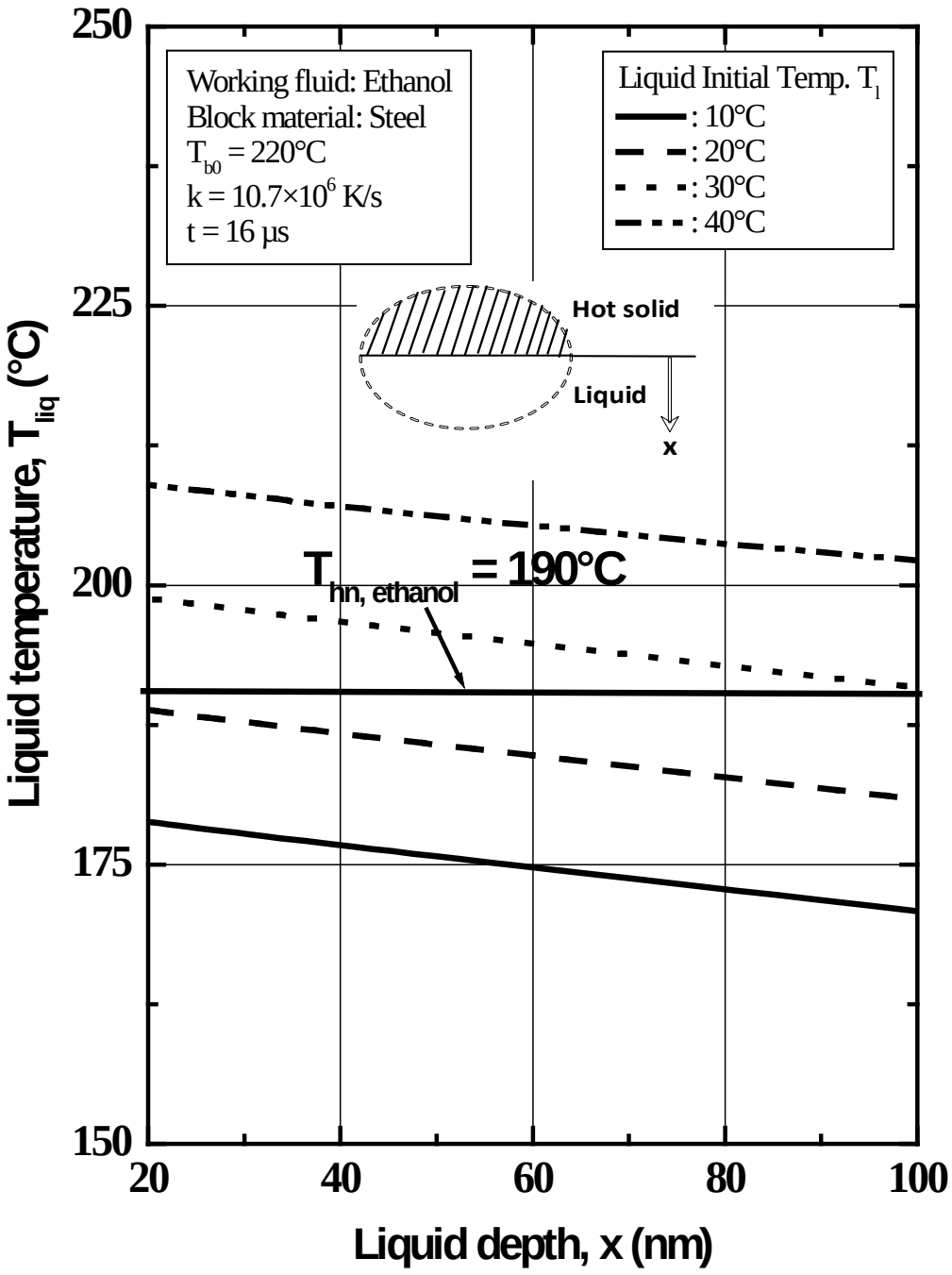

Figure 3.1.3 Effect of jet initial temperature on variation of liquid temperature with liquid depth for ethanol in TST case

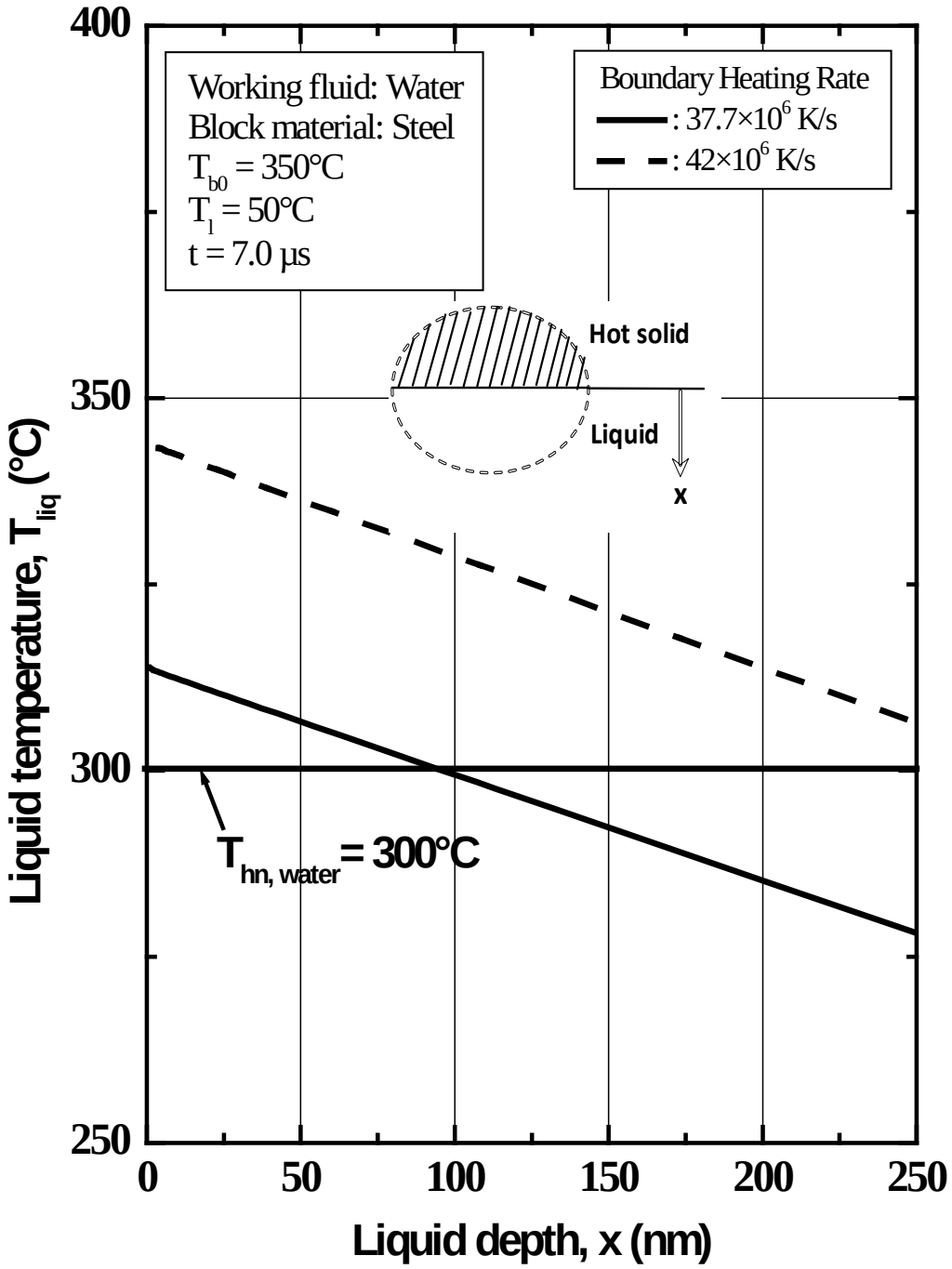

Figure 3.1.4 Effect of boundary heating rate on variation of liquid temperature with liquid depth for water

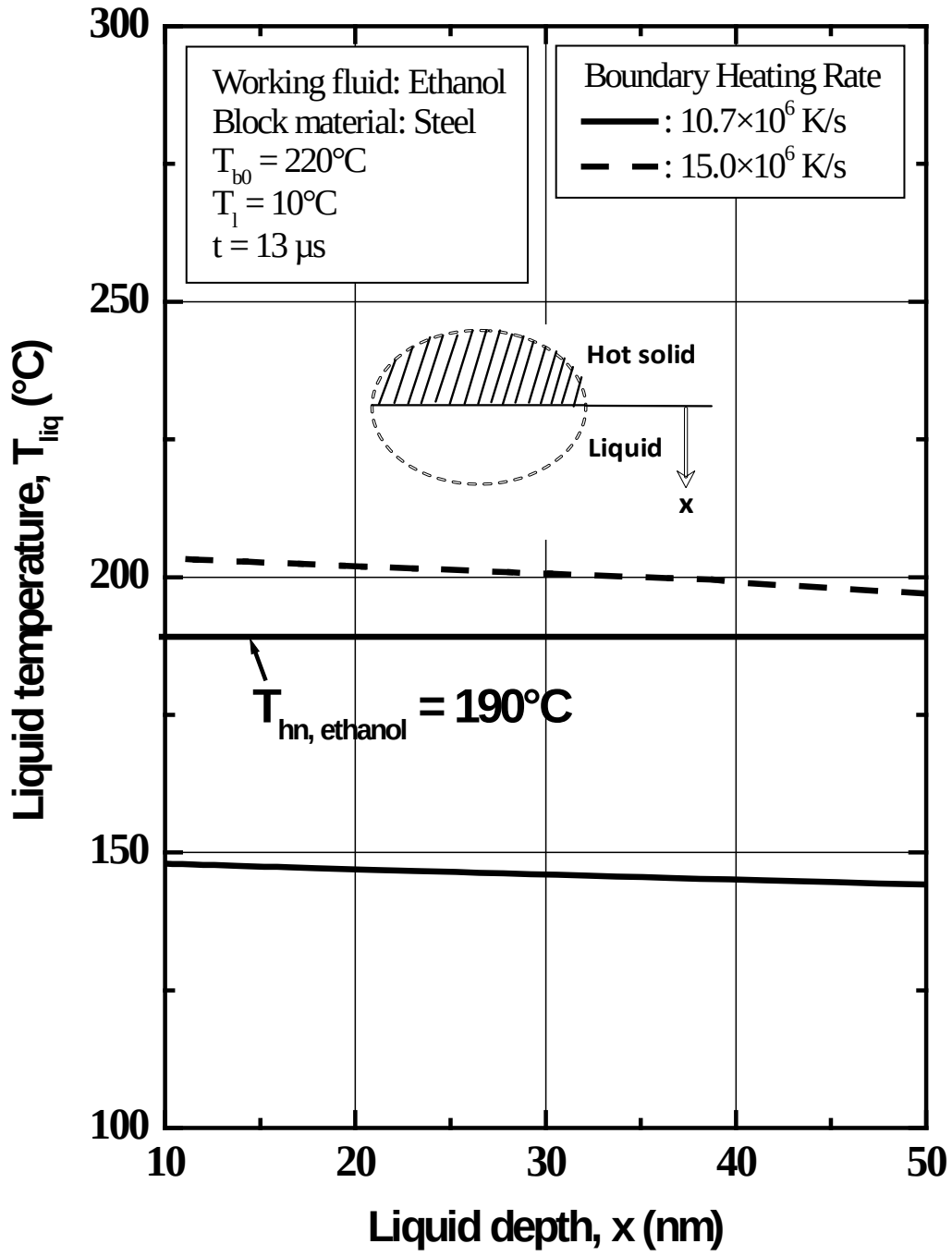

Figure 3.1.5 Effect of boundary heating rate on variation of liquid temperature with liquid depth for ethanol

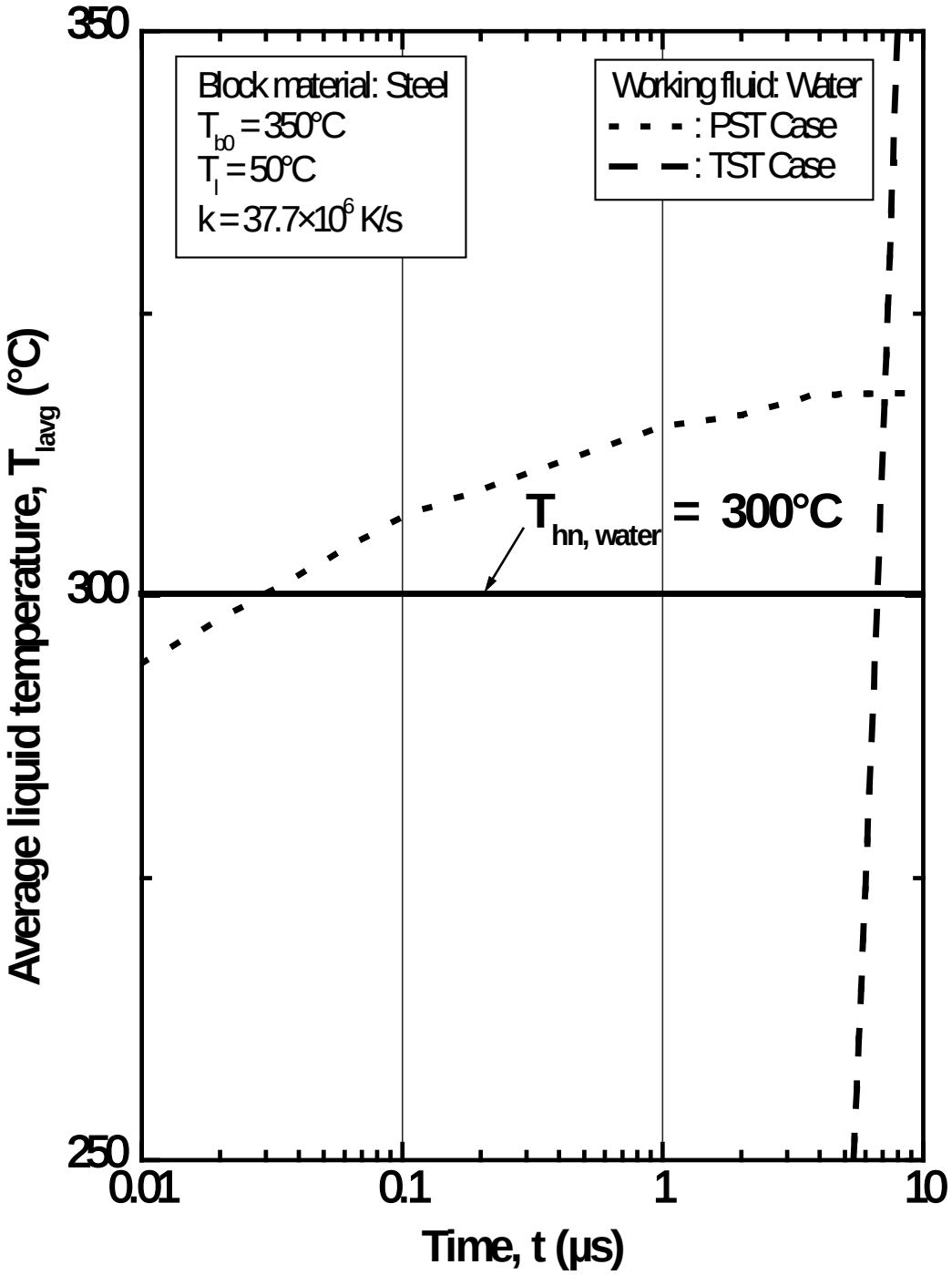

Figure 3.2.1 Variation of average liquid temperature with time for water

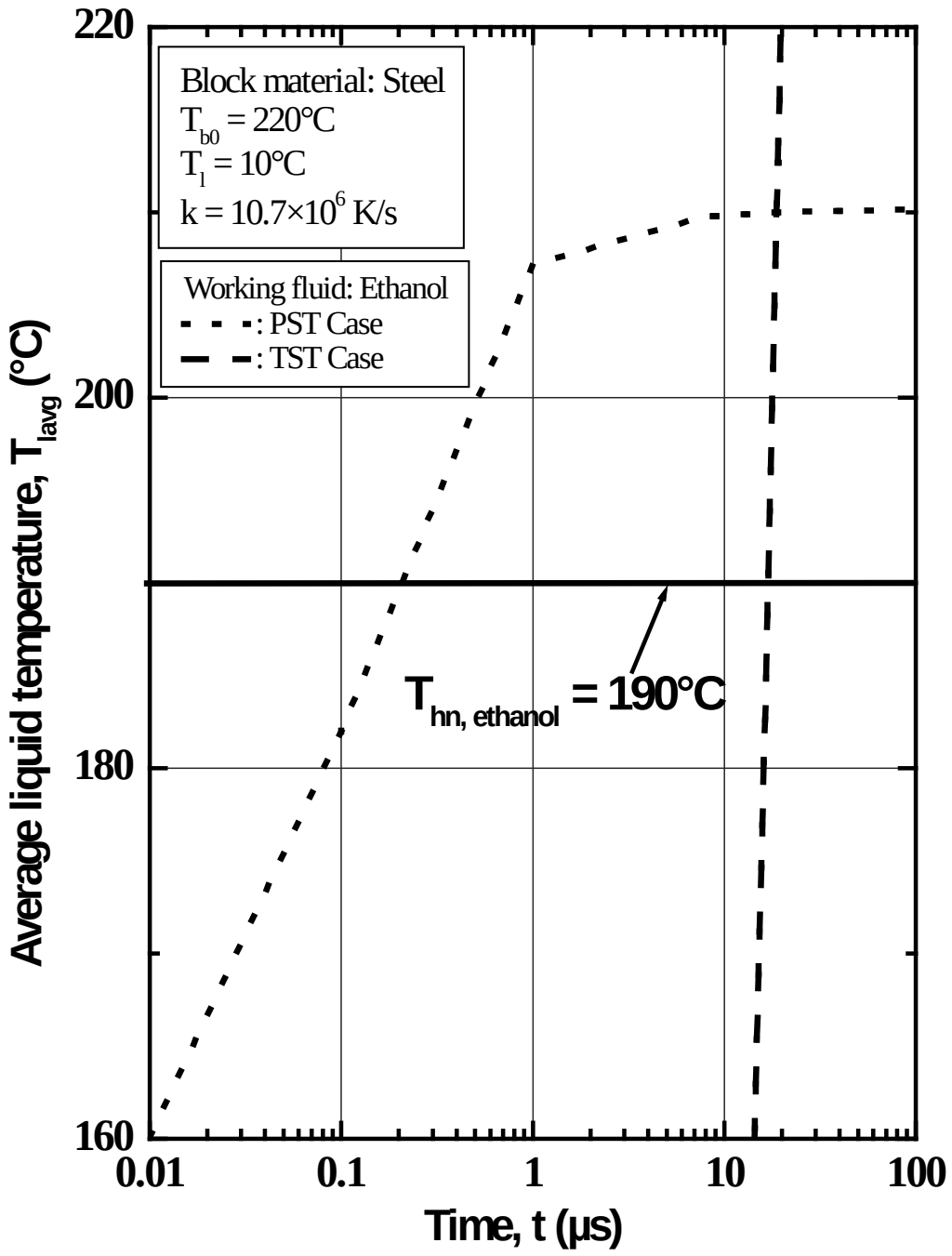

Figure 3.2.2 Variation of average liquid temperature with time for ethanol

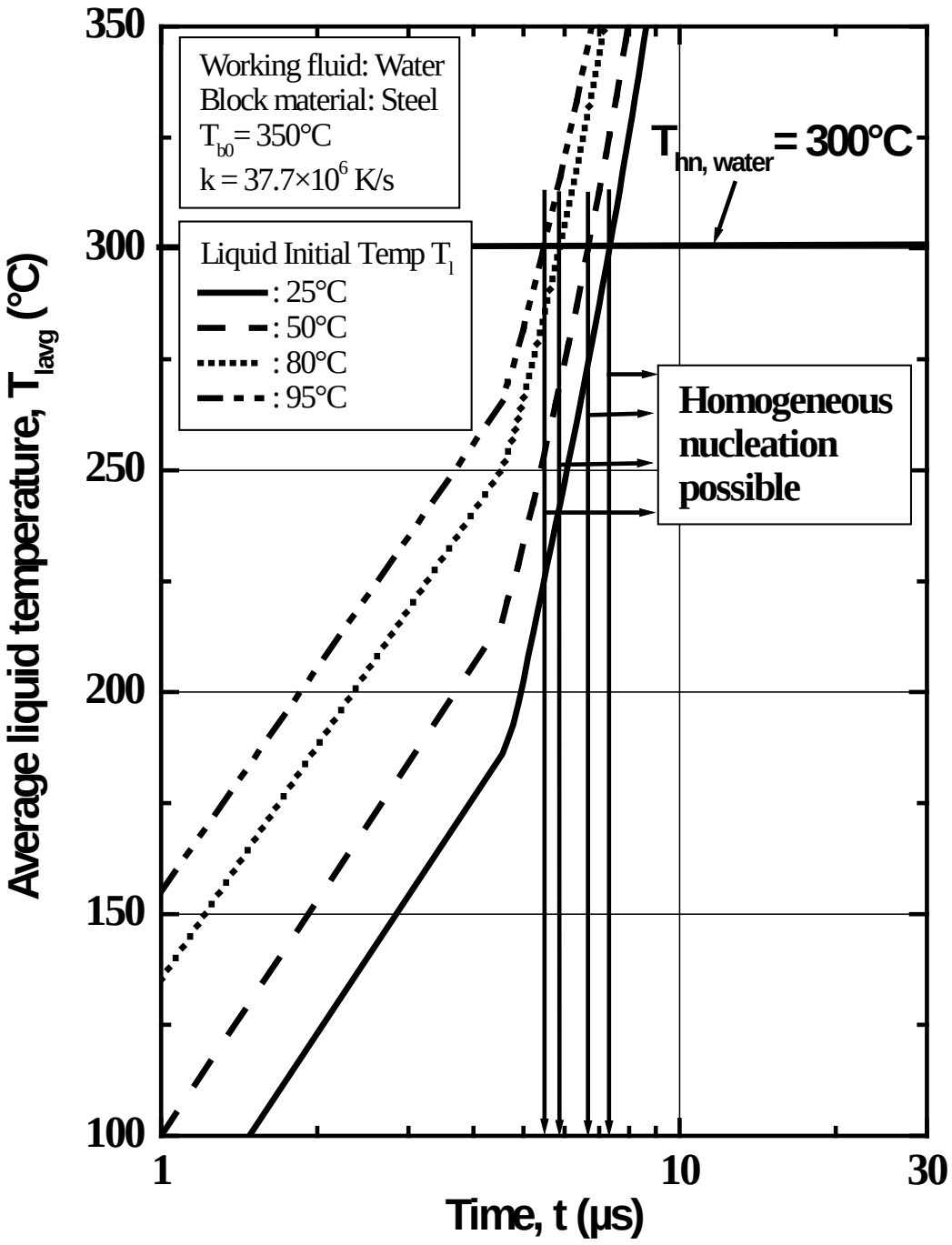

Figure 3.2.3 Effect of jet initial temperature on the variation of average liquid temperature with time for water in TST case

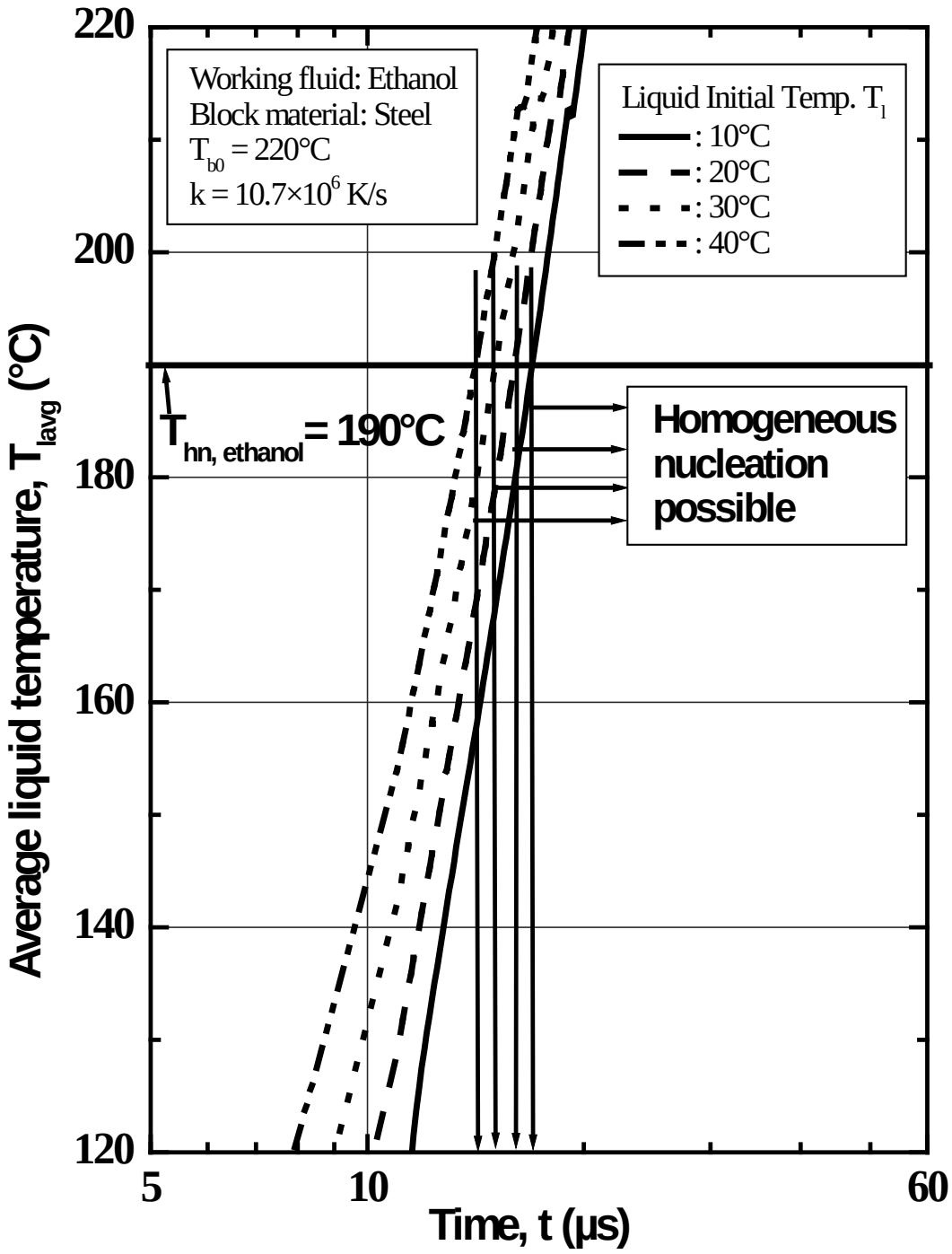

Figure 3.2.4 Effect of jet initial temperature on the variation of average liquid temperature with time for ethanol in TST case

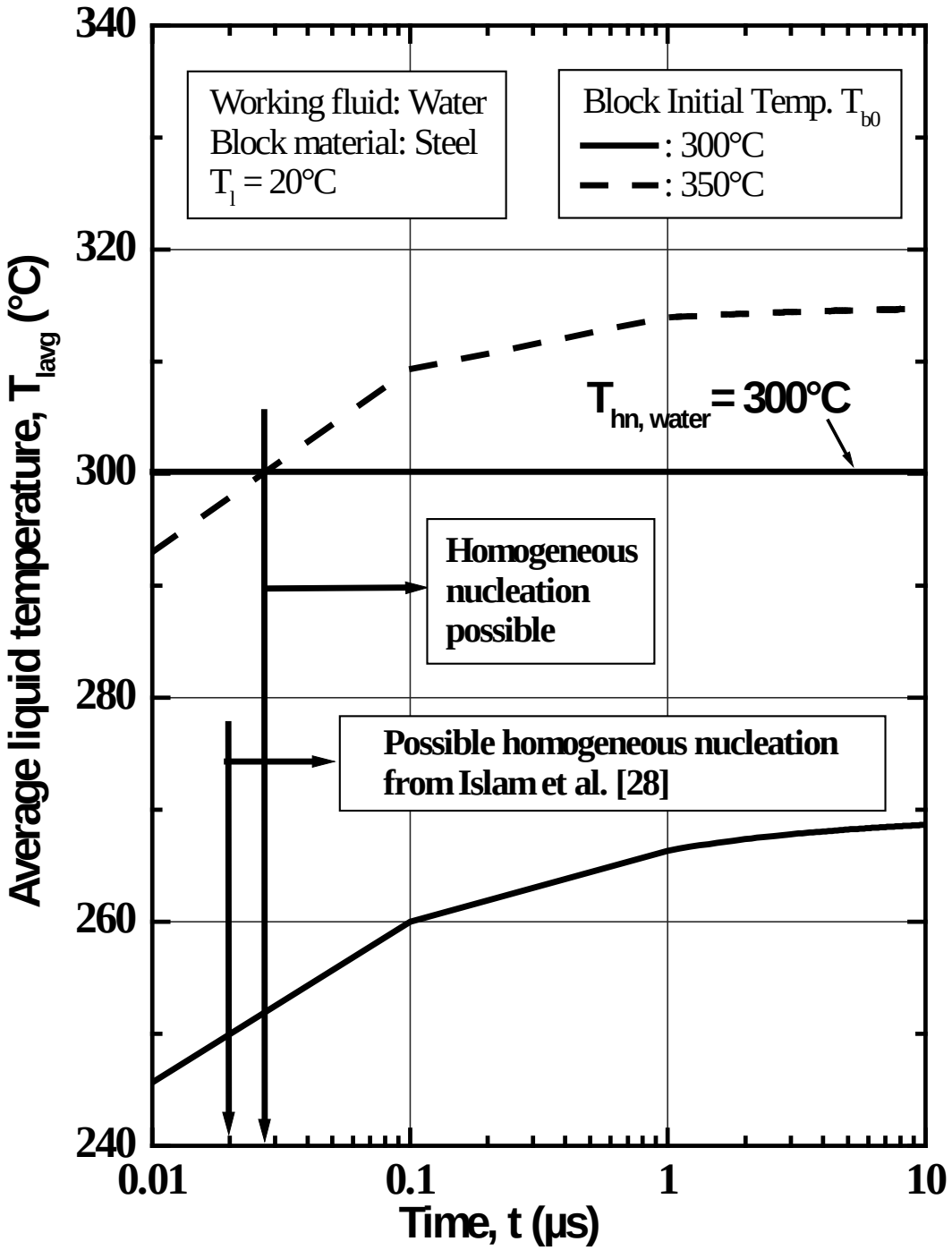

Figure 3.2.5 Effect of block initial temperature on the variation of average liquid temperature with time for water in PST case

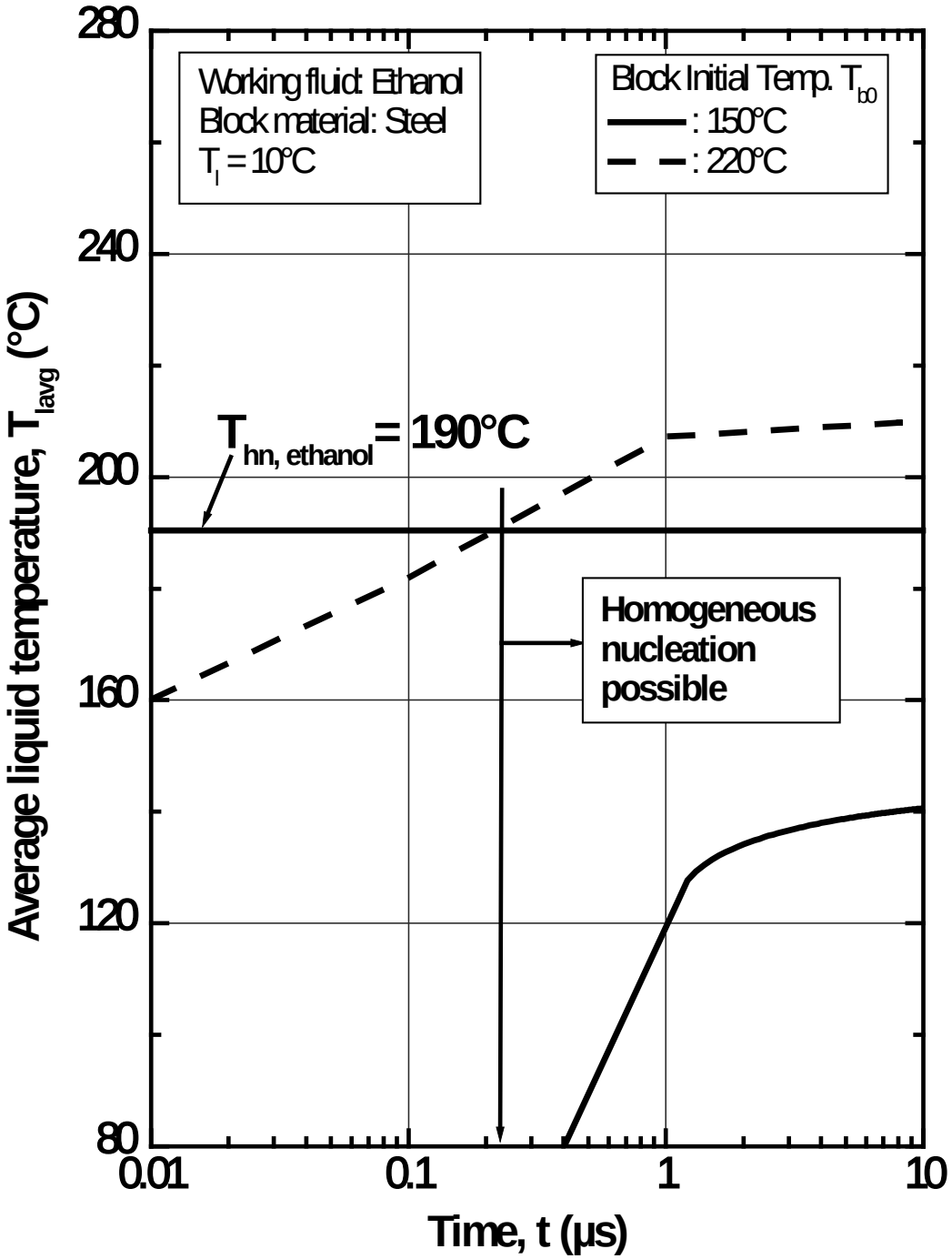

Figure 3.2.6 Effect of block initial temperature on the variation of average liquid temperature with time for ethanol in PST case

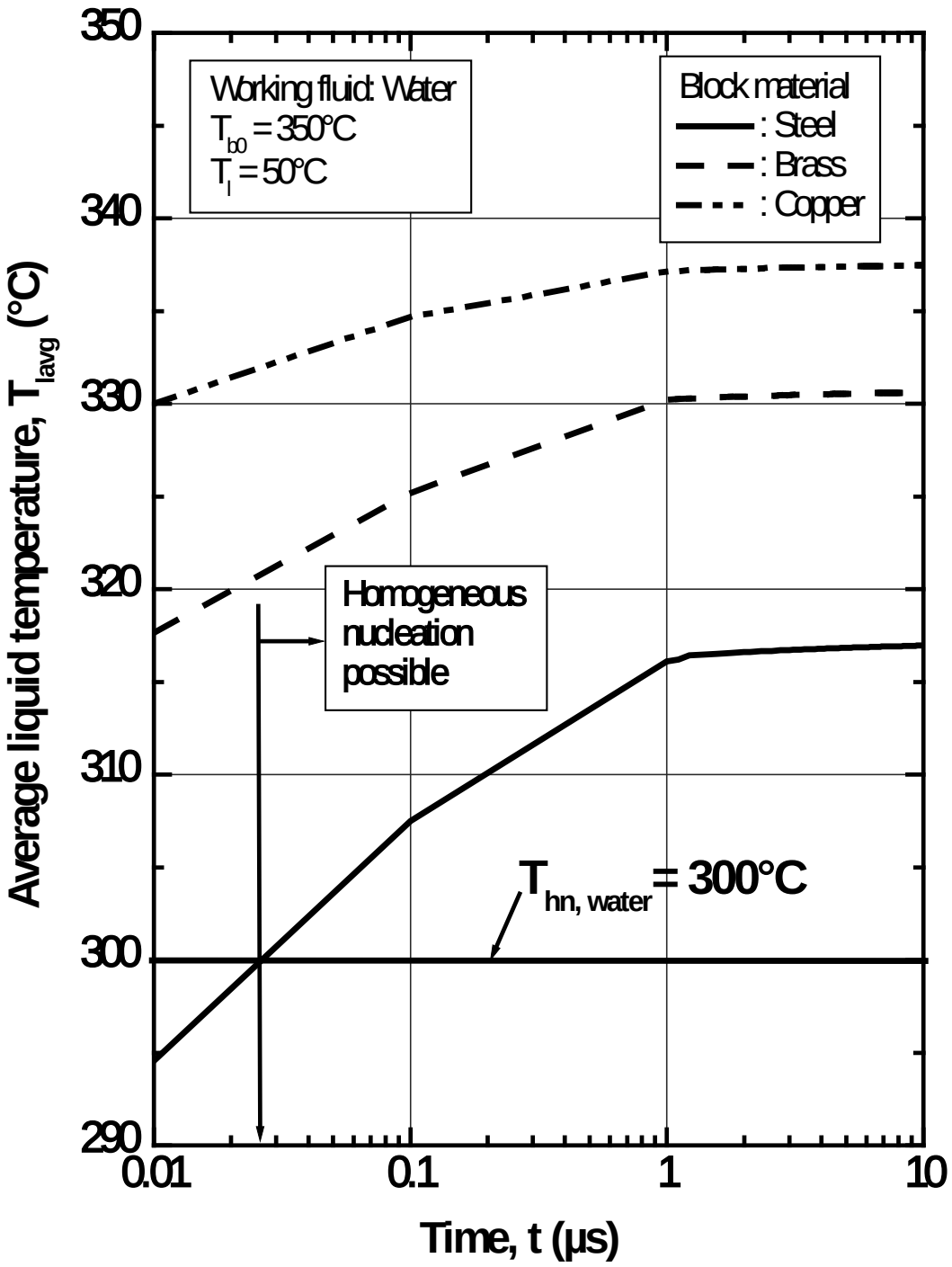

Figure 3.2.7 Effect of block material on the variation of average liquid temperature with time for water in PST case

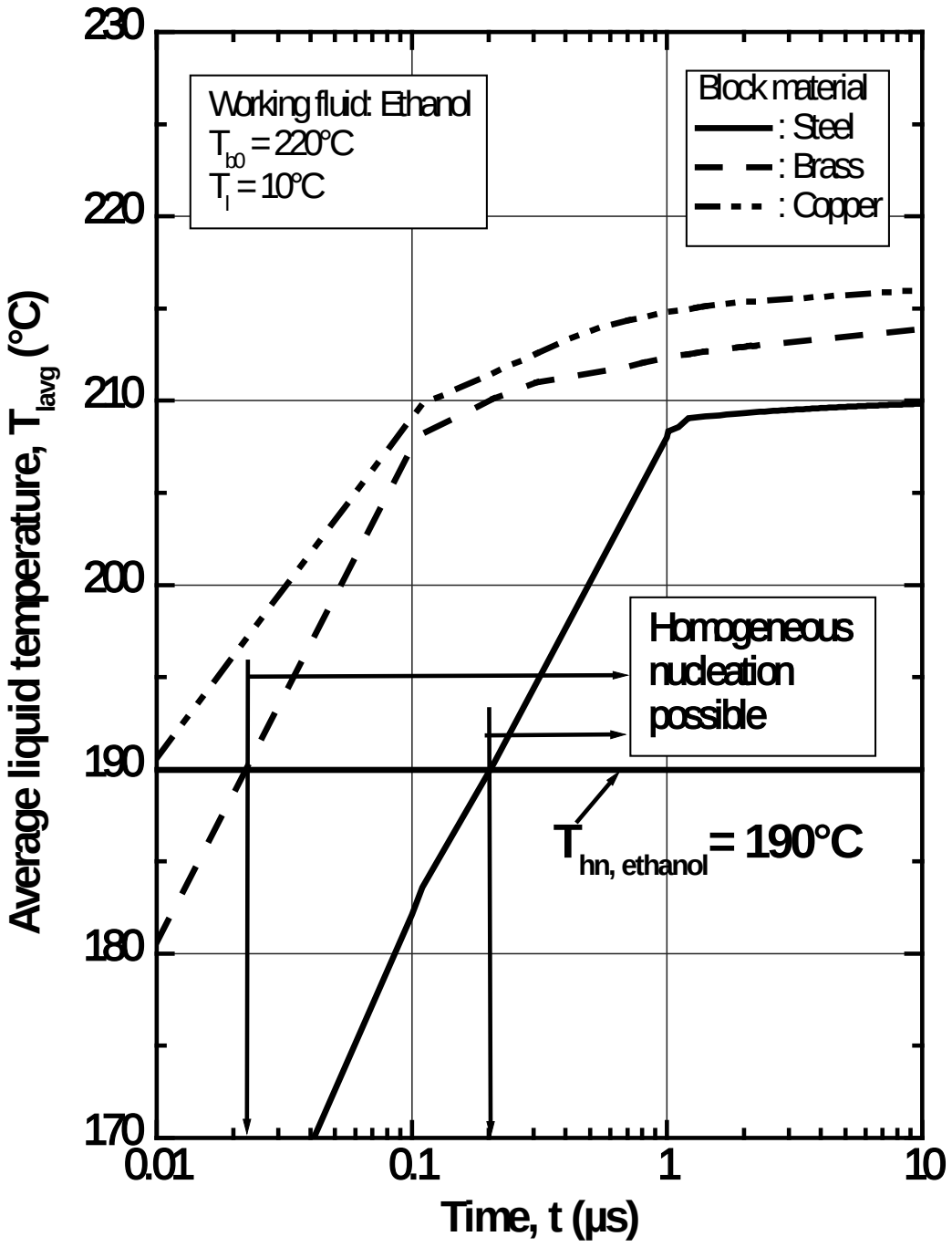

Figure 3.2.8 Effect of block material on the variation of average liquid temperature with time for ethanol in PST case

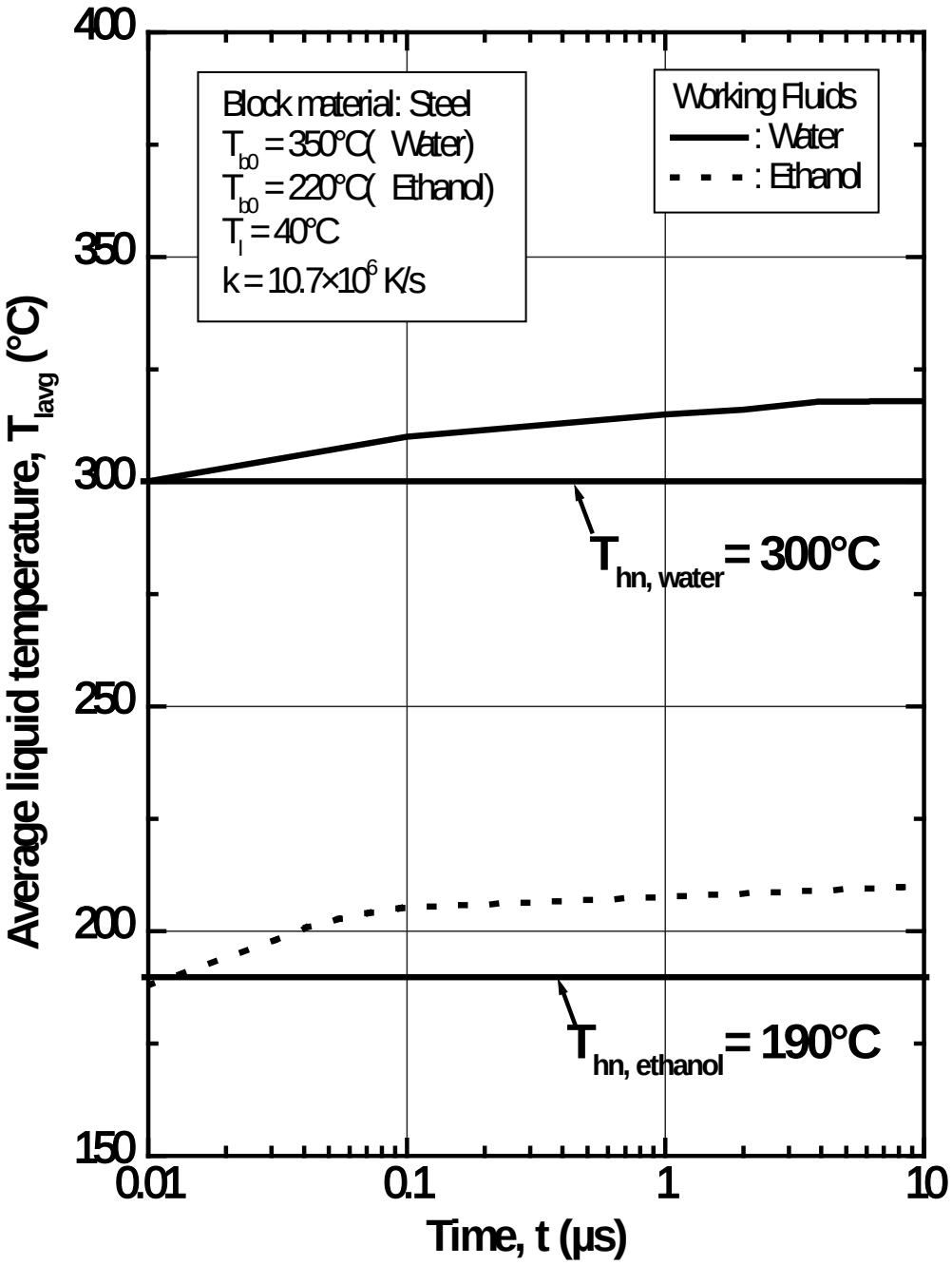

Figure 3.2.9 Effect of working fluids on the variation of average liquid temperature with time in TST case

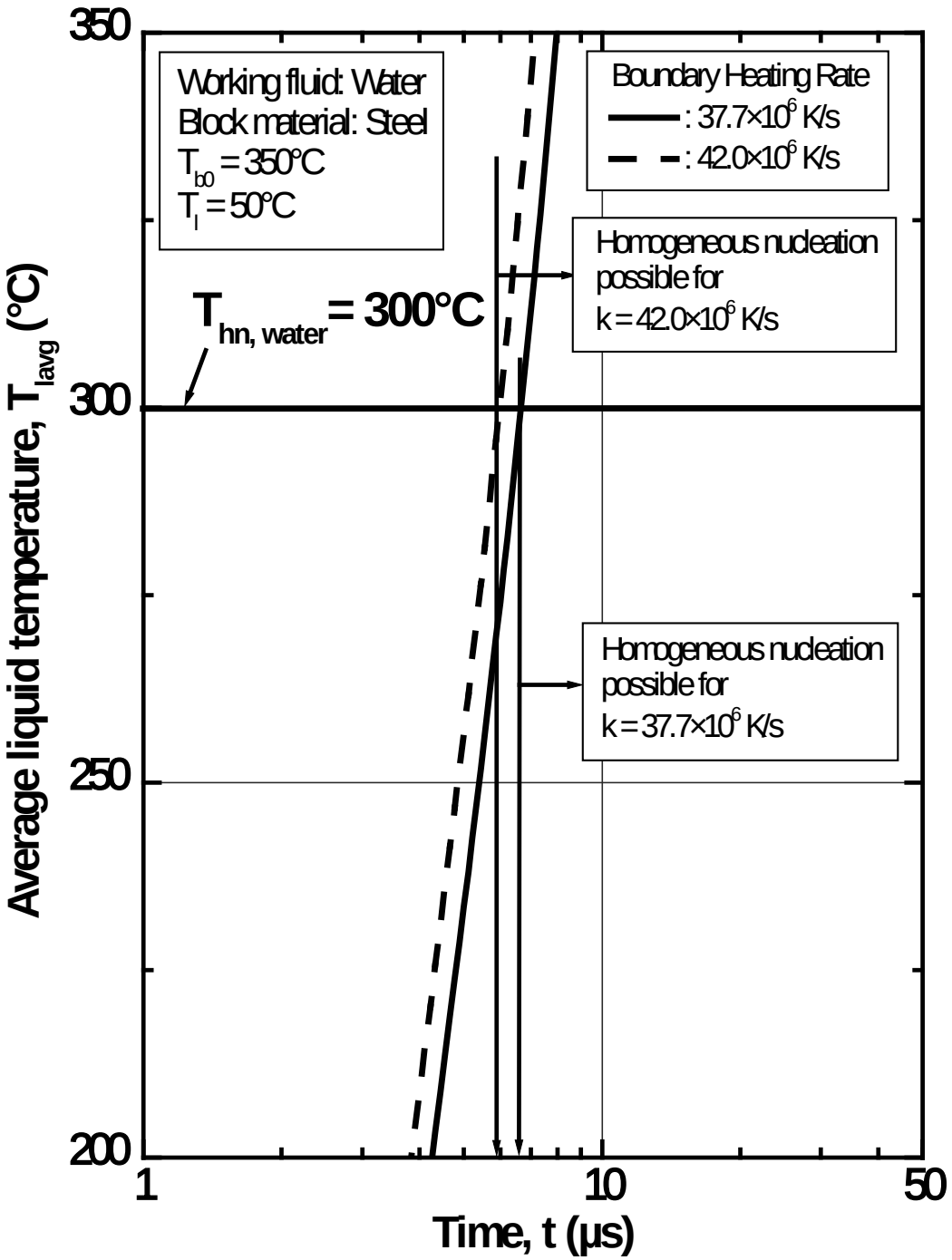

Figure 3.2.10 Effect of boundary heating rate on the variation of average liquid temperature with time for water

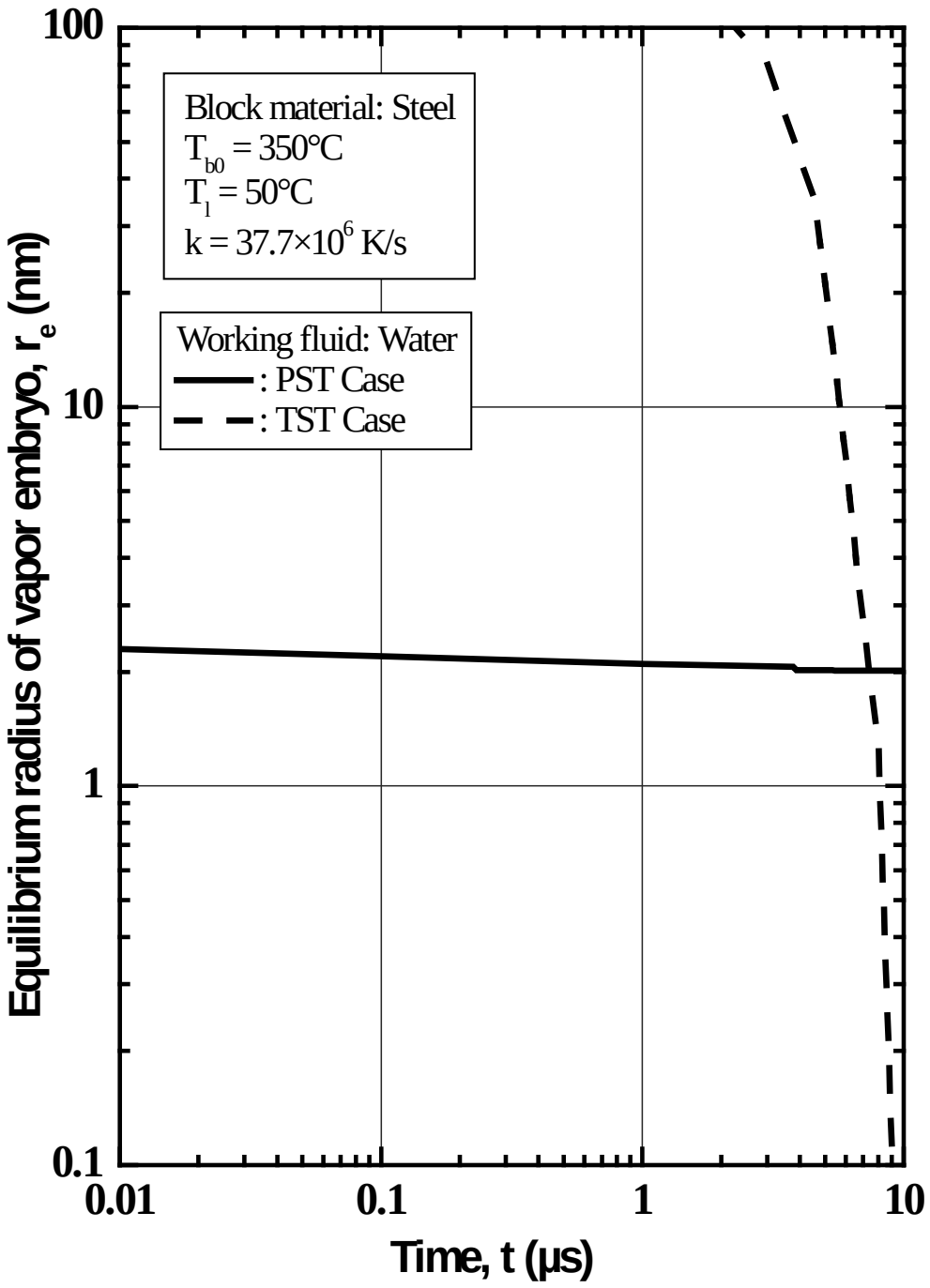

Figure 3.3.1 Variation of equilibrium radius of vapor embryo with time for water

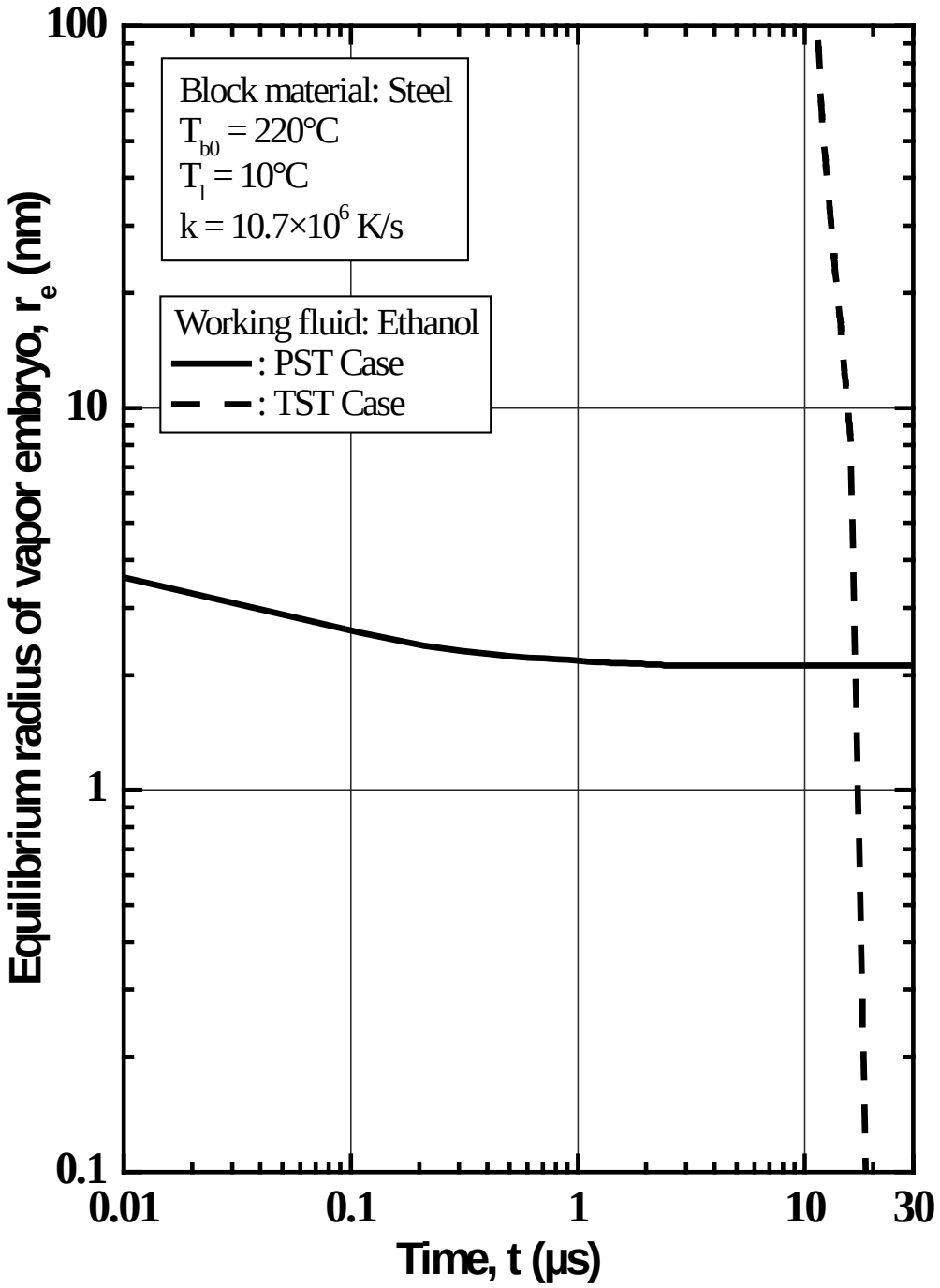

Figure 3.3.2 Variation of equilibrium radius of vapor embryo with time for ethanol

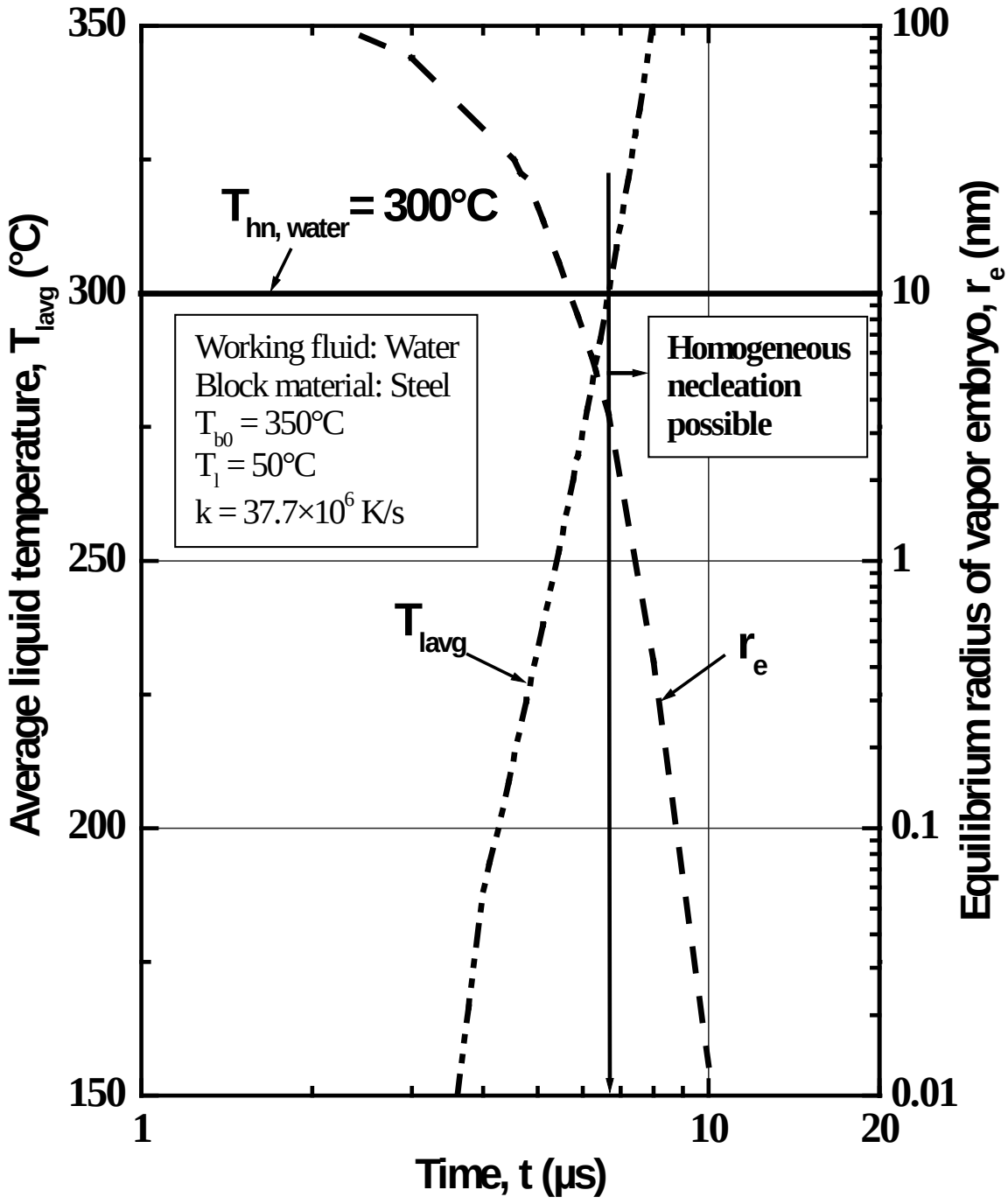

Figure 3.3.3 Variation of equilibrium radius of vapor embryo and average liquid temperature with time for water in TST case

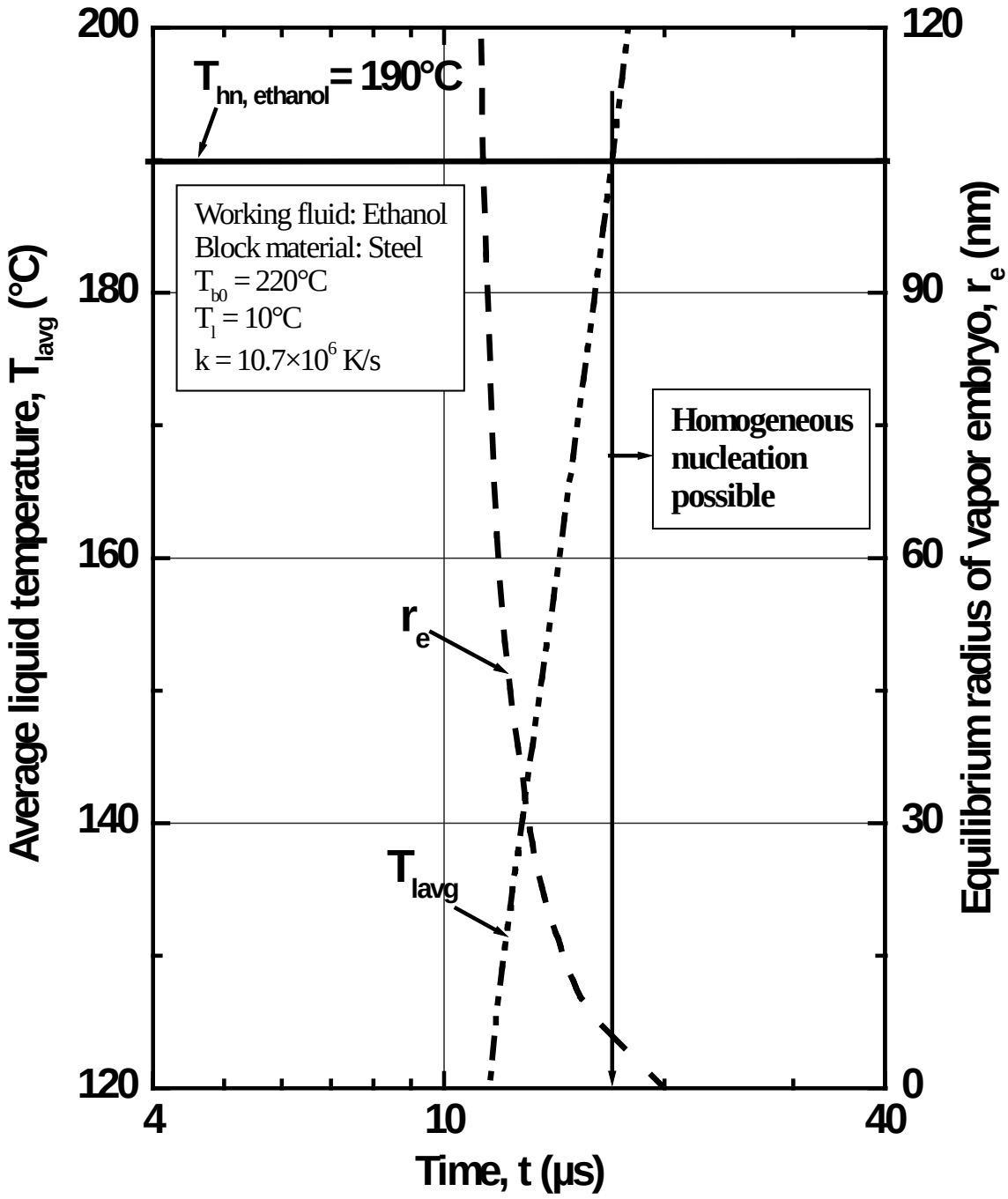

Figure 3.3.4 Variation of equilibrium radius of vapor embryo and average liquid temperature with time for ethanol in TST case

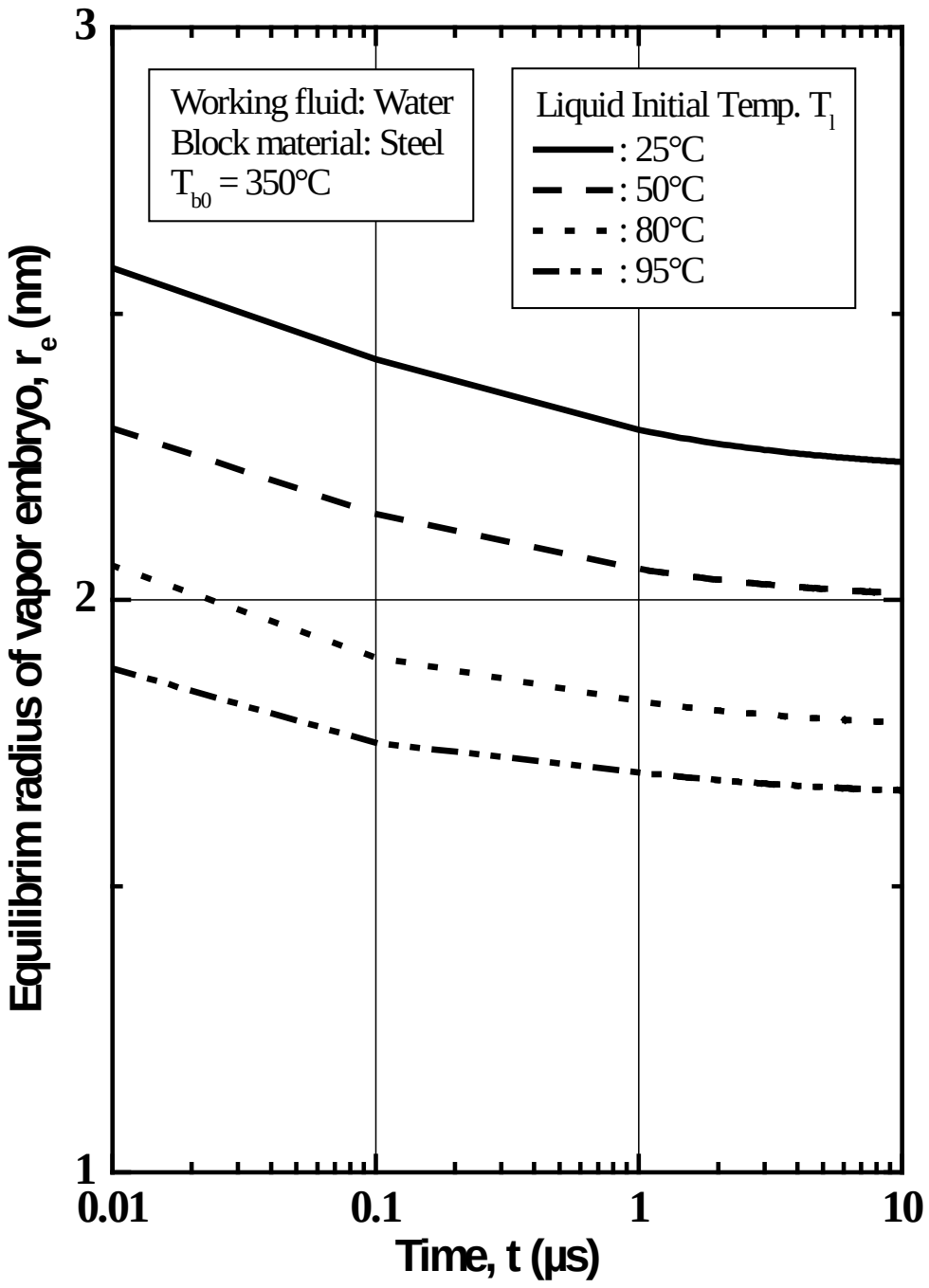

Figure 3.3.5 Effect of jet initial temperature on the variation of equilibrium radius of vapor embryo with time for water in PST case

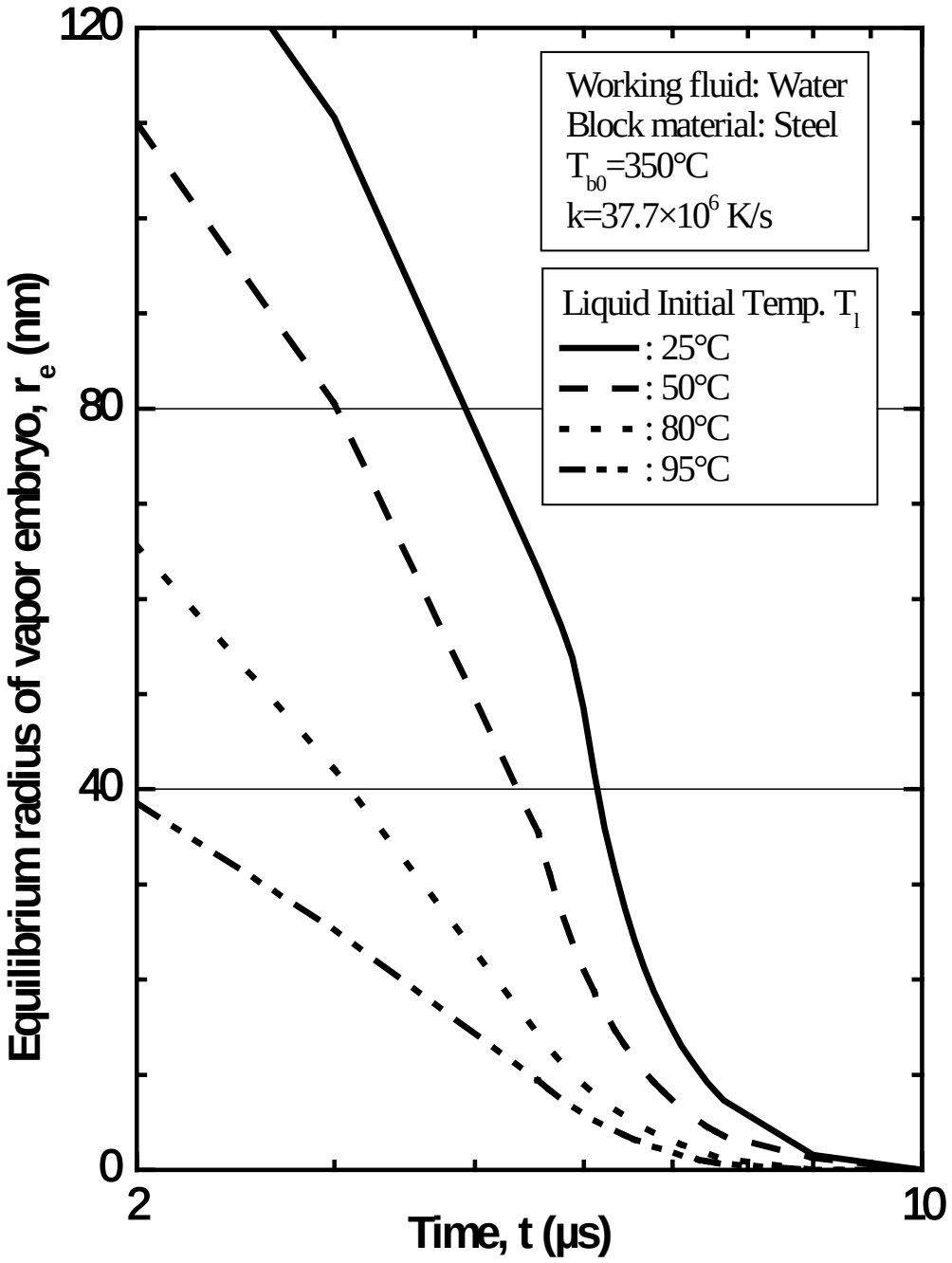

Figure 3.3.6 Effect of jet initial temperature on the variation of equilibrium radius of vapor embryo with time for water in TST case

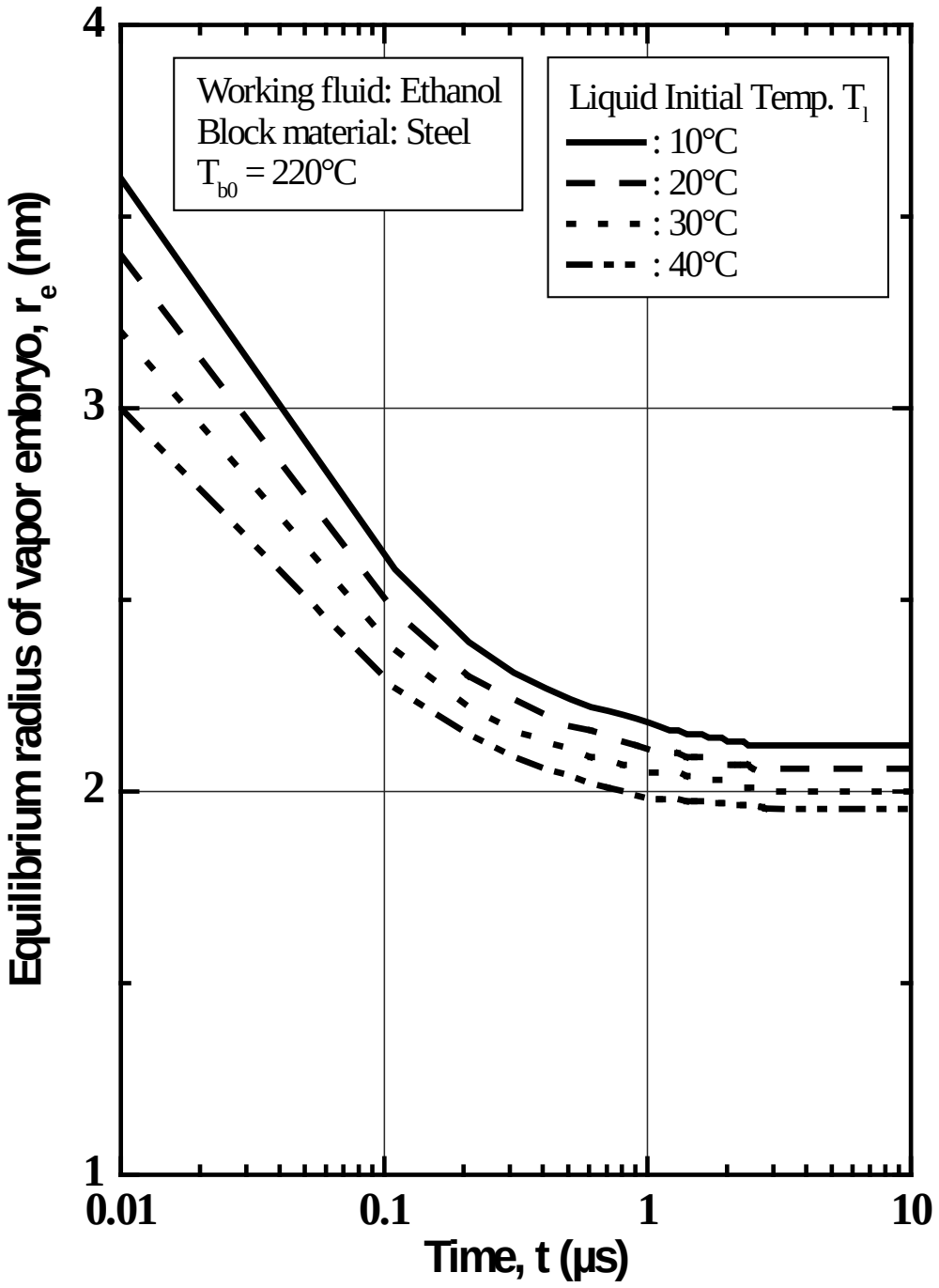

Figure 3.3.7 Effect of jet initial temperature on the variation of equilibrium radius of vapor embryo with time for ethanol in PST case

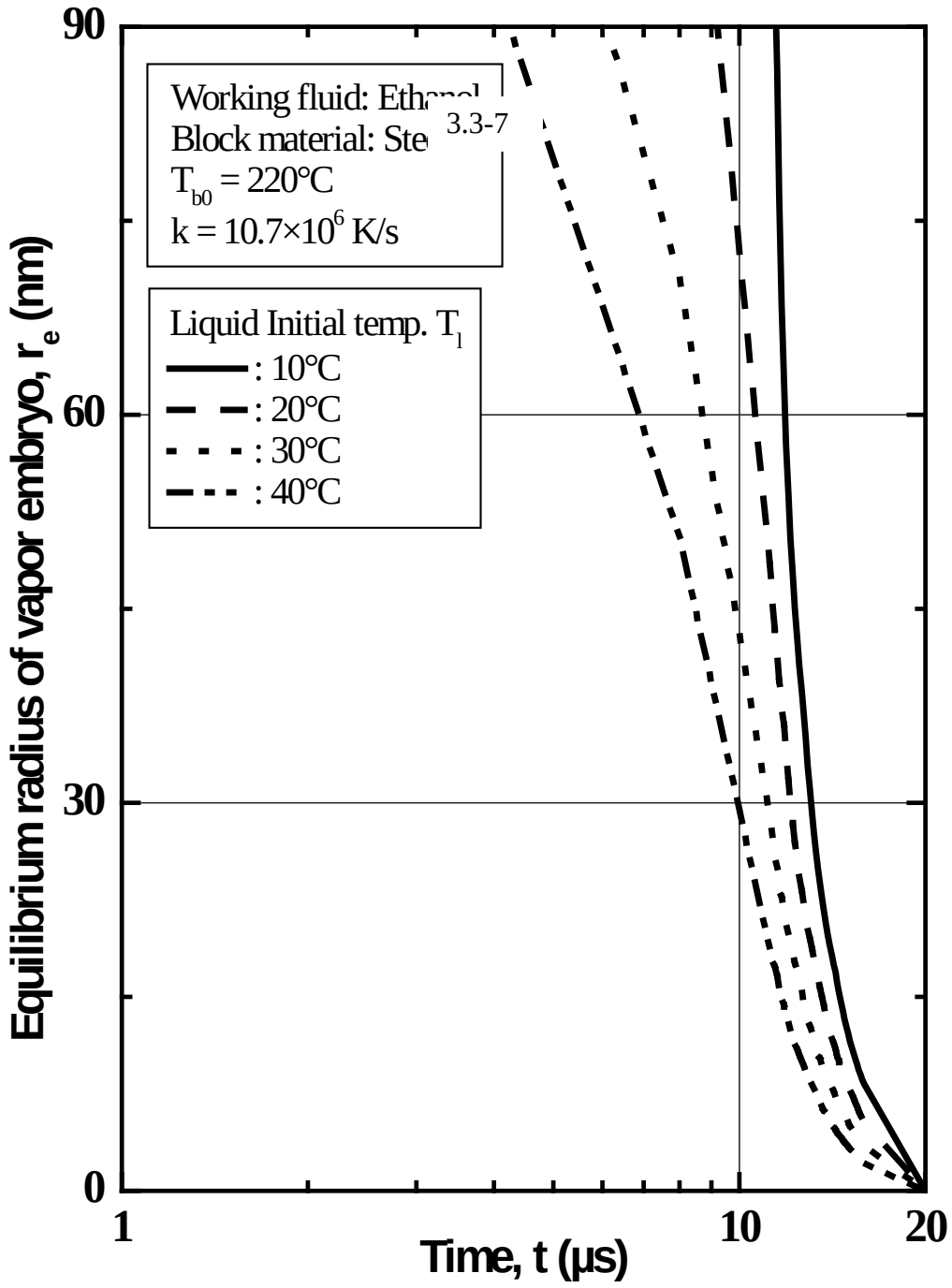

Figure 3.3.8 Effect of jet initial temperature on the variation of equilibrium radius of vapor embryo with time for ethanol in TST case

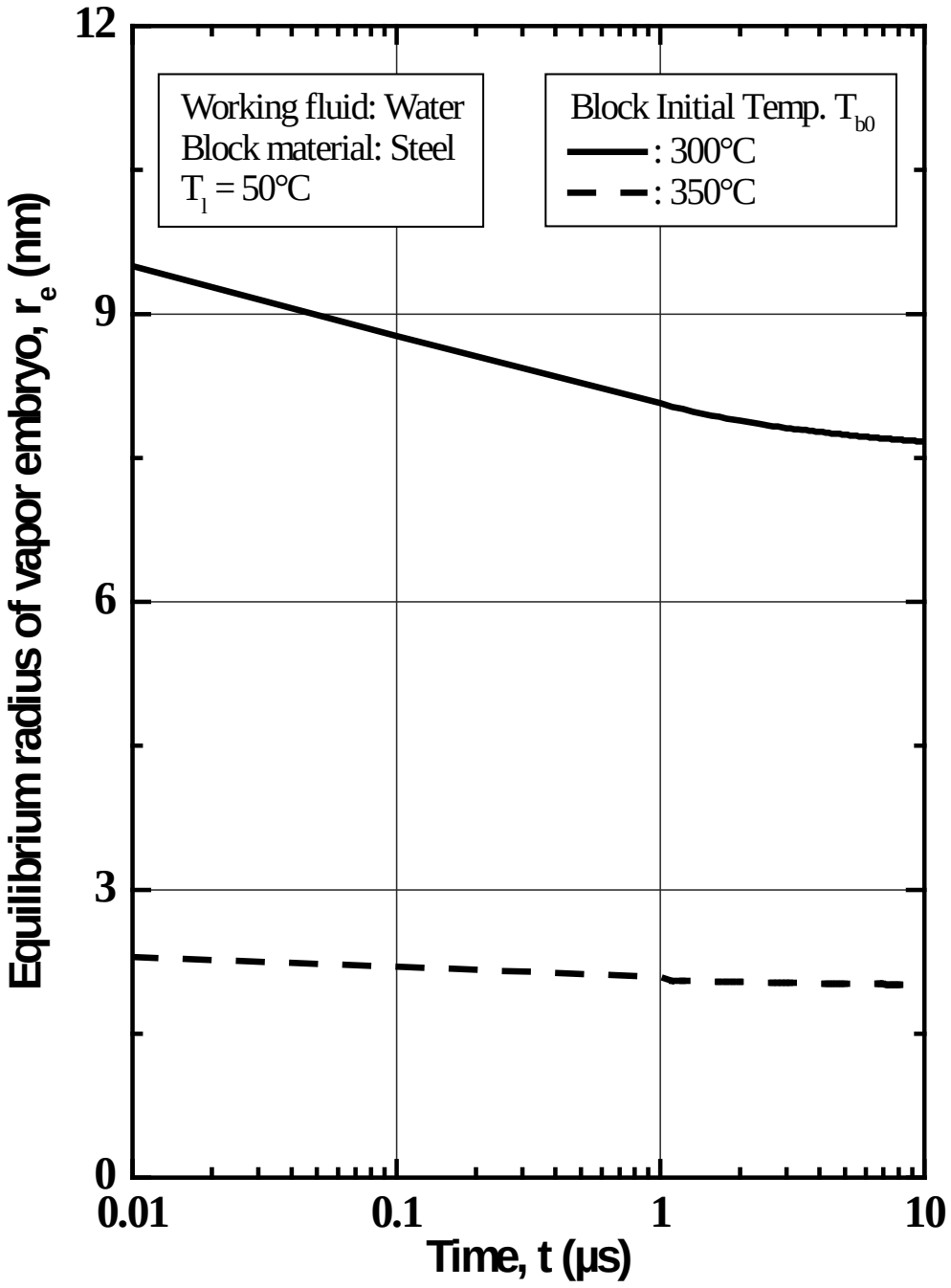

Figure 3.3.9 Effect of block initial temperature on the variation of equilibrium radius of vapor embryo with time for water in PST case

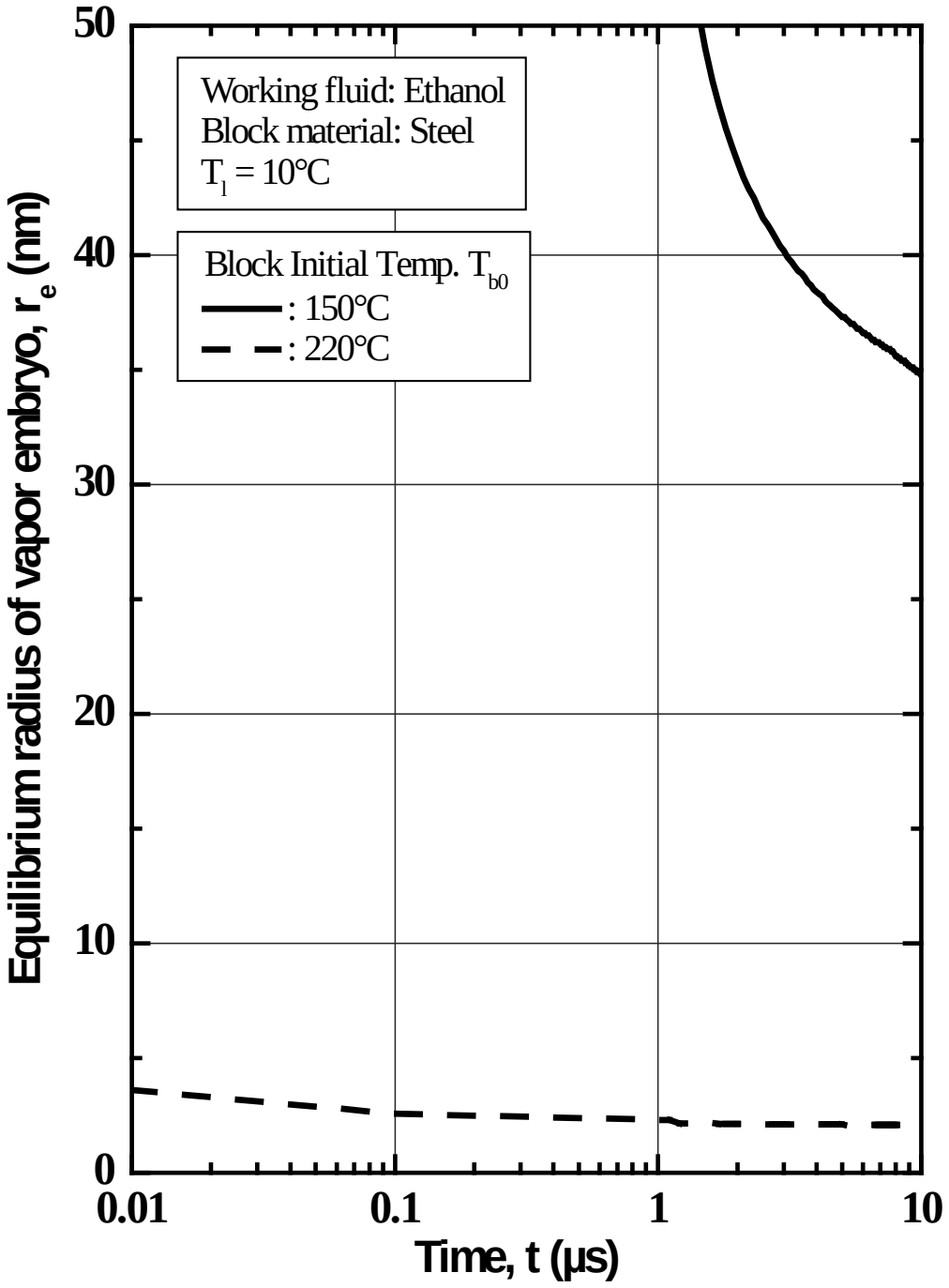

Figure 3.3.10 Effect of block initial temperature on the variation of equilibrium radius of vapor embryo with time for ethanol in PST case

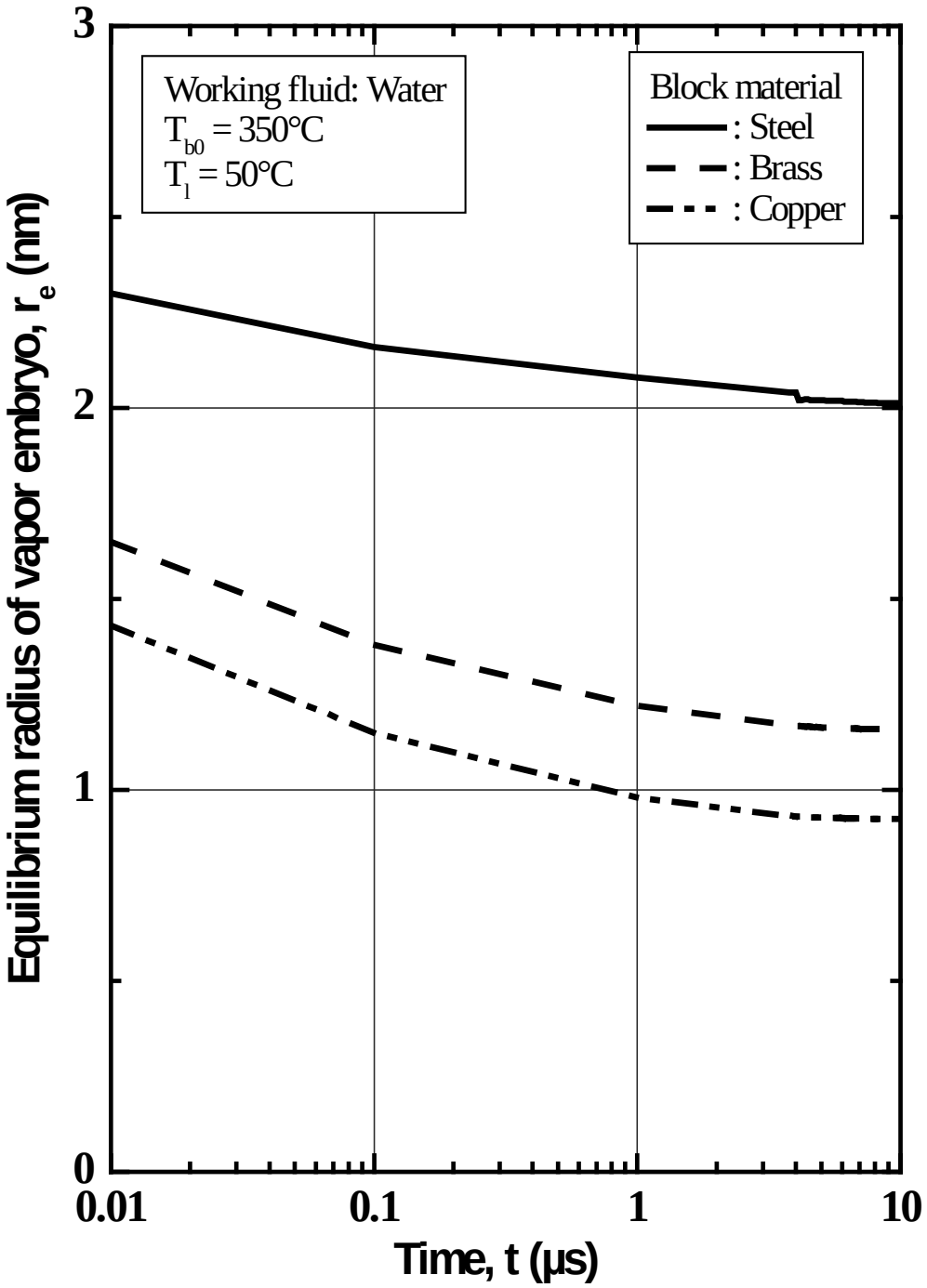

Figure 3.3.11 Effect of block material on the variation of equilibrium radius of vapor embryo with time for water in PST case

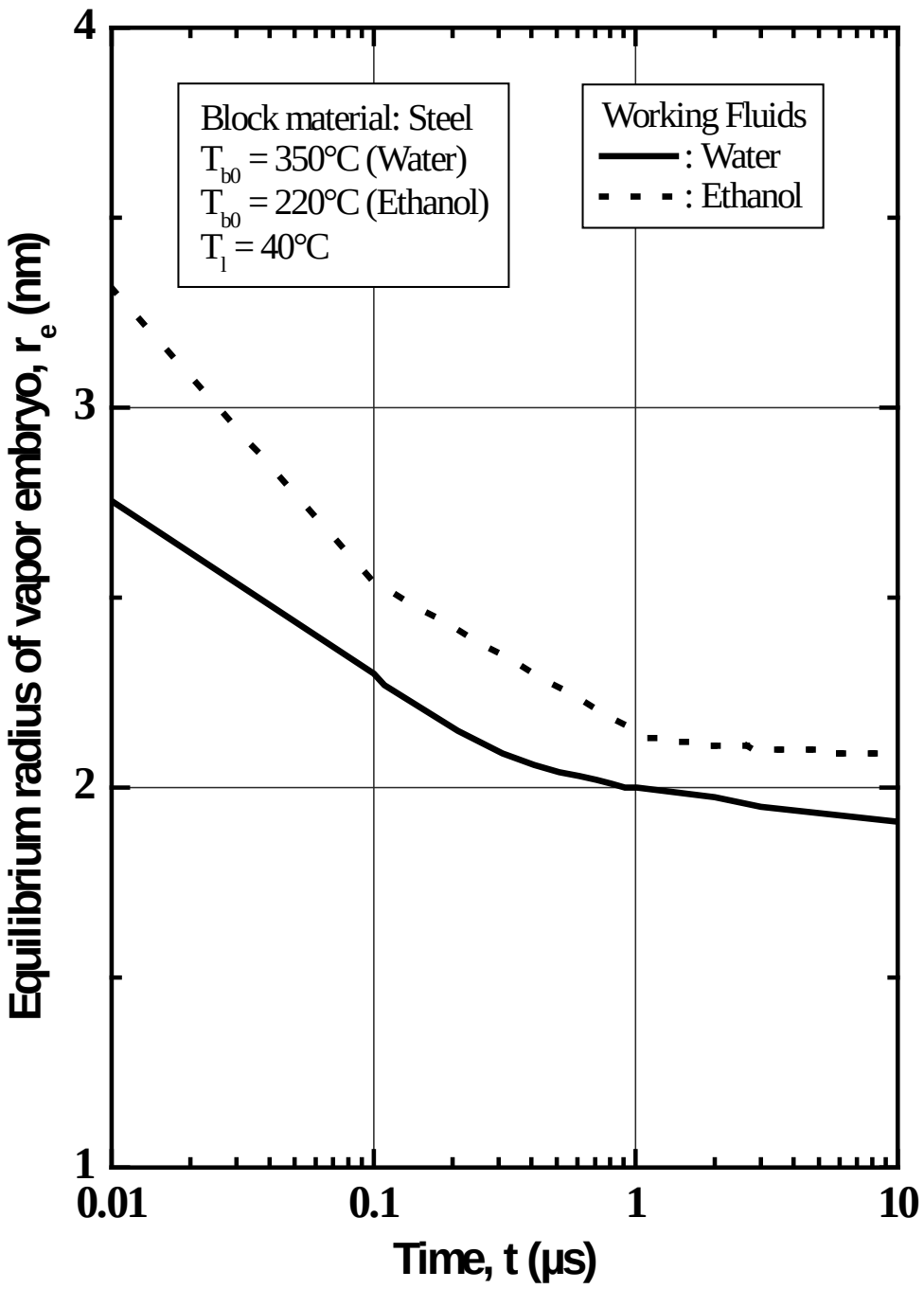

Figure 3.3.12 Effect of working fluids on the variation of equilibrium radius of vapor embryo with time in PST case

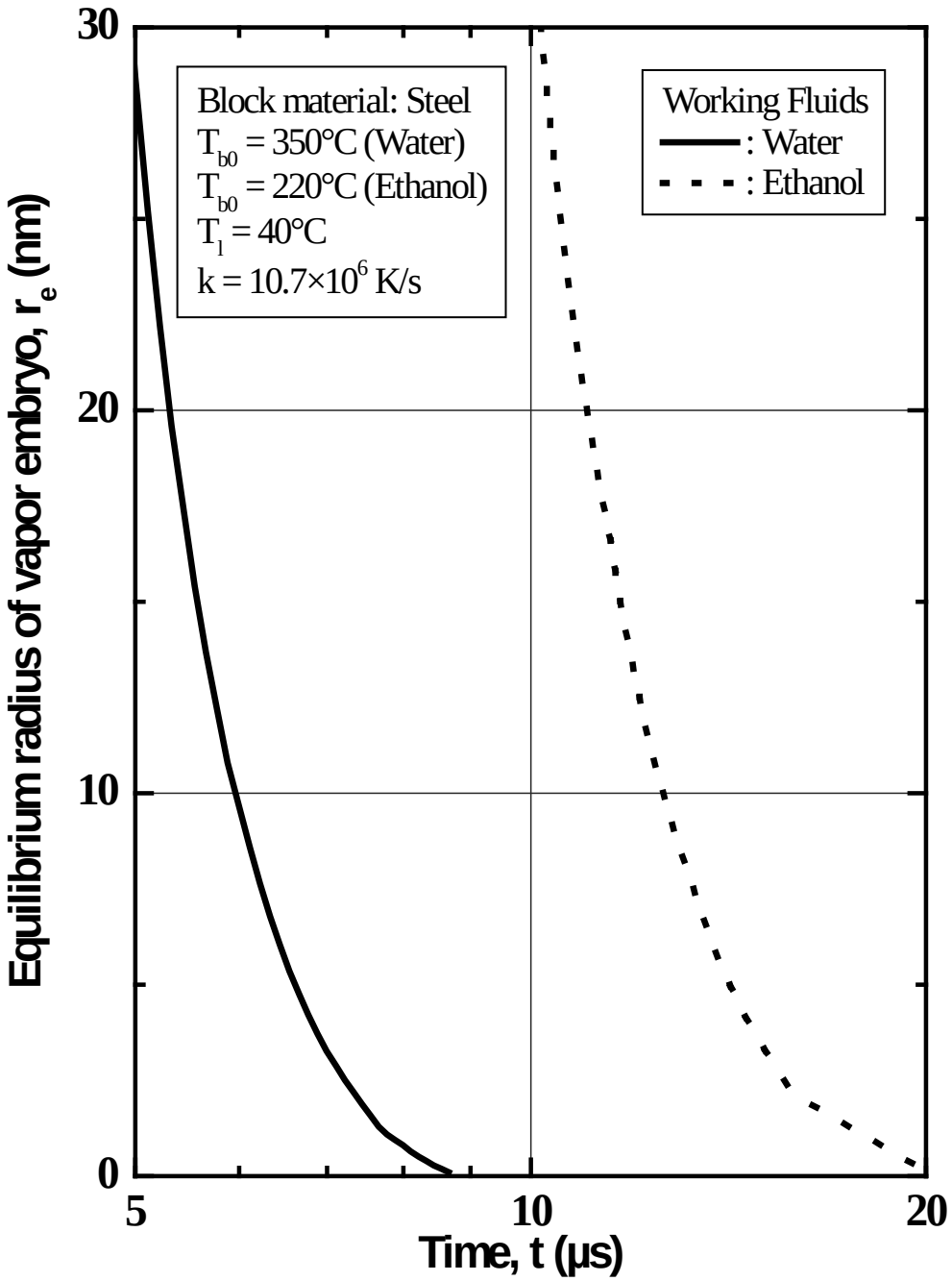

Figure 3.3.13 Effect of working fluids on the variation of equilibrium radius of vapor embryo with time in TST case

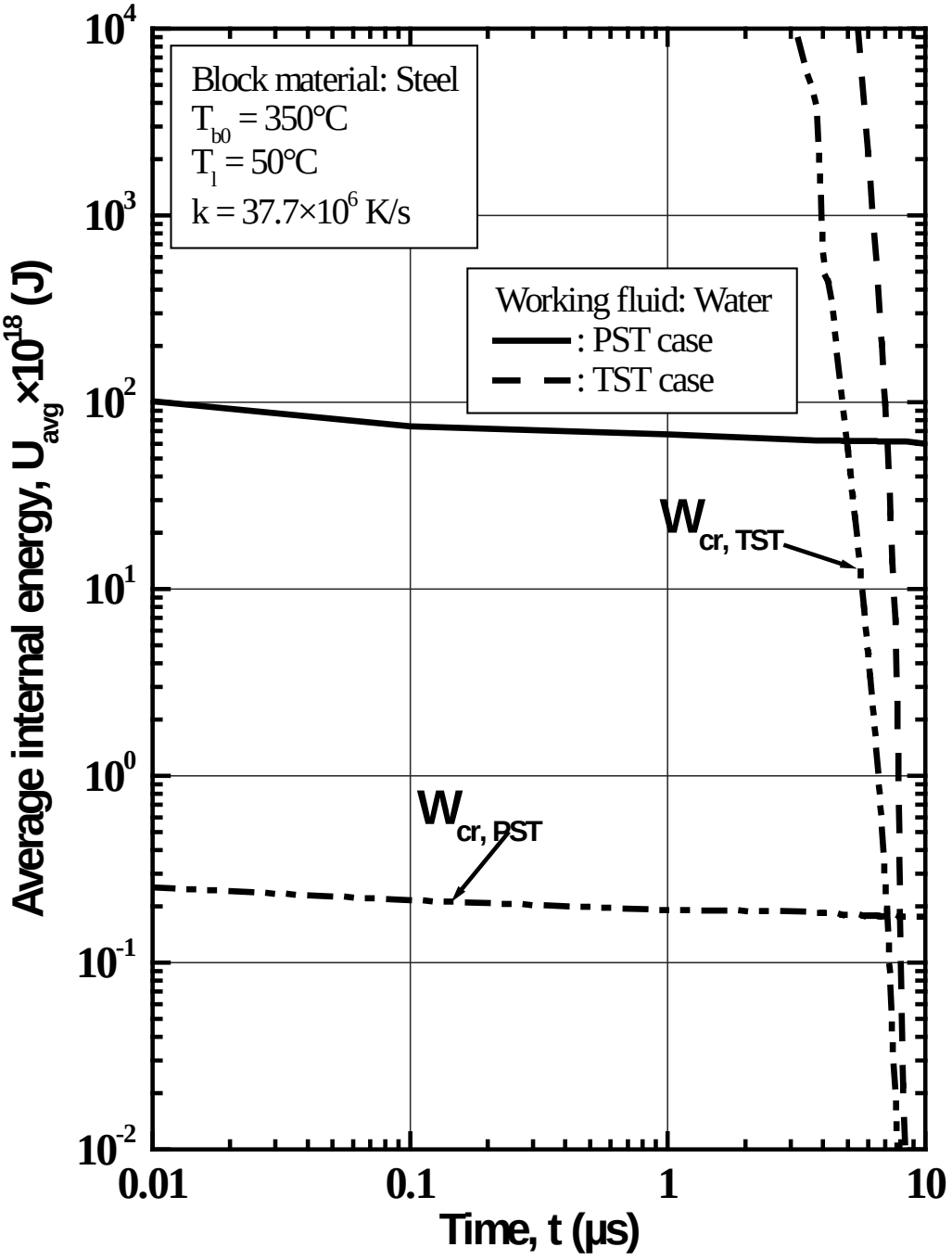

Figure 3.4.1 Variation of average internal energy with time for water

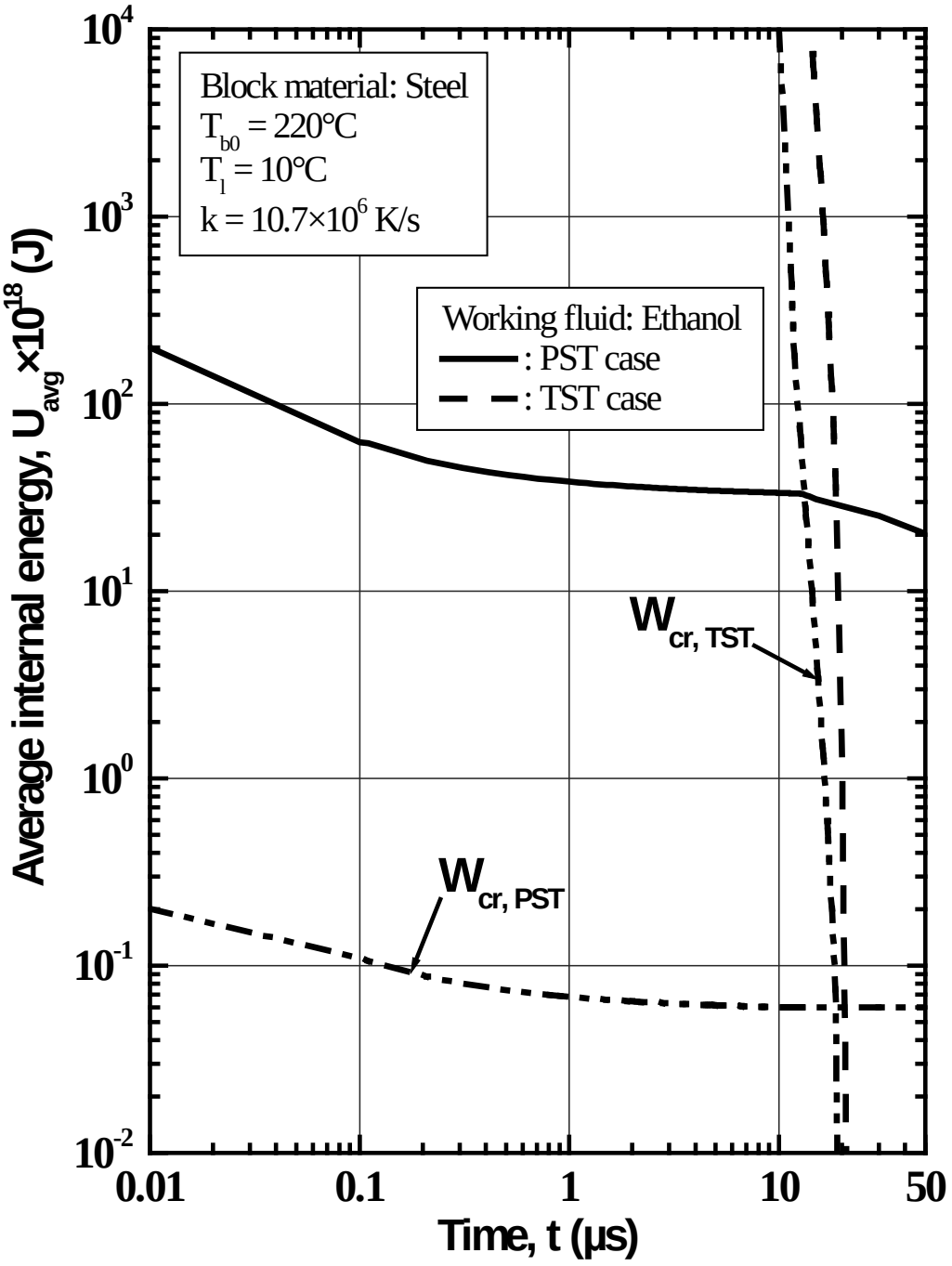

Figure 3.4.2 Variation of average internal energy with time for ethanol

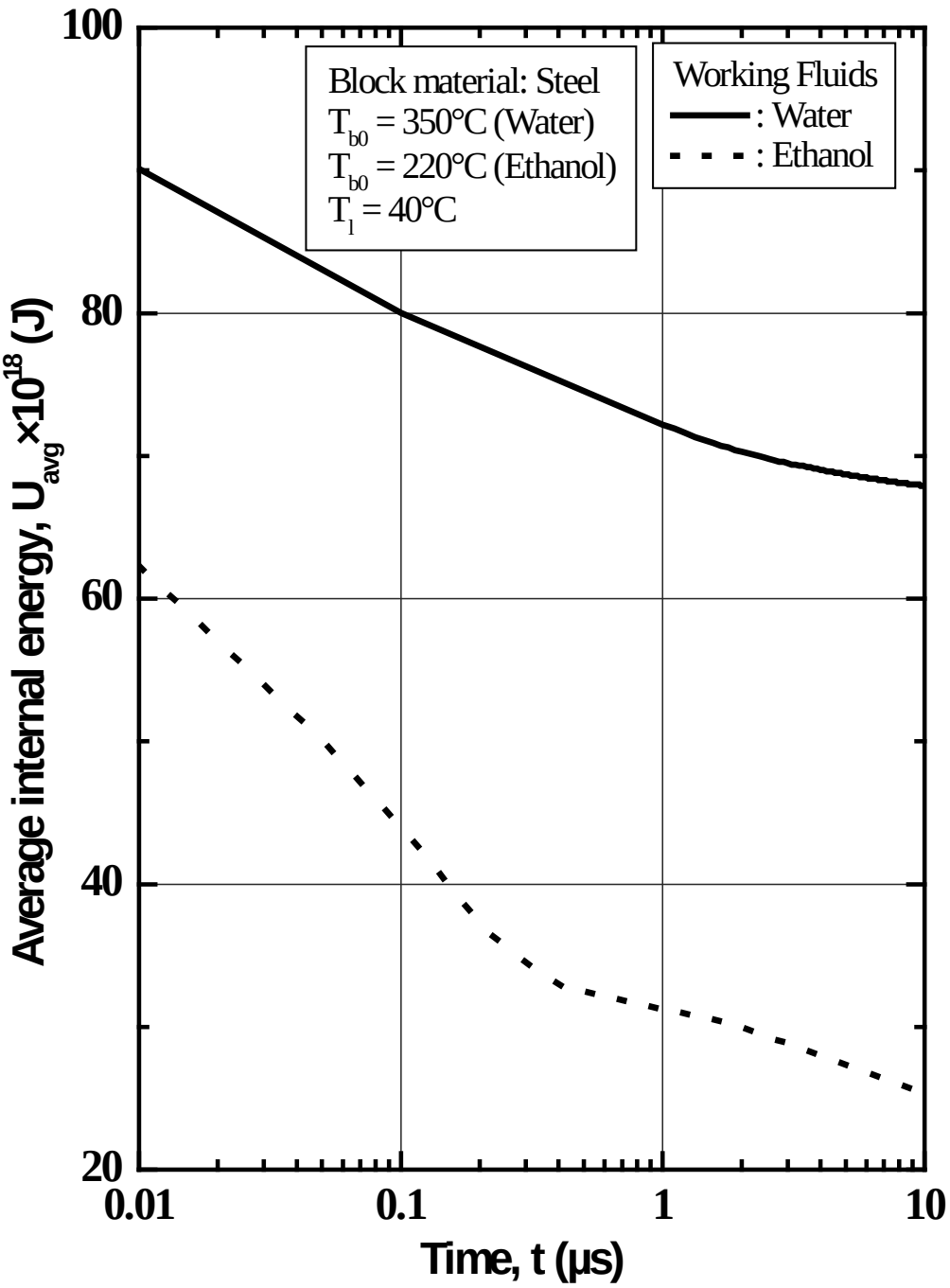

Figure 3.4.3 Effect of working fluids on the variation of average internal energy with time in PST case

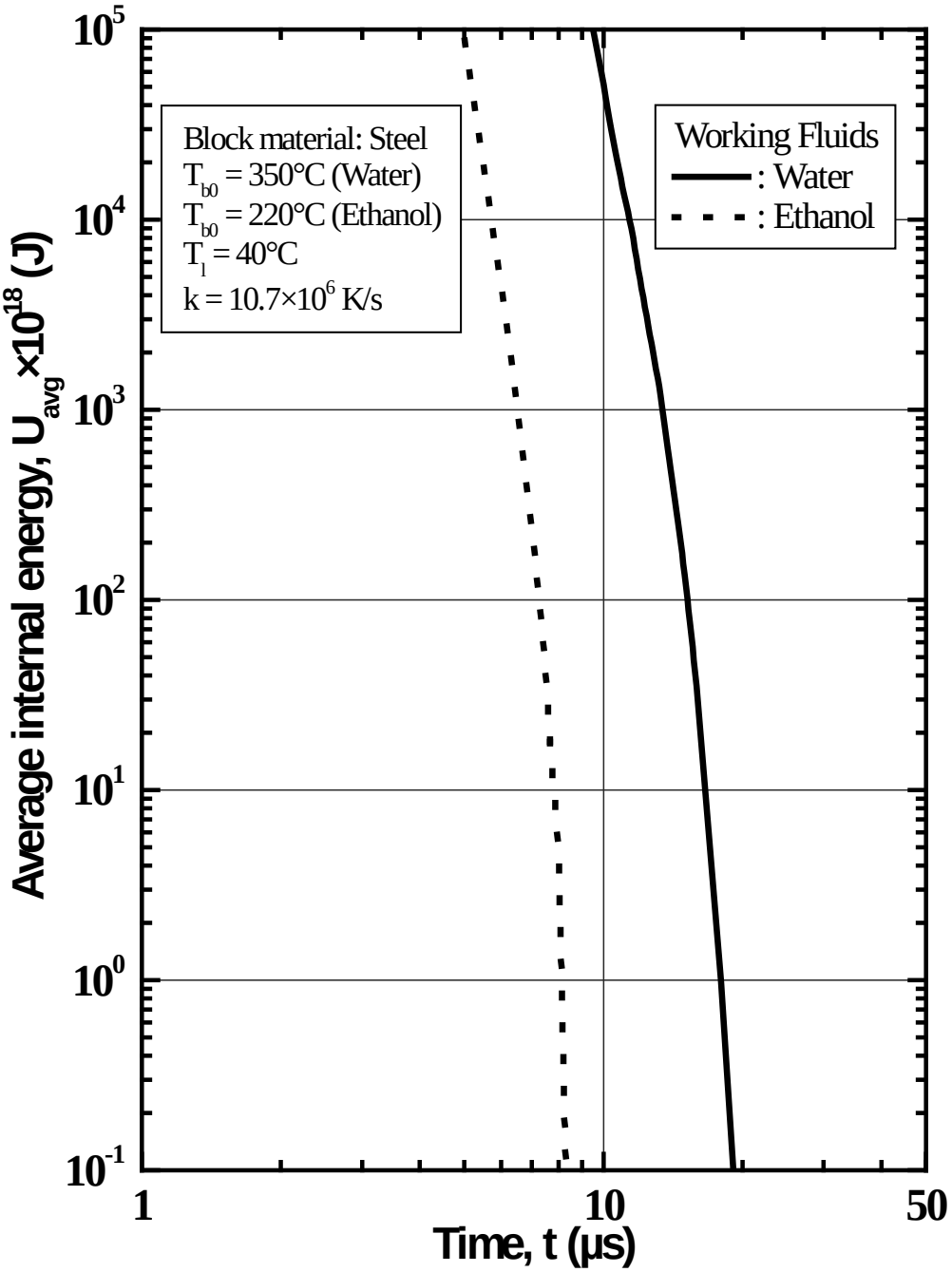

Figure 3.4.4 Effect of working fluids on the variation of average internal energy with time in TST case

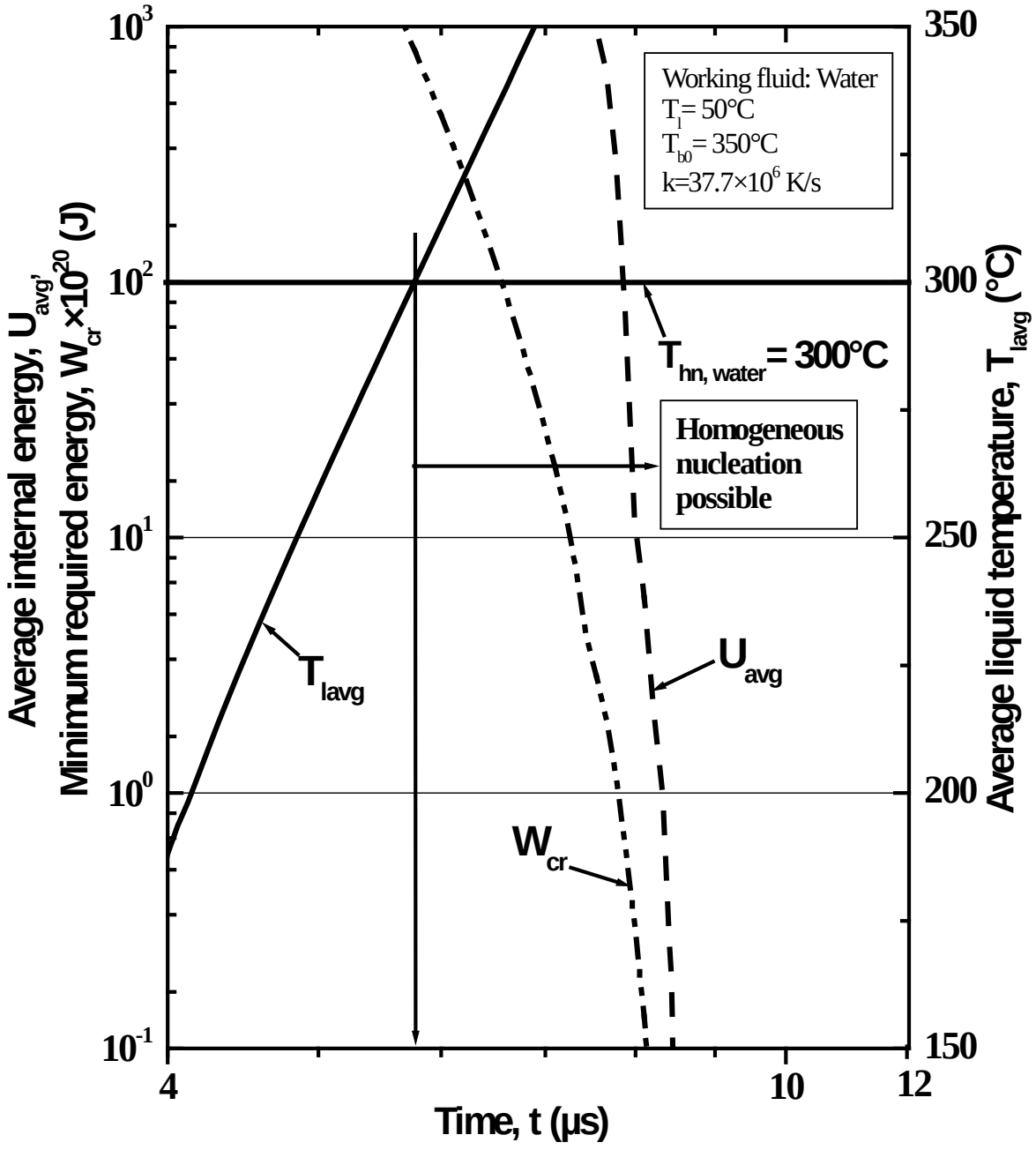

Figure 3.4.5 Variation of average internal energy, minimum required energy to form a bubble and average liquid temperature with time for water in TST case

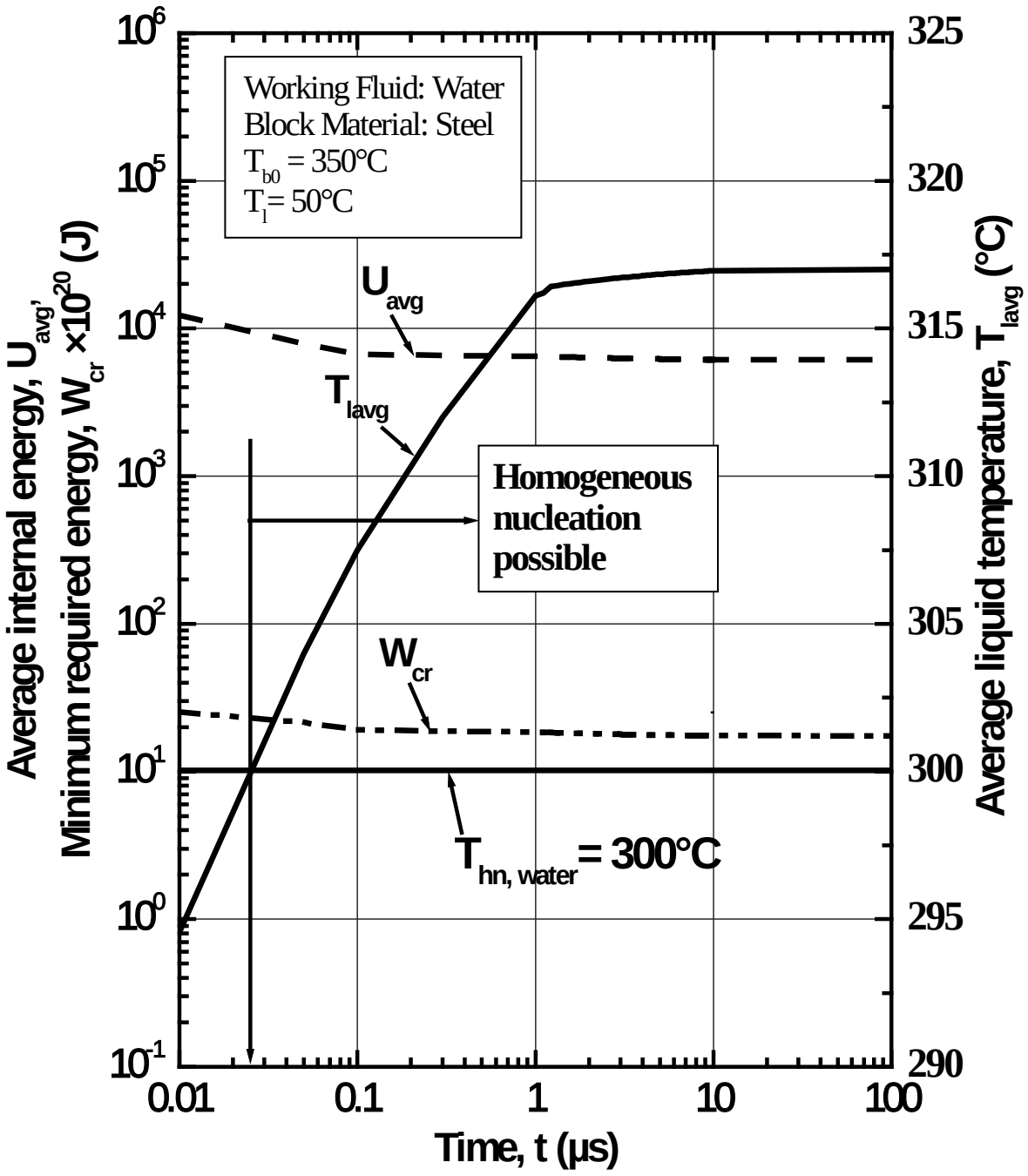

Figure 3.4.6 Variation of average internal energy, minimum required energy to form a bubble and average liquid temperature with time for water in PST case

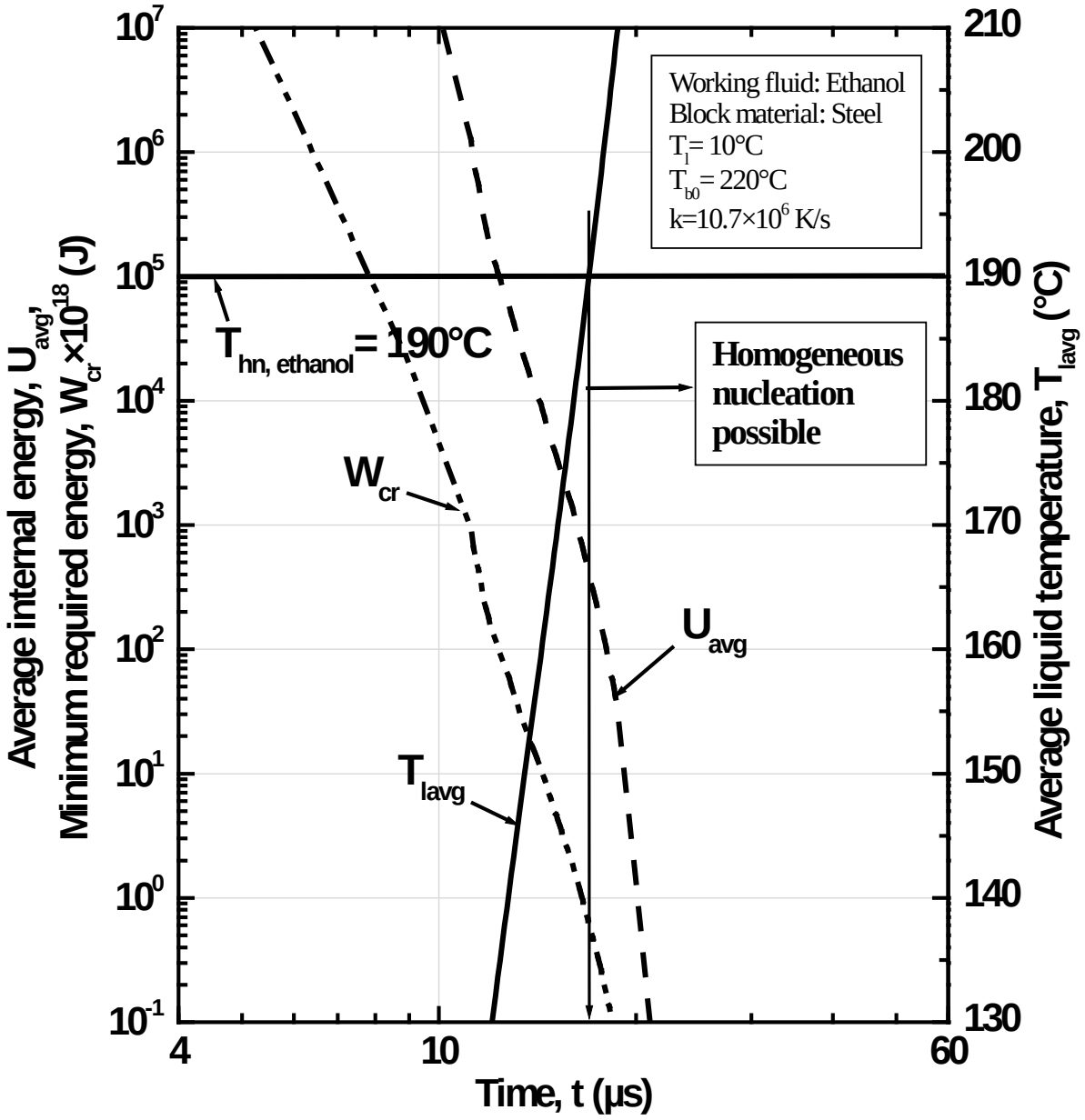

Figure 3.4.7 Variation of average internal energy, minimum required energy to form a bubble and average liquid temperature with time for ethanol in TST case

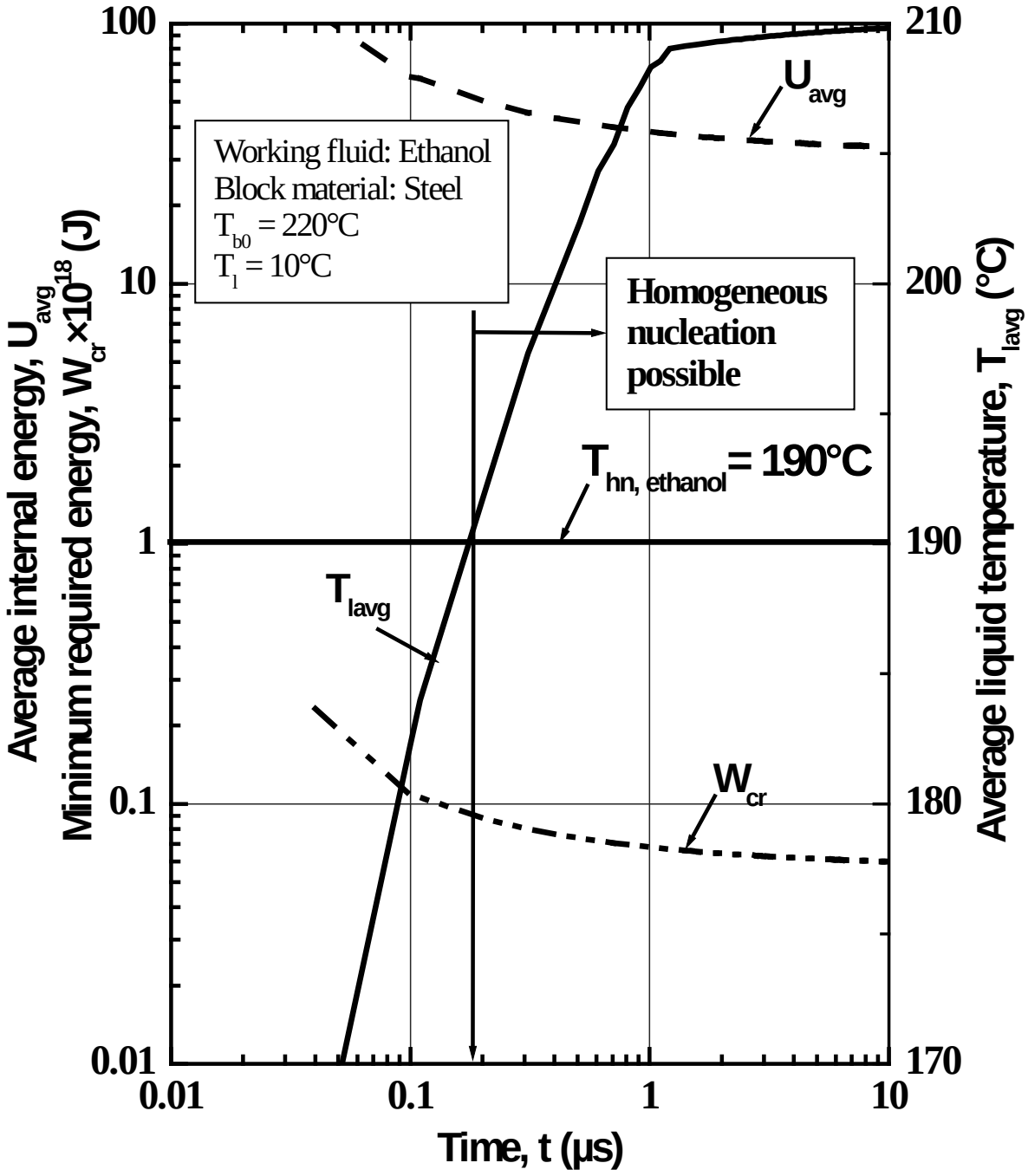

Figure 3.4.8 Variation of average internal energy, minimum required energy to form a bubble and average liquid temperature with time for ethanol in PST case

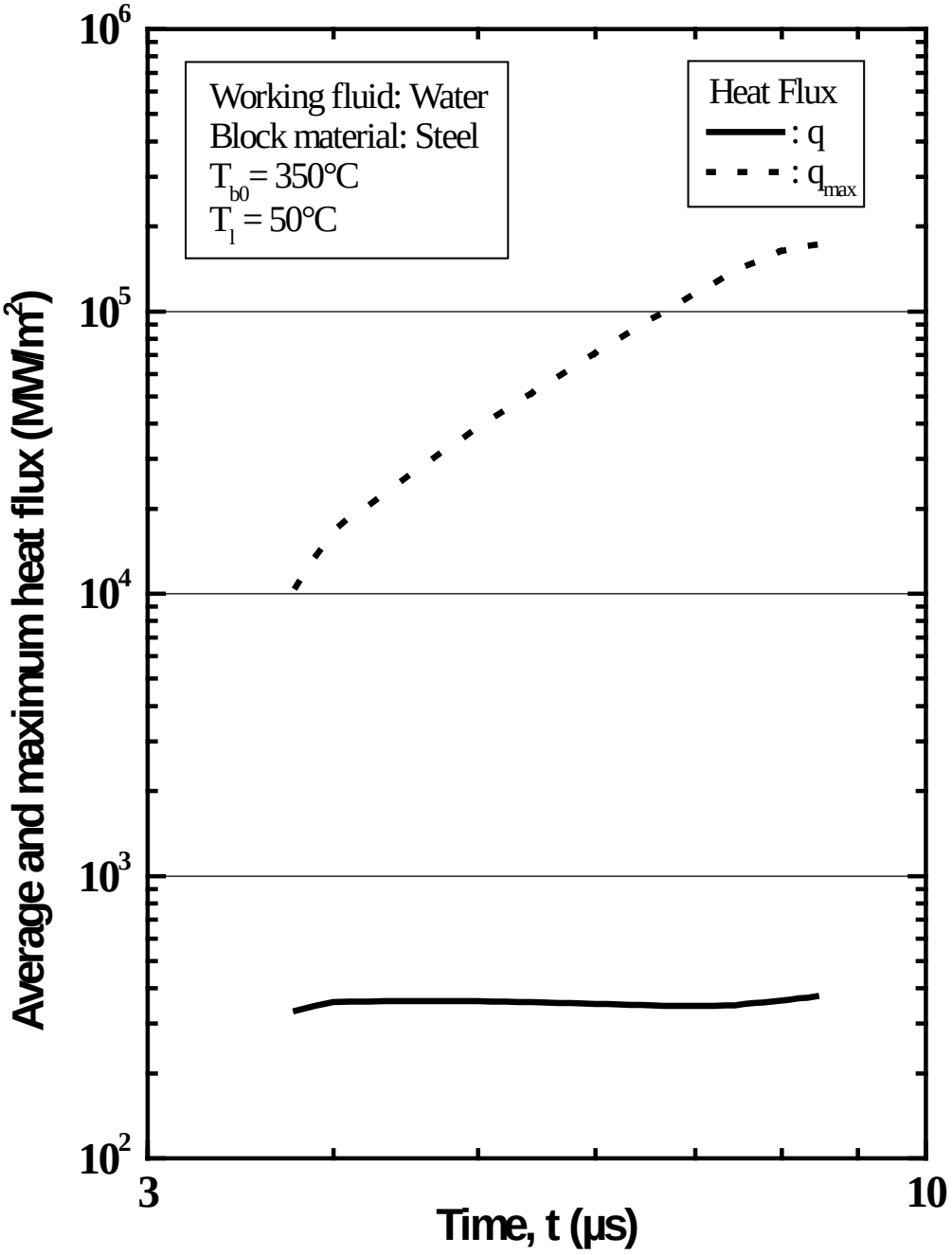

Figure 3.5.1 Variation of average and maximum heat flux with time for water in TST case

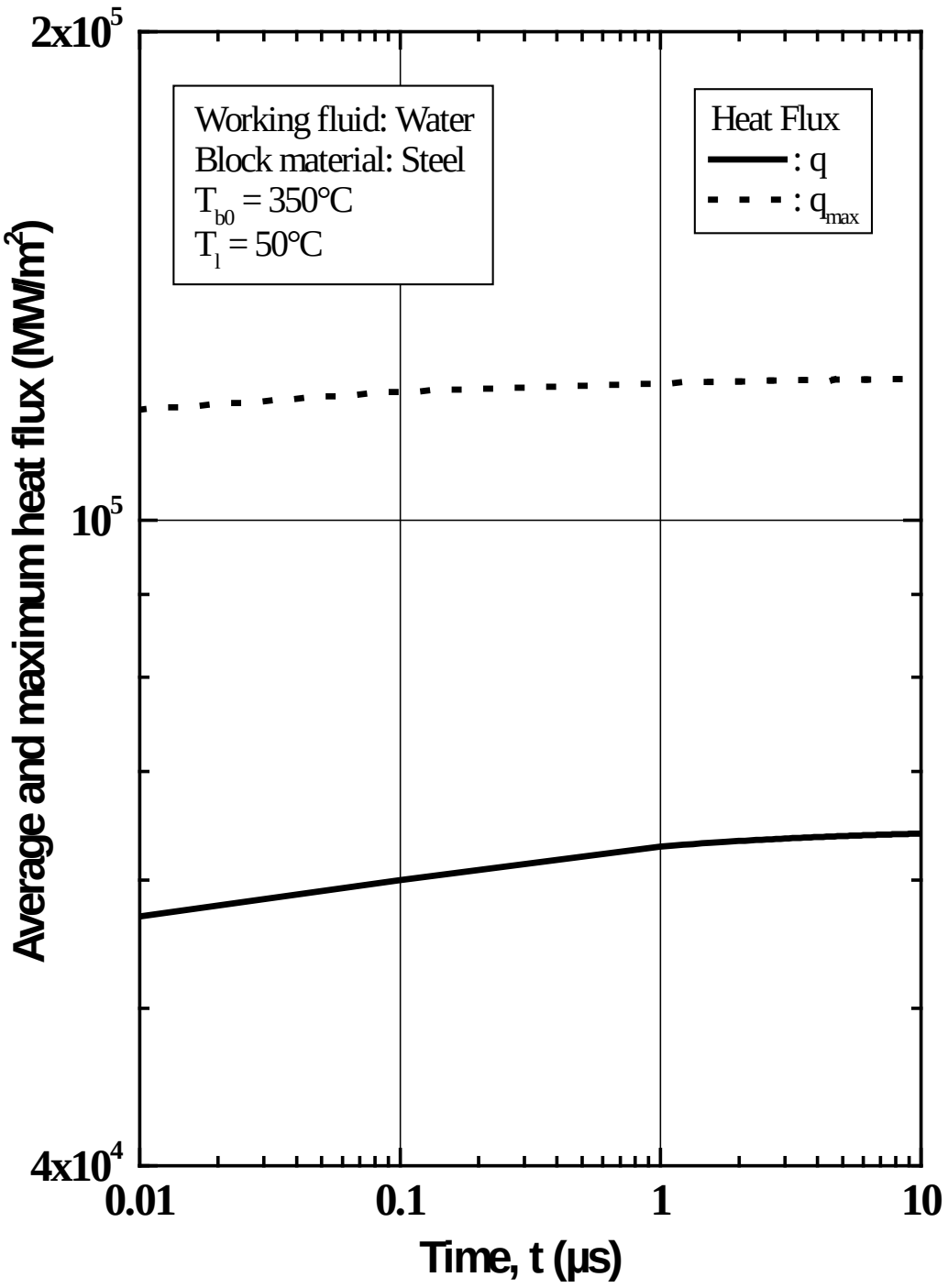

Figure 3.5.2 Variation of average and maximum heat flux with time for water in PST case

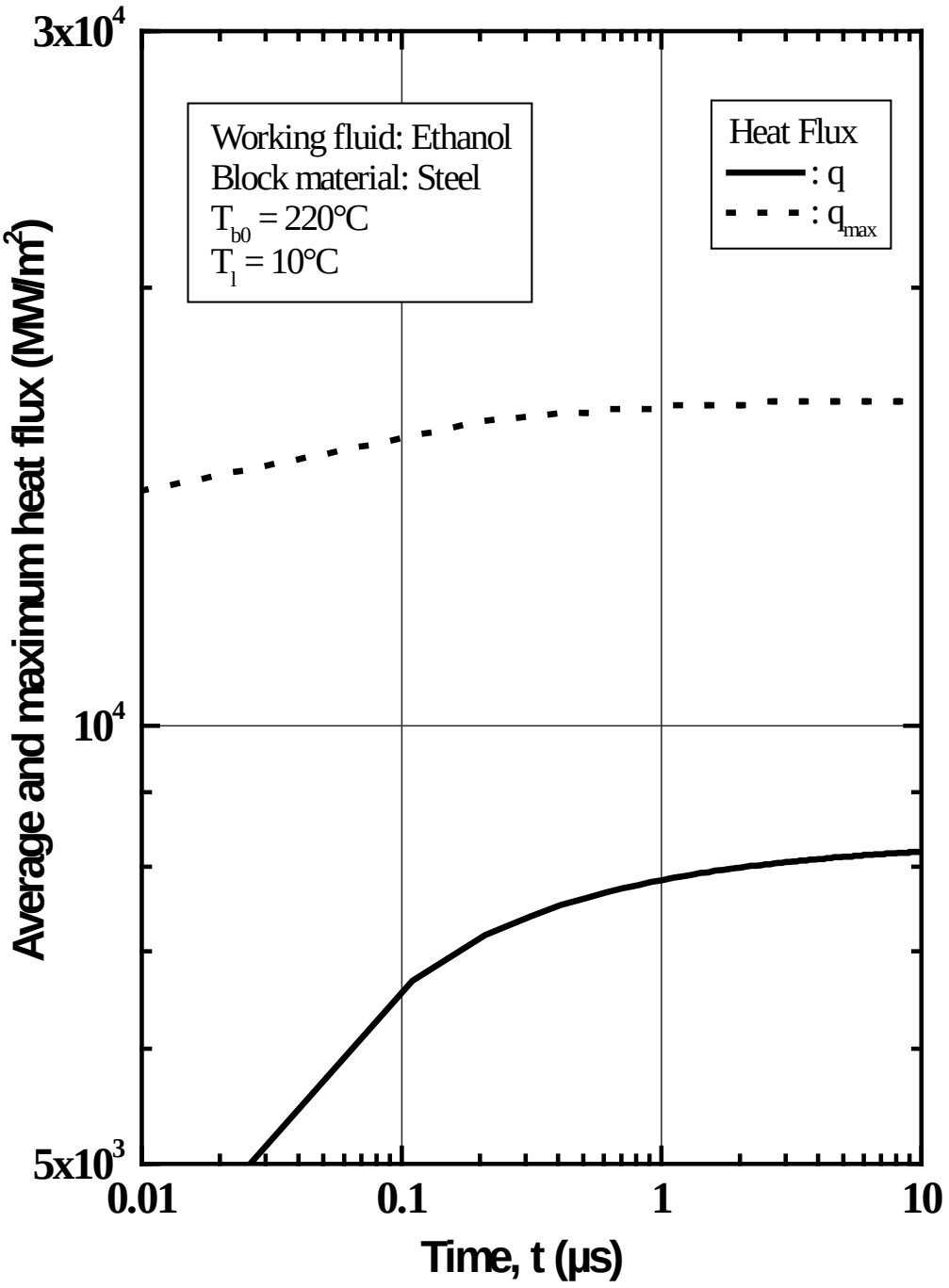

Figure 3.5.3 Variation of average and maximum heat flux with time for ethanol in PST case

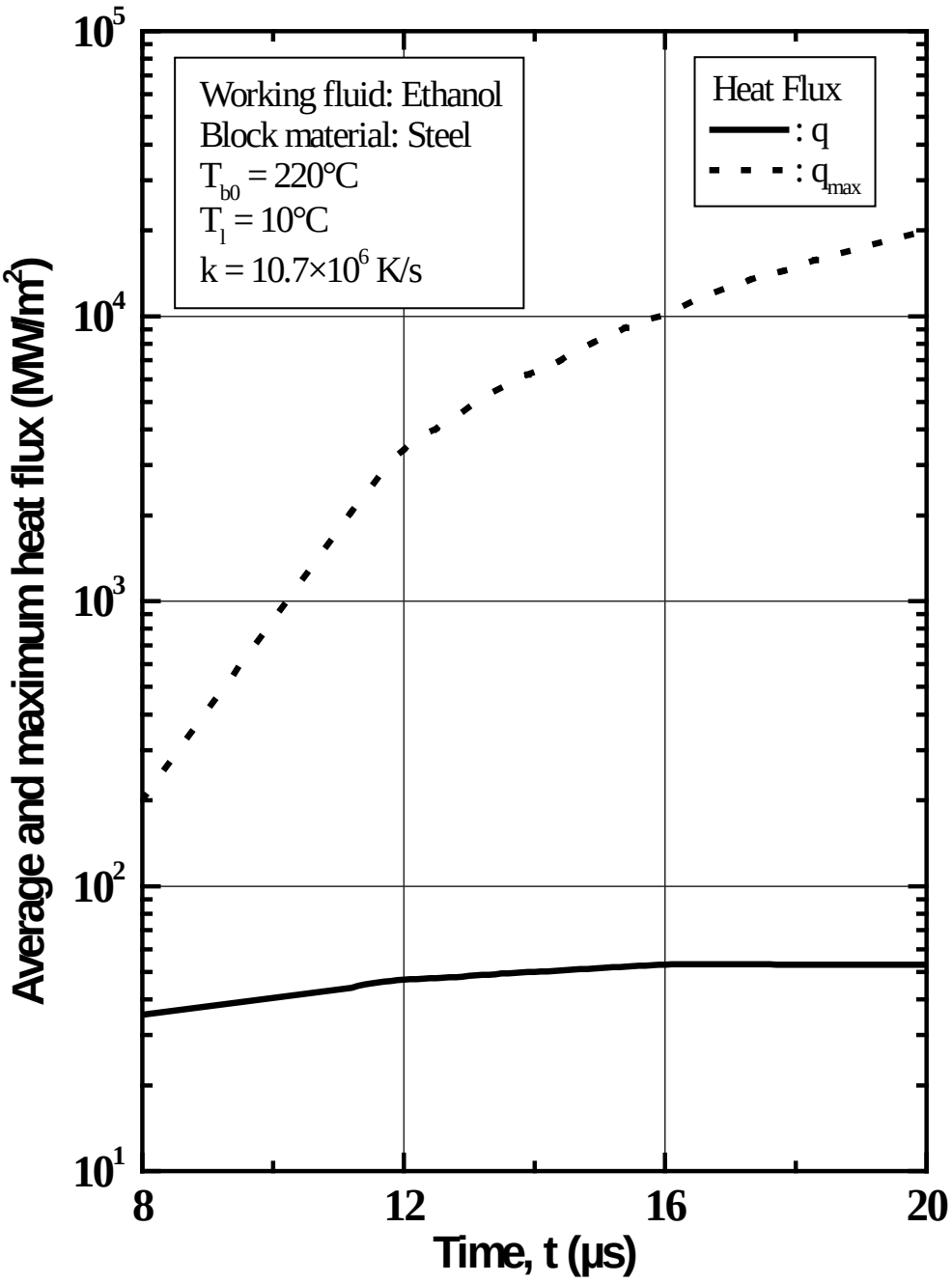

Figure 3.5.4 Variation of average and maximum heat flux with time for ethanol in TST case

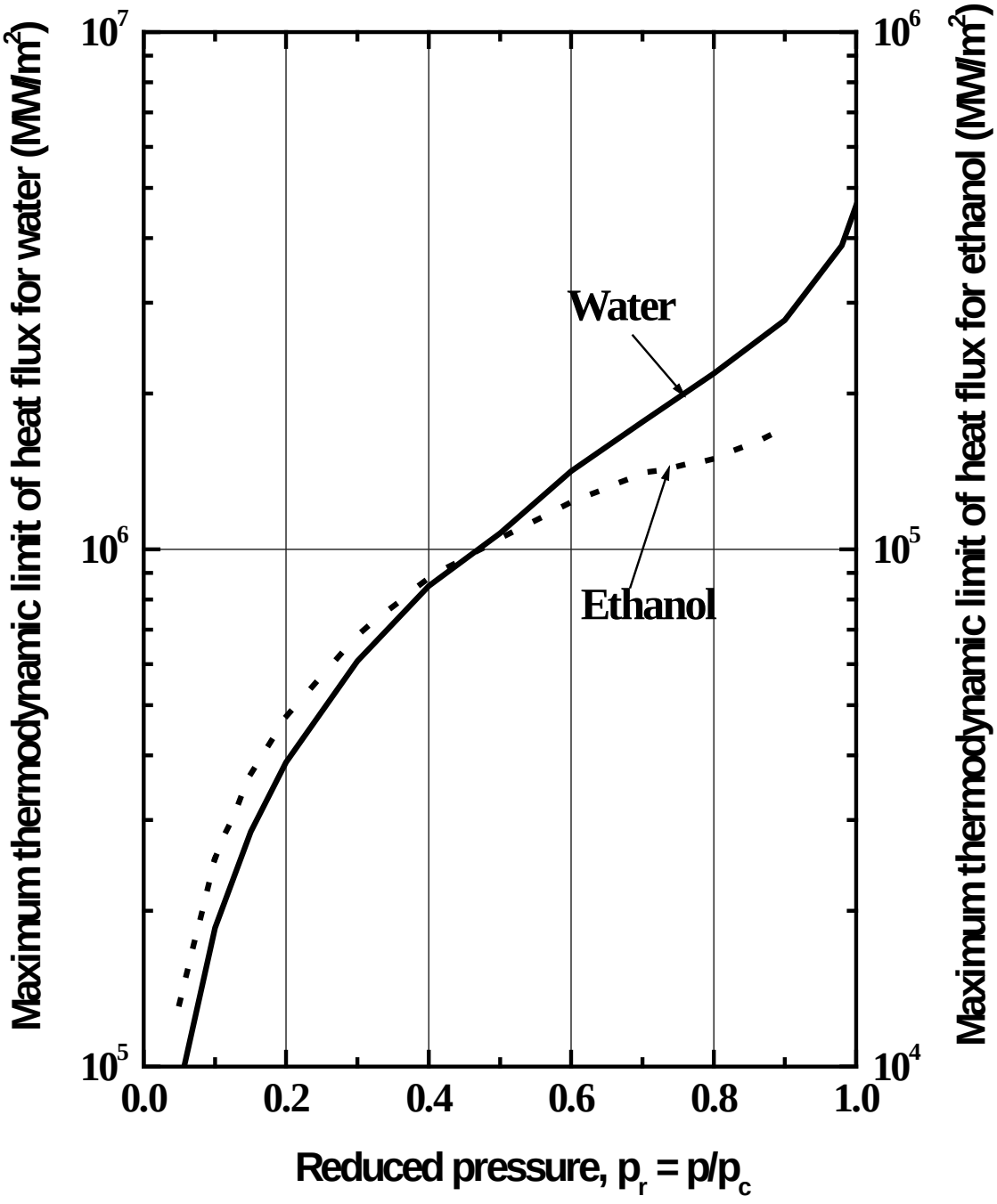

Figure 3.5.5 Variation of maximum thermodynamic limit of maximum heat flux for different working fluids

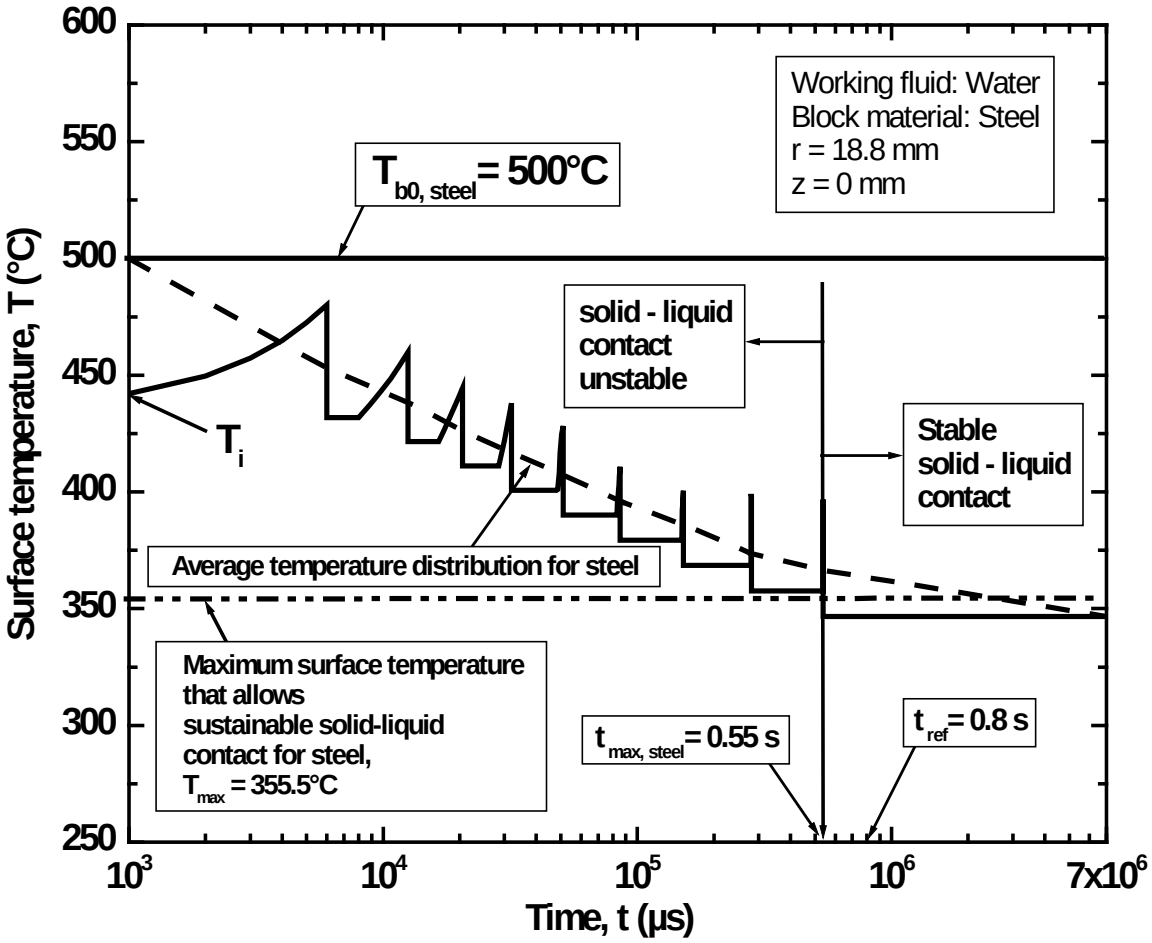

Figure 3.6.1 Variation of solid surface temperature with time for steel at early stages of jet impingement quenching

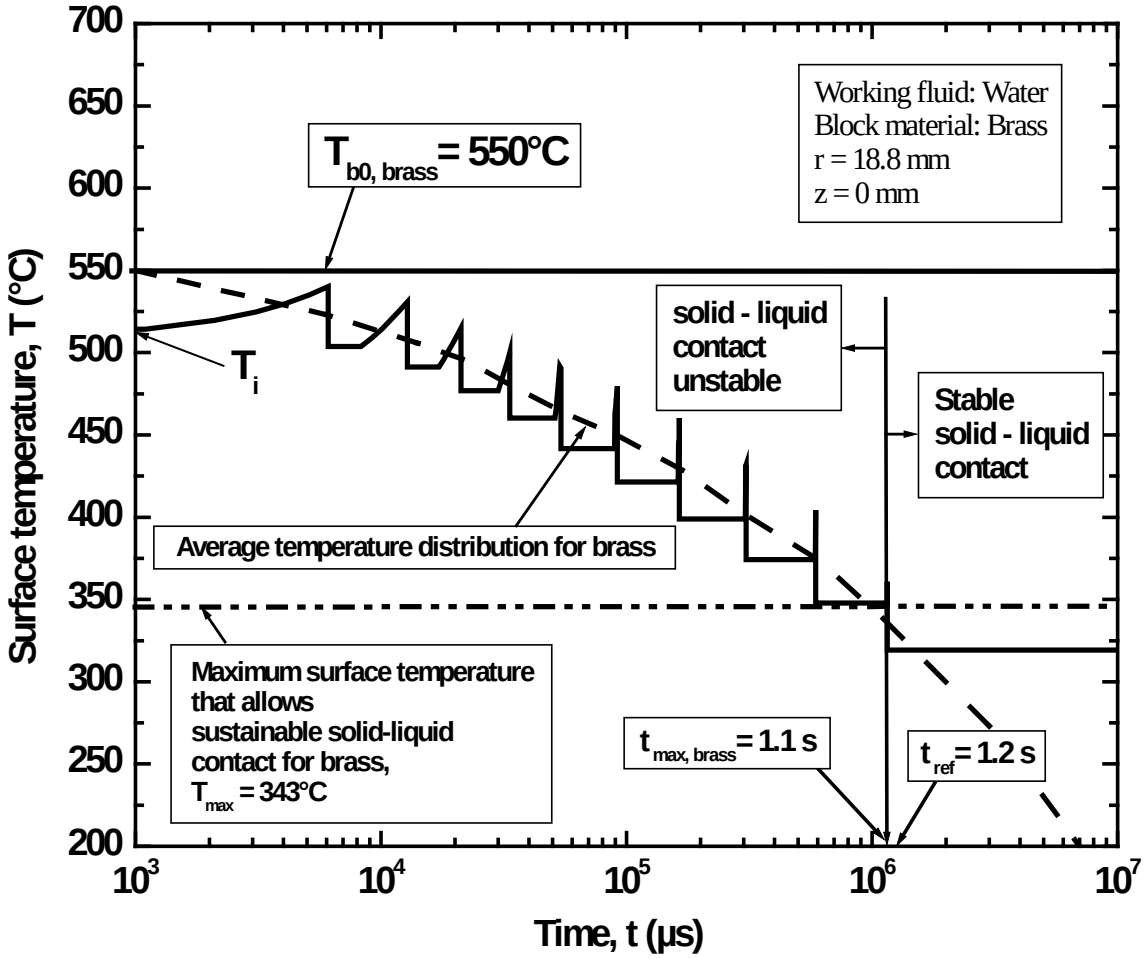

Figure 3.6.2 Variation of solid surface temperature with time for brass at early stages of jet impingement quenching

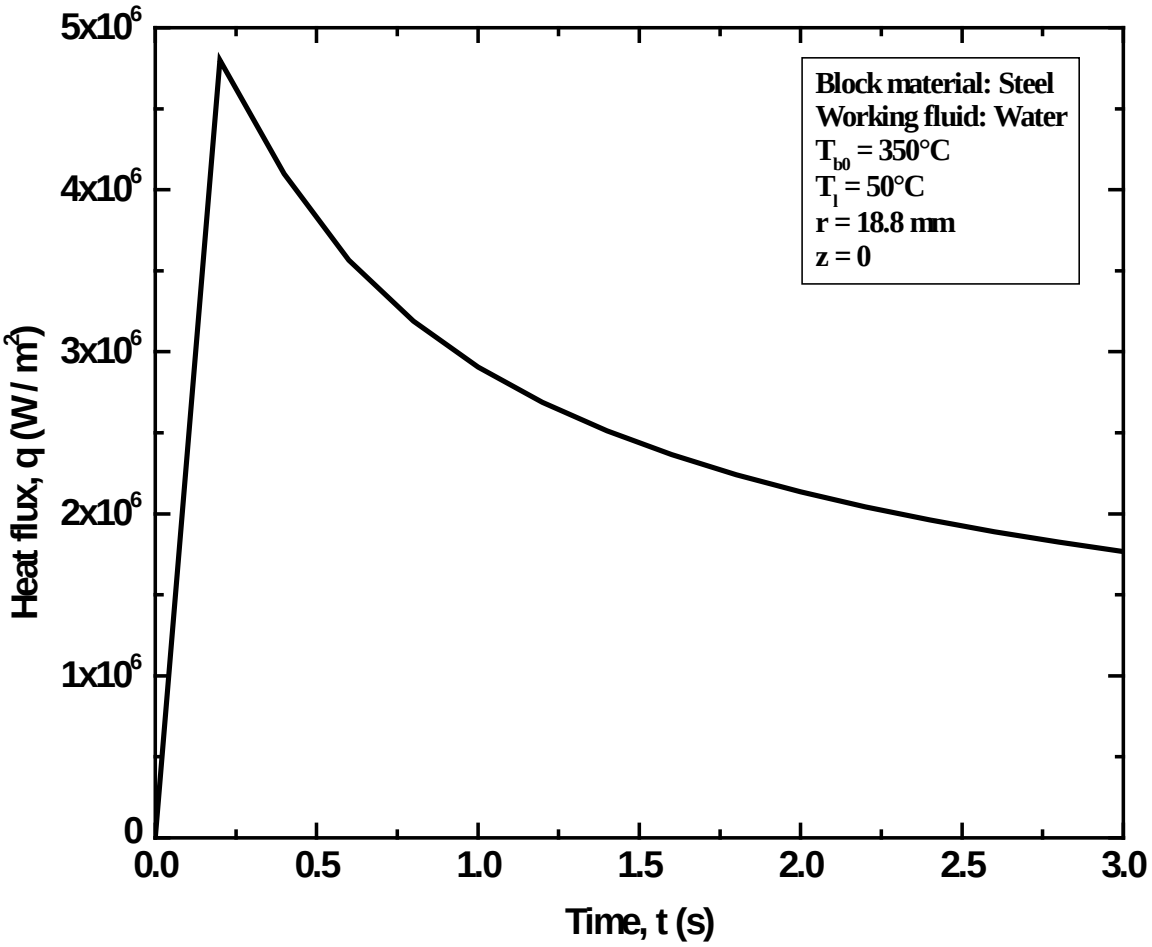

Figure 3.7.1 Variation of surface heat flux with time

REFERENCES

[1] Clemens, J. M. L. and Simons, R. E., “Advances in high-performance cooling for electronics,” Electronics Cooling, Vol. 7, No. 6, Nov. 2005.

[2] Lasance, C., “Technical data column,” Electronics Cooling, January 1997.

[3] Ellsworth, J. M. and Simons, R. E., “High-powered chip cooling-air and beyond,” Electronics Cooling, Vol. 5, No. 3, Aug. 2005.

[4] Simons, R. E., “Electronics cooling applications,” Electronics Cooling, Vol. 1, No. 1, Jan. 2008.

[5] Skripov, V. P., “Metastable Liquids,” John Wiley and Sons, 1974.

[6] Gibbs, W., “The Scientific Papers,” Vol. 1, Dover Publ. Inc., NY, 1961.

[7] Lienhard J. H. and Karimi, A., “Homogeneous Nucleation and The Spinodal Line,” *ASME J. of Heat Transfer*, Vol. 103, pp. 61-64, 1981.

[8] Blander, M. and Katz, J. L., “Bubble Nucleation in Liquids,” *AIChE Journal*, Vol. 21, No. 5, pp. 833-848, 1975.

[9] Volmer, M. and Weber, A., “Keimbildung in Ubersattigten Gebilden,” *Zeit. Physik. Chemie*, Vol. 119, pp. 277-301 1926.

[10] Farkas, L., “The Velocity of Nucleus Formation in Supersaturated Vapors,” *J. Physik Chem.* pp. 125, 236, 1927.

[11] Becker, R. and Doring, W., “The Kinetic Treatment of Nuclear Formation in Supersaturated Vapors,” *Ann. Phys.*, Vol. 24, pp 719, 752 1935.

[12] Zeldovich, J. B., “On the Theory of New Phase Formation: Cavitation,” *Acta Physicochimica, USSR*, Vol. 18, pp. 1-22 1943.

[13] Frenkel, J., “Kinetic Theory of Liquids,” John Wiley and Sons, 1955.

[14] Carey, V. P., “Liquid-Vapor Phase Change Phenomena,” Taylor and Francis, Copyright © 1992 by Hemisphere Publishing Corporations.

[15] Blake, F. G., “The tensile strength of liquids; A review of the literature,” Harvard Acou. Res. Lab. Rep. TM9. 1949.

[16] Bernath, L., "Theory of Bubble Formation in Liquids," *Ind. Eng. Chem.*, Vol. 44, No. 6, pp. 1310-1313, 1952.

[17] Cole, R., "Boiling Nucleation," *Adv. Heat Transfer,* Vol. 10, pp. 86-166, 1970.

[18] Piggot, B. D. G., White, A. P. and Duffey, R. B., "Wetting Delay Due to Film and Transition Boiling on Hot Surfaces," *Nucl. Eng. Des.,* Vol. 36, pp. 169-181, 1976.

[19] Ishigai, S., Nakanishi, S. and Ochi, T., "Boiling heat transfer for a plate water jet impinging on a hot surface," in *Proceedings of the 6th International Heat Transfer Conference*, 1978, pp. 445-450.

[20] Hatta, N., Kokado, J. and Hanasaki, K., "Numerical Analysis of Cooling Characteristics for Water Bar," *Trans. Iron Steel Inst. Jpn,* Vol. 23, pp. 555-564, 1983.

[21] Wolf, D.H., Incropera, F.P. and Viskanta, R., "Jet Impingement Boiling," *Advances in Heat Transfer,* Vol. 23, pp.1-132, 1993.

[22] Liu, Z. and Wang, J., "Study on Film Boiling Heat Transfer for Water Jet Impingement on High Temperature Flat Plate," *Int. J. Heat Mass Transfer,* Vol. 44, pp. 2475-2481, 2001.

[23] Hammad, J., Monde, M. and Mitsutake, Y., "Characteristics of Heat Transfer and Wetting Front during Quenching by Jet Impingement," *Therm. Sci. Eng.,* Vol. 12, pp. 19–26, 2004.

[24] Woodfield, P.L., Monde, M. and Mozumder, A. K., "Observations of High Temperature Impinging-Jet Phenomena," *Int. J. Heat Mass Transfer,* Vol. 48, pp. 2032-2041, 2005.

[25] Mozumder, A. K., Monde, M. and Woodfield, P. L., "Delay of Wetting Propagation during Jet Impingement Quenching for a High Temperature Surface," *Int. J. Heat Mass Transfer*, Vol. 48, pp. 5395-5407, 2005.

[26] Islam, M. A., Woodfield, P. L., Mozumder, A. K., Mitsutake, Y. and Monde, M., "Boiling and wetting phenomena of hot surface during jet impingement quenching," *Proc. 13-IHTC*, Sydney, Australia, pp. 1-12 (BOI-09 on CD), 2006

[27] Islam, M. A., Monde, M., Woodfield, P. L. and Mitsutake, Y., "Jet Impingement Quenching Phenomena for Hot Surfaces Well Above the Limiting Temperature for Solid-liquid Contact," *Int. J. Heat and Mass Transfer*, Vol. 51, pp. 1226-1237, 2008.

[28] Islam, M. A., Monde, M., Woodfield, P. L., Mitsutake, Y. and Mozumder, A. K., "Jet Impingement Boiling in Hot Surfaces Well Above the Limiting Temperature for Solid-liquid Contact," *Multiphase Science and Technology*, Vol. 19, No. 2, pp. 167-181, 2007.

[29] Islam, M. A., Monde, M. and Roy, P., "An analytical study of heat transfer during jet impingement quenching," *International Conference on Mechanical Engineering (ICME 07)*, Paper No. TH-36, Dec. 2007.

[30] Islam, M. A., "Study of homogeneous bubble nucleation during jet impingement quenching," CASR Report, Bangladesh University of Engineering and Technology (BUET), June 2008.

[31] Schrage, R. W., "A Theoretical Study of Interphase Mass Transfer," Columbia University Press (1953), New York, Chap. II.

[32] Gambill, W. R. and Green, N. D., "Boiling Burnout with Water in Vortex Flow," *Chem. Engr. Prog.*, Vol. 54, No. 10, pp. 68-76, 1958.

[33] Gambill, W. R., Bundy, R. D. and Wansbrough, R. W., "Heat Transfer, Burnout and Pressure Drop for Water in Swirl Flow Through Tubes with Internal Twisted Tapes," *Chem. Engr. Prog. Symp. Series,* Vol. 57, No. 32, pp. 127-137, 1961.

[34] Gambill, W. R. and Bundy, R. D., "High-Flux Heat Transfer Characteristics of Pure Ethylene Glycol in Axial and Swirl Flow," *AIChE Journal*, Vol. 9, No. 1, pp. 55-59, 1963.

[35] Ornatskii, A. P. and Vinyarskii, L. S., "Heat Transfer Crisis in a Forced Flow of Underheated (Subcooled) Water in Small-Bore Tubes," *High Temp.,* Vol. 3, No. 3, pp. 881-882, 1965.

[36] Monde, M. and Katto, Y., "Burnout in High Heat-Flux Boiling System with an Impinging Jet," *Int. J. Heat Mass Transfer,* Vol. 21, pp. 295-305, 1978.

[37] Katto, Y. and Shimizu, M., "Upper Limit of CHF in the Forced Convection Boiling on a Heated Disc with a Small Impinging Jet," *ASME J. of Heat Transfer,* Vol. 101, No. 2, pp. 265-269, 1979.

[38] Tien, C. L. and Lienhard, J. H., "Solutions Manual to Accompany Statistical Thermodynamics," Revised Printing, Hemisphere, Washington, pp-13.

[39] Tien, C. L. and Lienhard, J. H., "Statistical Thermodynamics," Revised Printing, Hemisphere, Washington, pp-55.

[40] Skripov, V. P., and Pavlov, P. A., "Explosive Boiling of Liquids and Fluctuation Nucleus Formation," *Teplofizika Vysokikh Temperatur,* Vol. 8, No. 4, p. 833, 1969.

[41] Derewnicki, K. P., "Experimental Studies of Heat Transfer and Vapor Formation in Fast Transient Boiling," *Int. J. Heat Mass Transfer,* Vol. 28, No. 11, p. 2085, 1985.

[42] Iida, Y., Okuyama, K. and Sakuri, K., "Boiling Nucleation on a Very Small Film Heater Subjected to Extremely Rapid Heating," *Int. J. Heat Mass Transfer*, Vol. 37, No. 17, p. 2771, 1994.

[43] Iida, Y., Okuyama, K. and Sakuri, K., "Peculiar Bubble Generation on a Film Heater Submerged in Ethyl Alcohol and Imposed a High Heating Rate over 10^7 K/s," *Int. J. Heat Mass Transfer*, Vol. 35, No. 10, p. 2699, 1993.

[44] Glod, G., Poulikakos, D., Zhao, Z. and Yadigaroglu. G., "An Investigation of Microscale Explosive Vaporization of Water on an Ultrathin Pt Wire," *Int. J. Heat Mass Transfer*, Vol. 45, p. 367, 2002.

[45] Okuyama. K., Mori. S., Sawa. K. and Iida. Y., "Dynamics of Boiling Succeeding Spontaneous Nucleation of a Rapidly Heated Small Surface," *Int. J. Heat Mass Transfer*, Vol. 49, p. 2771, 2006.

[46] Hasan, M. N., Monde, M. and Mitsutake, Y., "Numerical simulation for homogeneous nucleation boiling," *Proceedings of JSME Thermal Engineering Conference 2009*, Paper number: B221.

[47] Carslaw, H. S. and Jaeger, J. C., "Conduction of Heat in Solids," Second Edition, Oxford University Press, 2001, pp. 87-89.

[48] Gambill, W. R., and Lienhard, J. H., "An Upper Bound for the Critical Boiling Heat Flux," *Journal of Heat Transfer*, Vol. 111, pp. 815-818, Aug. 1989.

[49] Woodfield, P. L., "The role of homogeneous nucleation boiling in impinging jet heat transfer at high temperature," 1st Year Report, Institute of Ocean Energy, Saga University, June 2004.

[50] Monde, M., "Heat Transfer Characteristics during Quenching of High Temperature Solid," *Journal of Thermal Science and Technology*, Vol. 3, No. 2, 2008.